NEXUS OF WATER AND ENERGY: RESILIENCE THROUGH DECENTRALIZED OPERATION

by

Govind Joshi

A thesis submitted to the Faculty and the Board of Trustees of the Colorado School of Mines in partial fulfillment of the requirements for the degree of Doctor of Philosophy (Electrical Engineering).

Golden, Colorado

Date_____

Signed: _____

Govind Joshi

Signed: _____

Dr. Salman Mohagheghi

Thesis Advisor

Golden, Colorado

Date _____

Signed: _____

Prof. Peter Aaen

Professor and Department Head

Department of Electrical Engineering

ABSTRACT

Natural disaster events are increasing around the globe in frequency, duration, and severity, thanks to the changing climate. Such incidents, e.g., severe weather events such as hurricanes, tornados, and flooding events, or geological phenomena such as tsunamis and earthquakes, can potentially cause damages to critical infrastructure including power and water networks. Not surprisingly, socially vulnerable groups are disproportionately affected by outages in power and water. The focus of this research is on proposing strategies for reliable and resilient operation of power and water networks, while considering their interdependencies. The ultimate goal here is to enhance the resilience of communities and neighborhoods affected by natural disasters by enabling them to continue to operate their energy and water networks in a decentralized fashion, upon need. Considering the nexus of water and energy offers an opportunity to improve the overall performance of both systems and to provide added reliability and resilience in the wake of large-scale disturbances. In this thesis, a framework is proposed for optimal design and optimal operation of community energy and water systems by utilizing, as much as possible, local energy and water resources. This is achieved in multiple steps as outlined below.

First, an optimal control strategy is presented for a decentralized municipal wastewater treatment plant (WWTP) in order to reduce its overall energy footprint, which will make it more suitable for standalone applications. The system studied uses a sequencing-batch membrane bioreactor (SBMBR). Using the proposed control strategy, the electromechanical components in the SBMBR plant can be controlled in a way that it minimizes the energy consumption of the entire system, while achieving the same treatment load. To model the energy demand of the WWTP, a mixed-integer nonlinear programming (MINLP) model is developed for the Mines Park

wastewater treatment facility located in Golden, CO. This formulation focuses on the operation schedules and speeds of air blowers, which affect the concentration of dissolved oxygen (DO), and the air scour blower (ASB) speed and permeation rate, which impact the transmembrane pressure (TMP) of the membranes. The MINLP model is solved to identify an optimal aeration and permeation control, which would minimize the energy footprint of the SBMBR system.

Next, it is mathematically demonstrated how a self-contained community can schedule available energy and water resources optimally so that both demands are met with minimal external support. It is assumed that distributed energy resources (DER) such as PV, wind, and a battery system, along with demand responsive loads are employed to meet energy demands, while a WWTP built in the community is used to treat and recycle wastewater for potable reuse. The problem is modeled as a multi-objective MINLP optimization model. Simulation results demonstrate that communities can successfully coordinate the locally available water and energy resources to meet both water and energy demands during a disturbance, for instance when the primary source of water or energy is not available. However, due to the uncertainty in both renewable energy generation and the electric/water consumption, ensuring a sustainable operation is a challenging task. To address this, a stochastic optimization approach is adopted that allows for modeling the uncertainties in generation and demand. An energy storage system in conjunction with local water storage and wastewater treatment offer the needed flexibility to counteract the variations in wind, solar, and demand. A two-stage stochastic programming model is hence formulated and solved to determine an optimal operation strategy for the combined system.

While the preceding work focuses on operation, a follow-up chapter addresses the problem from a design perspective. A multi-objective mixed integer nonlinear programming (MMINLP)

model has been presented to determine the optimal sizes of energy resources such as wind turbine, PV system, and the battery system, as well as the optimal size of the community storage tank (ST) to be able to supply the demand. The electrical power demand of residential customers and power demand of the water distribution system need to be supplied by the microgrid system, whereas, the ST will store clean water either purchased from external sources or obtained from water treatment facilities to supply the water needs of the community.

The proposed methodologies mentioned above can be implemented for rural communities where the centralized municipal water system, centralized wastewater facilities, and/or regional electric grid are not available due to geographical or cost limitations. This idea can also be applicable for small-scale communities whose water and energy networks are temporarily out-of-service as a result of natural or manmade disturbances. Should this happen, the main power system and/or the water network need to be broken into multiple subsystems for standalone and decentralized operation. This is the focus of the last section of this thesis where a solution is proposed to divide a power distribution grid and water distribution network into multiple microgrids and micronets to allow for localized supply of energy and water. In addition to allowing for continuous supply of power and water, such an approach will also help expedite power restoration efforts as the smaller portions of the network would be self-reliant until the service to the main power grid is restored. A graph theoretic approach is proposed, which is able to weigh nodes and edges based on their individual criticality levels as well as their overall impact on the integrity of the system.

TABLE OF CONTENTS

LIST OF FIGURES

LIST OF TABLES

LIST OF SYMBOLS

A. Indices and Sets

b	Index for the bioreactors
i	Index used for load points (customers) connected to the microgrid
k	Index used for time
m	Index for the membrane tanks (MT)
N	Set of load points in the community circuit
q	Index used for the objective functions in the multi-objective framework
s	Scenarios (realizations of a random parameter) representing uncertain demand and generation
S	Set of scenarios
t	Index for time
T	Time horizon of the problem
T_a	Time steps associated with the aerobic phase
τ	Time index (used for past time steps)
x	Index used for type 1 wind turbines. In this study these are large wind turbines (LWT)

y	Index used for type 2 wind turbines. In this study these are small wind turbines (swt)
X	Total number of type 1 wind turbines
Y	Total number of type 2 wind turbines

B. Parameters and Input Data

A^{WT}	Area swept by the rotor of the wind turbine (m^2)
A^{LWT}	Area swept by the rotor of the type 1 wind turbine (m^2)
A^{swt}	Area swept by the rotor of the type 2 wind turbine (m^2)
A^{br}	Area of each bioreactor (m^2)
A^{tank}	Area of each membrane tank base (m^2)
b_q	Goal (target) values for objective function q in the multi-objective framework
c^B/c^b	Price of using one deep discharge of the battery ($); determined based on the total cost of purchasing and maintaining the battery divided by the maximum number of deep discharges it can provide over its lifetime
c^u	Cost of power purchased from the utility ($/kW)
c^w	Cost of water purchase ($/$m^3$)
D_i	Contribution factor for customer i: fraction of total electric demand in the system consumed by customer i.

d_i	Non-shiftable load factor for a customer *i*, i.e., the percentage of customer *i* demand which is non-shiftable.
h_{max}^{br}	Maximum acceptable height of water in the bioreactors
h_{min}^{br}	Minimum acceptable height of water in the bioreactors
h_{min}^{mbr}	Minimum height required to be maintained in the MT in order to keep the pressure regulated
h_{base}^{mbr}	Base water height in the MT. In this study, this is considered to be 3.048 m (10 ft.). This height is associated with the volume of water that already exists in the MT)
k^{ww}	Portion of water consumed that will be discharged as waste, i.e. the ratio of water inflow to households to water outflow to sewer system
k_{sh}	Maximum allowable percentage of consumer load that can be shed during a dispatch period
M	Sufficiently large number
n_{rated}^{air}	Rated speed of the air blower in each bioreactor (rpm)
$n_{rated}^{grinder}$	Rated speed of the grinder pump (rpm)
n_{rated}^{mixer}	Rated speed of the mixer in each bioreactor (rpm)
n_{rated}^{ras}	Rated speed of return activated sludge (RAS) pump (rpm)
n_{rated}^{asb}	Rated speed of the ASB in each membrane tank (rpm)
n_{rated}^{p}	Rated speed of the permeate pumps (rpm)
N_{sh}	Maximum allowable number of times during a dispatch period that a consumer may experience load shedding. Naturally: $N_{sh} < T$

O_{des}	Desired amount of DO in each bioreactor (kg/m^3)
o_i	Number of occupants at the residence of customer *i*
P_{rated}^{air}	Rated power of the air blower in each bioreactor (kW)
P_{rated}^{asb}	Rated power of the ASB in each membrane tank (kW)
$P^{B,max}$	Maximum available power provided by the battery (kW). Also represented by $P^{BT,max}$ or $P^{b,max}$ in the thesis.
$P^{d}_{t,s}$	Total active power consumption at time *t* (kW) during scenario *s*
$P_{i,t}^{des}$	Desired active power consumption of consumer *i* at time *t* (kW)
P_{t}^{des}	Desired active power consumption of the entire microgrid at time *t* (kW)
$P_{i,t}^{d,NSH}$	Power consumed by non-shiftable loads of costumer *i* at time *t* (kW)
$P_{rated}^{grinder}$	Rated power of the grinder pump (kW)
P_{rated}^{mixer}	Rated power of the mixer pump in each bioreactor (kW)
P_{rated}^{p}	Rated power of the permeate pumps (kW)
$P^{PV,max}$	Maximum capacity of the PV solar panel (kW)
P_{rated}^{ras}	Rated power of RAS pump (kW)
$P^{WT,max}$	Maximum capacity of the wind turbine (kW)

$P^{LWT,max}$	Maximum capacity of each wind turbine of type 1 (kW)
$P^{swt,max}$	Maximum capacity of each wind turbine of type 2 (kW)
p_s	Probability of occurrence of scenario *s*
p^{ww}	Energy consumed at the wastewater treatment plant (WWTP) for treating one unit of wastewater (kWh/m^3)
p^{pump}	Power consumed to pump 1 m^3 of treated wastewater from the WWTP to the community water storage tank (ST) (kW/m^3)
$P_{i,t}^{PV}$	Power provided by PV panel of costumer *i* at time *t* (kW)
$P_{i,t,s}^{PV}$	Power provided by PV panel of costumer *i* at time *t* (kW) during scenario *s*
$P_i^{PV,STC}$	Power provided by PV panel of customer *i* under standard test condition (STC) (kW)
$P_{i,t}^{d,SH}$	Power consumption level of shiftable loads of costumer *i* at time *t* (kW)
P_t^W	Power provided by the wind turbine at time *t* (kW)
$P_{t,s}^W$	Power provided by the wind turbine at time *t* (kW) during scenario *s*
$Q_{t,s}^d$	Total water demand in the system at time t (m^3) during scenario *s*
$q_{i,t}$	Water consumption rate at consumer *i* at time *t* (m^3/s)
q^{min}	Minimum amount of water considered to be necessary to ensure basic daily needs. This is estimated by the World Health Organization to be between 50–100 liters (0.05–0.1 m^3) per person per day
q^{max}	Maximum water flow rate through pipes. This is limited by the designed flow rate for the water network (m^3/s)

$q_{rated}^{grinder}$	Rated flow rate of the grinder pump (m^3/s)
q_{rated}^{ras}	Rated flow rate of RAS pump (m^3/s)
q_{rated}^{p}	Rated flow rate of the permeate pumps (m^3/s)
SOC^{min}	Minimum allowable state-of-charge of the community battery (%)
SOC^{max}	Maximum allowable state-of-charge of the community battery (%)
SOC_0	State-of-charge of the battery at the beginning of study period (%)
T	Time horizon of the problem (hours, minutes, etc.)
TSH	Maximum allowable number of times during a dispatch period that a customer may experience demand shifting. Naturally: TSH < T
TMP^{max}	Maximum TMP in the MT (Pascal or N/m^2)
$V^{s,max}/V^{ST,max}$	Maximum permissible volume of water in the community ST (m^3)
$V^{s,min}/V^{ST,min}$	Minimum permissible volume of water in the community ST (m^3). This can be determined based on the minimum amount of water considered to be necessary to ensure basic daily needs for the community residents. The amount is estimated by the World Health Organization (WHO) to be between 50–100 liters (0.05–0.1 m^3) per person per day
$V^{ST,max}$	Capacity of the water ST (m^3)
$V^{ww,max}$	Maximum permissible volume of wastewater in the WWTP (m^3)
$V^{ww,min}$	Minimum permissible volume of wastewater in the WWTP (m^3)

V_{batch}	Batch volume, which is the volume of wastewater to be processed (m^3)
w_t	Wind speed at the wind turbine location at time *t* (m/s)
$w_{t,s}$	Wind speed at the wind turbine location at time *t* (m/s) during scenario *s*
α	Albert Betz constant
γ	Self-discharge rate of the battery (p.u.)
Δ	Duration of a single time step (s)
η^c/η^d	Charge/discharge efficiency for the battery (p.u)
ρ_a	Air density (kg/m^3)
$\Phi_{i,t}$	Incident solar irradiance at PV panel for consumer *i* at time *t* (W/m^2)
Φ^{STC}	Incident solar irradiance at STC (W/m^2)
Δ_t^{br}	Duration of one-time step t in bioreactors (minutes)
Δ_t^{mbr}	Duration of one-time step t in MT (minutes)
Δ_t^{p}	Duration of one permeation time step (minutes)
Δ_t^{bw}	Duration of one backwash time step (minutes)

C. Variables

λ	Auxiliary decision variable that provides an upper bound on the normalized deficiency variables in CGP
$\alpha_t^{grinder}$	Binary variable indicating whether the grinder pump is ON (1) or OFF (0) during time step *t*
α_t^{ras}	Binary variable indicating if RAS pump is ON (1) or OFF (0) during time step *t*
$\beta_{b,t}^{air}$	Binary variable indicating if blower in bioreactor *b* is ON (1) or OFF (0) during time step *t*
$\beta_{b,t}^{mixer}$	Binary variable indicating if mixer in bioreactor *b* is ON (1) or OFF (0) during time step *t*
$h_{b,t}$	Water level in bioreactor *b* at time step *t* (m)
$n_{b,t}^{air}$	Speed of air blower in bioreactor *b* at time step *t* (rpm)
$n_t^{grinder}$	Speed of the grinder pump at time step *t* (rpm)
n_t^{mixer}	Speed of mixer in bioreactor *b* at time step *t* (rpm)
n_t^{ras}	Speed of RAS pump at time step *t* (rpm)
$n_{m,t,k}^{asb}$	Speed of ASB blowing air into tank m at time step *t* during sub time step k (rpm)
$n_{m,t,k}^{P,p}$	Speed of permeate pump in membrane tank m at time step t during sub time step k (rpm)
$n_{m,t,k}^{P,bw}$	Speed of permeate pump in membrane tank *m* at time step t during sub time step k (rpm)
$o_{b,t}$	DO in bioreactor *b* during time step *t* (kg/m^3)
O_q	Value of objective function *q* in the multi-objective framework

p_q	Deficiency variables used in CGP
$P^{BT,\,cap}$	Installed capacity of the battery (kW)
$P_t^{B,c}$	Power provided to charge the battery at time *t* (kW)
$P_t^{B,d}$	Power discharged by the battery at time *t* (kW)
$P^{d}_{i,t}$	Active power consumption at load point *i* at time *t* (kW)
$P_{i,t}$	Power consumed by consumer *i* at time *t* (kW)
$P_{b,t}^{air}$	Power consumed by air blower in bioreactor *b* at time step *t* (kW)
$P_t^{grinder}$	Power consumed by grinder pump at time step *t* (kW)
$P_{b,t}^{mixer}$	Power consumed by mixer pump in bioreactor *b* at time step *t* (kW)
P_t^{ras}	Power consumed by RAS pump at time step *t* (kW)
$P^{PV,\,cap}$	Installed capacity of the PV solar panel (kW)
$P^{PV,\,STC}$	Power provided by the PV solar panel under STC (kW)
P_t^{ww}	Power consumed by the WWTP at time *t* (kW)
P_t^{PV}	Power provided by the community PV solar panel at time *t* (kW)
P_t^{WT}	Power provided by the wind turbine at time *t* (kW)

$P_{x,t}^{LWT}$	Power provided by type 1 wind turbine *x* at time *t* (kW)
$P_{y,t}^{swt}$	Power provided by type 2 wind turbine *y* at time *t* (kW)
$P^{WT,cap}$	Installed capacity of each wind turbine at time *t* (kW)
$P_t^{P,p}$	Power consumption of permeate pump during time step *t* in permeation mode (kW)
$P_t^{P,bw}$	Power consumption of permeate pump during time step *t* in backwash mode (kW)
$P_t^{asb,p}$	Power consumption of ASB during time step t in permeation mode (kW)
$P_t^{asb,bw}$	Power consumption of ASB during time step t in backwash mode (kW)
P^u	Power purchased from the utility to charge the battery at the beginning of study period (kW)
$P_{i,t,s}^{d,\ NSH}$	Power consumed by non-shiftable loads of costumer *i* at time *t* (kW) during scenario *s*
$P_{i,t,s}^{d,SH}$	Power consumption level of shiftable loads of costumer *i* at time *t* (kW) during scenario *s*
$P_{t,s}^{b,c}$	Power provided to charge the battery at time *t* (kW) during scenario *s*
$P_{t,s}^{b,d}$	Power discharged by the battery at time *t* (kW) during scenario *s*
$P^d_{i,t,s}$	Active power consumption at load point *i* at time *t* (kW) during scenario *s*
$q^d_{i,t,s}$	Water consumption rate at customer *i* at time *t* (m^3/s) during scenario *s*
$q_{t,s}^{ST,out}$	Outgoing flow rate from the ST at time *t* (m^3/s) during scenario *s*

$q_t^{ST,out}$	Outgoing flow rate from the storage tank at time t (m^3/s)
$q_{t,s}^{ww,eff}$	Effluent flow rate from the wastewater management plant at time *t* (m^3/s). This is the amount of untreated wastewater discharged to make sure the tank does not go over capacity during scenario *s*
$q_{t,s}^{ww,in}$	Incoming flow rate to the WWTP at time *t* (m^3/s) during scenario *s*
$q_{t.s}^{ww,out}$	Outgoing flow (treated wastewater) from the WWTP at time *t* (m^3/s) during scenario *s*
$q_{b,t}^{bf}$	Flow rate back feed into bioreactor tank *b* from spill way during time *t* (m^3/s)
$q_{i,t}^{d}$	Water consumption rate at customer *i* at time *t* (m^3/s)
$q_t^{s,in}$	Incoming flow rate to the ST at time *t* (m^3/s)
$q_t^{s,out}$	Outgoing flow rate from the ST at time *t* (m^3/s). Also represented by $q_t^{ST,out}$ in the thesis
$q_t^{ww,eff}$	Effluent flow rate from the wastewater management plant at time *t* (m^3/s). This is the amount of untreated wastewater discharged to make sure the tank does not go over capacity
$q_t^{ww,in}$	Incoming flow rate to the WWTP at time *t* (m^3/s)
$q_t^{ww,out}$	Outgoing flow (treated wastewater) from the WWTP at time *t* (m^3/s)
$q_{b,t}^{in}$	Input flow rate into bioreactor *b* during time step *t* (m^3/s)
$q_{b,t}^{out}$	Output flow rate from bioreactor *b* during time step *t* (m^3/s)
$q_t^{grinder}$	Flow rate through grinder pump during time step *t* (m^3/s)
q_t^{ras}	Flow rate through RAS pump during time step *t* (m^3/s)

$q_{m,t,k}^{P,p}$	Permeate flow rate in membrane tank m at time step t during sub step k (m^3/s)
$q_{m,t,k}^{P,bw}$	Backwash flow rate in membrane tank m at time step t during sub step k (m^3/s)
q_{est}^{P}	Estimated permeation flow rate based on the available batch size (m^3/s)
SOC_t	State-of-charge of the community battery at time *t* (%)
$SOC_{t,s}$	State-of-charge of the community battery at time *t* (%) during scenario *s*
$TMP_{m,t,k}$	TMP in membrane tank m at time step t during sub step k (Pa)
u_x^{LWT}	Binary variable indicating if type 1 wind turbine *x* is online or offline (=1: online, 0: offline*)*
u_y^{swt}	Binary variable indicating if type 2 wind turbine *y* is online or offline (=1: online, 0: offline*)*
$u_{t,s}^{b,c}$	Binary variable indicating if the battery is charged at time *t* (= 1: charged, 0: not charged) during scenario *s*
$u_{t,s}^{b,d}$	Binary variable indicating if the battery is discharged at time *t* (= 1: discharged, 0: not discharged) during scenario *s*
$u_t^{B,c}$	Binary variable indicating if the battery is charged at time *t* (= 1: charged, 0: not charged). Also represented by $u_t^{BT,c}$ in the thesis.
$u_t^{B,d}$	Binary variable indicating if the battery is discharged at time *t* (= 1: discharged, 0: not discharged). Also represented by $u_t^{BT,d}$ in the thesis.
$v_{i,k,t,s}$	Binary variable indicating if the shiftable appliance load has been shifted from time *k* to a later time *t* (=1: shifted, 0: not shifted) during scenario *s*
$V_{t,s}^{ST}$	Volume of water at the community ST at time *t* (m^3) during scenario *s*
$V_{t,s}^{ww}$	Volume of wastewater at the WWTP at time *t* (m^3) during scenario *s*

$V^{ST,in}$	Volume of water purchased and stored in ST for the community so that it can use during daytime (m^3)
$v_{i,t}$	Binary variable indicating if consumer i is experiencing load shedding at time t (=1: load shed, 0: desired demand met)
$v_{i,\tau,t}$	Binary variable indicating if the shiftable appliance load has been shifted from time τ to a later time *t* (=1: shifted, 0: not shifted)
V_t^s	Volume of water at the community ST at time *t* (m^3)
V_t^{ST}	Volume of water at the community storage tank at time t (m^3)
$V^{ST,cap}$	Installed capacity of the water tank (m^3)
V_t^w	Volume of water received from external resources at time t (m^3)
V_t^{ww}	Volume of wastewater at the WWTP at time *t* (m^3)
$v_{b,t}$	Volume of fluid in bioreactor *b* during time step *t* (m^3)
V_{ras}	Volume processed by the RAS pump over the time horizon T (m^3)
V_m^p	Volume of permeated water from membrane tank *m* (m^3)

ACKNOWLEDMENTS

This thesis would not have been possible without the help and guidance of several individuals who have contributed and extended their valuable time and assistance in the preparation and completion of this research.

First and foremost, I offer my utmost gratitude to my PhD advisor, Dr. Salman Mohagheghi, for his support throughout the development of this thesis with his expertise. He provided me the tools and necessary support in every step of this PhD journey. I am also very grateful to my thesis committee Prof. Tzahi Cath, Prof. Abd Arkadan, and Dr. Payam Nayeri for their suggestions and ideas that helped improve this work. I am particularly thankful to Prof. Tzahi and his team for their insightful advice and help in development of some of the topics in this research. I also would like to thank my friend and colleague, Dr. Moein Choobineh, for his support during my PhD at Colorado School of Mines.

I express my deepest gratitude to my parents (Khagi Raj Joshi and Sita Devi Joshi) as well as my brother, Kosh Raj Joshi, and sister, Yashoda Joshi, for their endless support and love. I appreciate all the supports that I received from my uncle, Rajendra Awasthi, and aunt, Kacie Awasthi, throughout my stay in Colorado. I would not have made it this far without their help. Last but not least, I appreciate all the love and care I received from my wife, Purnika Joshi, throughout this journey.

CHAPTER 1

THESIS OVERVIEW

1.1 Scope and Problem Statement

Access to water and energy systems are critical for the well-being and growth of societies, but in the recent years, natural and manmade hazards have posed an increasing threat to the reliability and resilience of these critical resources. Disturbances such as hurricanes, flooding events, droughts, earthquakes and tsunamis, and winter storms, as well as manmade threats such as cyber-attacks on control centers, can lead to widespread and prolonged disruption of services in energy and water systems. The modern power grid is an interconnected network of a large number of generators and motors, DERs, and other power transmission and distribution equipment. As the power grid typically expands over a large geographical area connecting millions of customers with many critical loads, there is an increased risk of losing power due to damages to grid components. This is due to the fact that power system components that are located thousands of miles apart are still electrically connected together and unavailability of one component may affect the operation of a group of other components or, in extreme cases, the entire network. One way to prevent such failures from propagating across the entire network is to adopt a strategy to isolate the affected component(s) from rest of the grid. Of course, this is not limited to networks impacted by disturbances. There are many isolated communities in rural and remote regions that are located far away from the main generation resources. While they may rely on certain level of external support to be able to operate, these isolated communities must be self-reliant as much as possible. In this thesis, reliable and resilient operation of electrical power grid is studied from the viewpoint of decentralized operation. A similar concept is extended to water distribution systems that may rely

on water reuse and localized supplies. Together, the nexus of energy and water is studied for the purpose of achieving resilience and reliable operation of both water and energy networks.

Power system resilience is the ability of the network to withstand natural or manmade low-frequency high-impact disasters and reduce the risk of interruption in the supply of power. There is an increasing number of threats to the power grid resilience imposed by natural and manmade disturbances that have the capability to disrupt power supply for a nonnegligible period of time to a large portion of the population. Losing multiple transmission lines or generators due to such disturbances in the grid can force transmission and distribution system operators to issue forced power outages across their territories to balance the load and generation [1]. The damages incurred by these events significantly affect the livelihood of the communities affected, and in addition to often long-term economic consequences, may lead to serious mental, emotional, and physical health issues [2]–[5]. Depending on its severity and scope, a natural disaster may cause severe damages to the critical infrastructure such as roads, power grid, water treatment and wastewater management facilities, telecommunication systems, and suchlike. Lack of access to these basic services can significantly impact the health and wellbeing of the residents in the affected regions and disrupt disaster recovery efforts. While evacuation is one option, it may not be easy (e.g., in densely populated urban areas), feasible (e.g., damages to roads and other transportation systems), or desirable (e.g., for residents with financial concerns or health or disability issues) [6]. Not surprisingly, socially disadvantaged communities are disproportionately affected by the social and economic impacts of natural disasters [7], [8], and research has shown that widespread poverty increases the population's vulnerability to many natural hazards [9], [10]. In order to be prepared for the future disasters, the regulating agencies must work together to build a plan and implement

policies to strengthen the power grid and other critical infrastructure so that the future events can be monitored in advance and impacts can be minimized.

One of the important solutions that many researchers have proposed and discussed in the literature is the concept of an electric microgrid. Electrical microgrids can be a part of larger power system network or in remote areas, can operate as an isolated and decoupled power system that has its own generating stations, distribution lines, and other necessary equipment to serve its loads. Microgrids span over smaller geographical regions compared to the main power grid. When connected to the main grid, they have the capability to island from it upon need, for instance during large-scale disturbances and outages. By utilizing locally available generators, the communities connected to the microgrid can receive power without having to suffer from the impacts of the power grid disturbance or outage.

Another equally critical infrastructure for communities is the water network, which needs to be designed and planned in advance to better withstand future disasters. The concept of decentralized operation in the power network can be expanded to water systems as well. Similar to the power grid, the traditional municipal water distribution system covers a large geographical region with a large population and a complex infrastructure. Natural and manmade disturbances can threaten the operation and availability of the water distribution systems. For example, contamination in reservoirs, breakdown of major water distribution lines, power supply disruption to water treatment facilities and pumping station can all disrupt water services and cause water supply outage for millions of people in the affected region. The system operators must plan ahead to ensure reliable water supply for the communities when primary sources of water may become unavailable due to disturbances and disasters.

In this thesis, the combined operation of energy and water networks is studied from both design and operation perspectives. Electrical power is used in the water system to run water treatment facilities, control systems, and pumping systems. Power system planners, designers, and system operators must consider the critical nature of the energy demand in water systems in order to maintain the load generation balance in the grid. In case of the potential loss of the main power grid, the system operator needs to coordinate locally available energy resources to meet the energy needs of the water network as well as other critical loads in the power system. This thesis presents the coordinated optimal design and operation of water and energy networks that rely on local energy resources such as DERs and water resources such as storage tanks and wastewater treatment facilities. Multi-objective optimization models have been proposed to meet the multiple and, at times contradictory, objectives of the power and water networks. Case studies have been presented as proof-of-concept to demonstrate the applicability of the proposed solutions.

1.2 Thesis Outline

The rest of this thesis is organized as follows. CHAPTER 2 provides a detailed introduction to the problem statement studied in this dissertation and a review of the literature as related to the various aspects of optimal design and operation of the combined water and energy systems. This chapter discusses in detail how energy and water systems are interconnected and how the combined operation of both systems is beneficial for their overall efficiency. The concepts of an electric microgrid and a water micronet have been discussed. Furthermore, this chapter highlights the increasing threats to energy and water systems as well as the importance of energy-water nexus to maintain resiliency of a community against potential disturbances. Finally, an introduction is provided into stochastic programming and multi-objective optimization.

In CHAPTER 3, an optimal energy management strategy is proposed for wastewater treatment plants (WWTPs), together with a case study to demonstrate the application of the proposed mathematical model. Various electromechanical components that are used to treat wastewater have been modeled so that their operation can be optimized to achieve minimum energy consumption in the system. In addition, electrochemical activities that occur during the water treatment process have been modeled using a data driven approach. This chapter discusses the time-series modeling of these activities to predict future state of the biochemical reactions in bioreactors and membrane tanks of a WWTP.

CHAPTER 4 presents the problem formulation and a proof-of-concept case study for an energy-water co-optimization problem, with the goal of ensuring the resiliency of both water and energy systems in an isolated neighborhood. A deterministic multi-objective mathematical model has been presented to balance multiple goals across both systems and devise an optimal strategy to concurrently run both energy and water distribution systems.

In CHAPTER 5, a strategy is proposed for optimal design of a combined microgrid/micronet system. A multi-objective mixed-integer non-linear optimization model has been presented with a deterministic set of data. The optimal sizes of a battery system, wind turbine, and PV generator have been computed for reliable operation of microgrid. In addition, demand response (DR) has been identified as a solution to maintain the stability of the microgrid, i.e., when load shedding is necessary for ensuring load-generation balance. Similarly, the optimal size of the ST in the micronet has been determined based on the number of residents and their typical water consumption patterns. Two design options are considered, i.e., considering the possibility of

curtailment of energy resources when generation exceeds demand and absorbing all energy available (also known as maximum power point tracking (MPPT)).

CHAPTER 6 extends the work in CHAPTER 4 by considering the stochastic models of an energy-water system. Uncertainties in renewable generation, power demand, and water demand of the community have been considered to replicate a more realistic model of the system. A scenario-based approach has been implemented to solve the stochastic model, and a case study is presented as proof-of-concept.

CHAPTER 7 views the problem from the standpoint of forming microgrid/micronet systems. A strategy is proposed to of decompose a power and water network into multiple smaller microgrid/micronet systems so that each system (cluster) can operate independently to meet the local energy and water needs. This is especially necessary when the main power and/or water network are affected by a large-scale disturbance and cannot continue operating as normal. A graph theoretic approach is proposed, which is able to weigh nodes and edges based on their individual criticality levels as well as their overall impact on the integrity of the main system. The approach also takes into account the possibility of power exchanges between different clusters with the goal of improving the overall reliability and resiliency.

Finally, conclusions, a list of contributions, and suggestions for future work are presented in CHAPTER 8.

CHAPTER 2

INTRODUCTION AND LITERATURE REVIEW

2.1 Introduction

According to ecological theory, resilience of an ecosystem is defined as its ability to respond to and absorb a disturbance and to maintain the "basic normal functions" and essential relationships within all components of the system [11]–[13]. In the most general sense, an ecosystem represents a community of both living and nonliving components of the environment. In this thesis, we consider a residential community as the ecosystem. Modern cities and communities depend on some key resources such as food, water, and energy to survive and to build a resilient community, one must consider and understand its holistic picture, i.e. dependencies of human being on natural resources as well as the impacts of interruptions of those resources on human lives [14],[15]. This thesis focuses on the reliable and resilient operation of the two key resources, i.e. water and energy, and their nexus within cities and communities.

As the world population grows, so does the need for water and energy. As such, it becomes more important for communities to be either self-reliant in these two resources or to have the capability to operate independently of outside sources upon need. This way, the extent of damages of external disturbances on the livelihood of the community can be reduced or even eliminated. When exposed to disturbances, resilient communities adjust their operation so that post-disturbance impacts are minimal [16]. Community resilience is gaining more importance due to the climate-change induced rise in frequency and severity of natural disasters as well as increasing number of cyber threats to remote automation systems [17]–[24]. The critical infrastructure of

cities and communities, including water and energy networks, are equipped with multitude of software and hardware components, which are vulnerable to cyber intrusions and other security threats. Regardless of the source and cause of the disturbance, these events have the potential to affect a large number of people within a community or region. Unfortunately, socially vulnerable groups are disproportionately affected by such impacts. For example, people with compromised health conditions or lower income may not be able to evacuate to safety as easily as those members of the community who are healthy and more affluent [25], [26]. Furthermore, people of lower socioeconomic status are likely to live in homes that are more vulnerable to natural disasters, which could in turn result in more dire consequences [27]. Currently, many sophisticated technologies are being researched and/or implemented in order to enhance the reliability of water and energy systems. These may include smart sensors, advanced control systems, and faster communication systems to allow for fast response to disturbances [28]–[30]. In addition, in order to improve a community's responsiveness to or preparedness against large-scale disturbances, one must develop contingency plans and organize resources to reduce post-disturbance impacts on people's health and livelihood. Making community resilient helps protect people against overwhelming and stressful experiences that they would have otherwise felt from not having access to their basic needs for survival. It also helps to use innovations to push the entire community forward towards improved environmental, social, and economic wellbeing [31]–[34].

One of the most critical infrastructures for maintaining resiliency of a community is the electrical power system. This is because electrical power is essential for running almost all the services that the community needs to survive. For example, electricity is needed in water treatment and wastewater management facilities, machines used for food processing and storage, and heating and cooling of buildings, the telecommunication systems, transportation systems, to name a few.

The electric power grid has evolved from historical one-way power networks where a single generation unit served a small number of predictable loads to modern-day power systems which is the largest running machine ever built by humans, spanning thousands of miles, and connecting millions of components. The modern power system is not only expanding in size but is also becoming more complex due to increasing penetration of variable energy resources, energy storage systems, electric vehicles, and variable power electronics-controlled loads [35]. As more aspects of our daily lives depend on electricity, access to reliable power is becoming the cornerstone of the modern society. Recently, this was further underlined by the winter storm Uri in the state of Texas in February 2021 [36], [37]. During the event, the Electric Reliability Council of Texas (ERCOT) had to order transmission service providers (TSPs) and distribution service providers (DSPs) to perform rolling power outages across their territories to prevent a statewide blackout. There are many examples that show the vulnerability of the power grid to natural disasters and manmade disturbances [1], [38].

Although various reinforcement strategies can in theory be adopted to protect the grid against such events, most are either not efficient or cost prohibitive. This is in part due to the severities of the events, but also due to the lack of accurate mathematical models that can predict their timing and/or geographical scope with reasonable accuracy. As such, adaptive resilience solutions are needed to allow for more flexible operation during and in the aftermath of a natural disaster. One such solution is the concept of electric microgrid. This is a small-scale power system that is equipped with DER and controllable loads and has the capability to island from the grid and support its load locally upon need. Many researchers have looked into breaking the original power system into microgrids [39]–[42]. Grid-connected microgrids can island from the grid upon detecting a disturbance on the utility side and continue supplying the loads locally. This can help

with the resilience of the grid when exposed to large-scale events such as natural disasters and can be envisioned to be deployed more frequently at residential neighborhoods. The concept of electrical microgrids has been analyzed at length in the literature, and its role in providing reliable power supply to remote communities or during times of large-scale disturbances has been discussed [43], [44]. Literature show that many microgrids rely on renewable energy generation such as rooftop PV and/or small-scale wind turbines and these resources pose operational challenges in microgrids due to their intermittent and stochastic nature. For a small power network with variable generators, volatility of one would have a higher overall impact on the entire network compared to integrated power system. Further, there is likely less reserves available to counteract their variability. However, studies show that these issues can be mitigated by using energy storage systems, e.g., community energy storage (CES), in conjunction with variable resources [45], [46].

A similar concept has been extended to water distribution networks, where the original water distribution and supply network is broken into smaller-scale sections known as micro-nets [47]–[50]. These micro-nets can be small-scale water systems that are built on top of the existing water supply network infrastructure (i.e. not a fully decentralized facility). It is important to note that during normal operation, micro-nets are typically connected, forming a more reliable large-scale water network. As the concept of microgrids and micro-nets are critical to maintain the resiliency of energy and water systems, many researchers have discussed how future communities should be designed and planned so that individual neighborhoods can be better prepared for the potential disturbances in the system [51]–[55]. Operating such a system requires simultaneous management of both energy and water resources. However, additional challenges are introduced due to the interconnection between the two networks, especially the dependence of the water network on the

power system. As such, a co-optimization strategy is needed to model both systems within a single framework.

2.2 Water and Energy Nexus

Water and energy systems are intertwined in our daily lives. On the one hand, water systems need energy for production, treatment, and distribution. According to U.S. Department of Energy (DOE) and U.S. Environment Protection Agency (EPA), energy use in drinking water and wastewater treatment accounts for a significant amount of annual budget for local governments across the U.S. Approximately 3-4% of the nation's electricity use is in water distribution and water treatment [56]–[58]. On the other hand, in order to generate electricity, water is heavily used in generation stations specially for cooling purposes, and significant water losses may occur as a result of evaporation in the power generation phase. Statistics show that US energy system accounts for approximately 40% of total water withdrawals in the country [59], [60]. Because of the interdependence between water and energy, loss reduction in one resource can be beneficial to both resources. Conversely, shortage of one resource could result in shortage of the other resource [61], [62].

Considering the nexus of water and energy provides an opportunity to improve the overall system performance of both sub-systems. Energy utilities could utilize the energy flexibility of water systems to serve power system loads without having to build new power plants. Similarly, water utilities could take advantage of dynamic electricity pricing and supply water demand at lower energy prices. While traditionally power and water networks had been studied in isolation, in recent years, the coordinated operation of the two, in the form of an energy-water nexus, has gained much attention [63], [64]. The notion of the energy-water nexus was first introduced to

highlight the interactions between water and energy resources and systems as well as human dependency on water, energy, and food [65], [66]. The recent studies have presented the combined operation of water and energy systems to improve overall system reliability, optimize cost of operation, and offer operational flexibility [67], [68] . Authors in [69] proposed a microgrid system that operated using a wind turbine, solar PV, battery system, and a pump that can also operate as a turbine and generate electricity. Authors in [70] showed how excess energy from renewables can be utilized by water pumps to store water in storage tanks for future use. Coordinating with a WWTP, the water distribution system provides flexibility in operating either the plant or the related water pumps whenever there is sufficient generation available from wind and PV, the pumps and WWTP can be turned off when there is higher electrical demand in the system. With proper plan and coordination, the clean water from the WWTP can be pumped from lower elevation to higher elevation and stored in water distribution tanks at the time of high generation. Once the tanks are filled to a desired height, gravitational force can be utilized to supply water demand to customers with little or no energy consumption. In addition to reducing power curtailment of PV or wind, combined operation of power and water networks allows for alleviating the volatility in the renewable energy resource as shown in [71], [72]. The water distribution system utilizes energy from the power grid to run pumps and the WWTP(s). A benefit in combining the two systems into a single framework is that excess generation (during times of low demand) can be utilized by the water network to avoid curtailing the otherwise useful energy.

2.3 Energy Utilization in Wastewater Treatment

In the United States, conventional wastewater treatment facilities (WWTF) are primarily centralized facilities in which a network of sewer lines conveys municipal and industrial

wastewaters to a single, large facility. In recent years, construction of decentralized facilities to serve smaller communities has become an attractive alternative to the centralized treatment paradigm [73], [74]; mainly due to drivers such as the aging conveyance infrastructure, increasing flows, increasingly stringent nutrient discharge limits, and water reuse. Decentralized WWTF are built to collect, treat, and distribute treated water near the point of generation of wastewater [75]. This reduces the need for building pipelines and tanks to transport larger volumes of water over long distances, which means that smaller pipe diameter, shallow installation depth, and pressurized sewers can help save the installation cost for decentralized system [76], [77]. Another benefit of decentralized WWTF (and other critical infrastructure) is the resilience they offer against large-scale failure events and disturbances such as natural disasters. In centralized systems, damages to critical parts of the system can lead to prolonged outages for all users. For example, earthquakes can lead to physical damages to a central facility or flooding events can damage pumping stations and other critical processes [78]. By using decentralized facilities, not only the scope of damages and the number of residents affected by them would be limited, repairs and replacements can also be faster and less expensive.

There are different ways a decentralized WWTF can be designed and configured [79], [80]. One example configuration is a SBMBR in which a batch biological treatment unit is coupled with a continuous membrane treatment unit [81]. SBMBRs allow for the decoupling of hydraulic and solids retention times, which allows for greater control and flexibility for biological intensification, higher quality effluent, and lower solids production [81], [82]. However, there is typically a higher cost for the operation of small-scale WWTFs, and specifically SBMBRs. In cases where decentralized facilities are space-limited, energy-intensive membrane-based processes are used in lieu of gravity-driven clarifiers [83]–[85]; thus, cost of water treatment at a decentralized facility

can be 20% higher than at a centralized facility in terms of energy consumption in Mega Joules per cubic meter of treated water volume, making energy-optimization imperative.

Current energy-optimization efforts have relied on physics-based models to calculate air blower and pump energy requirements for biological and membrane treatment units [86]–[88]; however, due to complex interactions between various process variables, physics-based models are frequently too inaccurate for real-time process control. There is therefore a need for a real-time, data-driven energy monitoring approach that can adapt with changing environmental conditions and operating strategies [89].

WWTFs monitor system flows, speed of various equipment, and other system parameters. Sensors installed to monitor the biochemical processes in a WWTFs can be used to estimate energy requirements and to control the most critical parameters in the system in real-time. Researchers have used different data-driven modeling techniques, including auto-regressive exogenous (ARX) and auto-regressive integrated moving average (ARIMA) techniques to model nonlinear dynamics such as prediction of total suspended solids, chemical oxygen demand, total phosphorous, and total nitrogen of biological WWTFs [90]–[93]. Auto-regressive models such as ARX, ARIMA, and ARIMA exogenous (ARIMAX) are time-series modeling techniques, which take input data from present and past times and in turn, predict the output in the future. The AR portion of the model represents the regression of a variable on its lagged (or past) values [94]. In essence, these models describe the underlying autocorrelations in the data in order to derive a pattern for forecasting purposes.

One objective of this thesis is to model and optimize the operation of electromechanical components used in an SBMBR system operated since 2009 at the Colorado School of Mines

(Mines), in Golden, Colorado. This work is presented in CHAPTER 3. While our approach is developed based on this system, it is generic enough that can be used for any decentralized SBMBR system. A data-driven approach has been used in the mathematical model formulation to optimize the water treatment process. The model is formulated as minimizing the energy consumption of all pumps and air blowers in the bioreactors (BR) and MT, and minimizing the deviation of DO concentration and TMP from the desired values over the time horizon of the optimization model. By modeling the key parameters such as DO and TMP, the required speed of blowers and pumps can be determined as a part of an energy optimization control strategy—to identify the most efficient operating conditions.

Furthermore, another related objective of this research is to design and operate a decentralized WWTP solely using renewable energy source like wind and PV. This way, the WWTP would be fully self-reliant in terms of its energy needs, and in case of power disruption from the grid, it can continue to treat the wastewater and provide clean water to the users. Since the power generation from PV and wind changes with the available sunlight and wind speed, respectively, a fuel-cell based generation system, or a battery energy storage system (BESS) can be used to counteract the volatility and intermittency of solar energy. This design can in particular benefit isolated communities, who either do not have access to a power grid or lack financial resources to purchase power from the grid or to run a diesel generator.

2.4 Electrical Microgrid and Water Micro-net

A typical power system consists of power generation plants, transmission lines, power substations, and distribution lines that need to be efficiently operated to deliver power to the end users. The operational characteristics of power systems depend on their internal characteristics, as

well as external factors. Some of the internal characteristics could be the types and capacities of generators (inverter based or rotational machines), ratings of power system equipment (conductors and transformers), protection system implemented in the network, and geographical location of generators and loads. The latter is particularly important since it can determine the availability of power during or in the aftermath of a large-scale disturbance.

In the recent years, the electrical power system has seen increased penetration levels of renewables into to the network both at the transmission and distribution levels [95]–[97]. This trend is driven by environmental, economic, and energy security drivers, as well as concerns over the long-term availability of fossil fuels and conventional technologies [24,25]. It is expected that the future of the power system will be in the form of an interconnected network of small-scale and self-contained microgrids supported by the large-scale bulk energy system [100]. The DER units, which are typically dispersed in the system, offer the possibility of running the network in the form of multiple islanded and independent microgrids. The skeleton of the grid will be used to provide connectivity among these localized microgrids. As the microgrids serve critical loads such as the water system, it is important to maintain connectivity between power and water networks for resilient operation of the community during a natural disaster. This is beneficial both during the course of a disaster, and at its aftermath when service needs to be restored to the grid.

The problem of microgrid design and operation has been studied extensively in the literature, especially when equipped with renewable energy resources and BESS [101]–[104]. In such systems, the presence of BESS is crucial to ensure that the excess generation of wind and PV can be stored for future use when the energy resource is not available. Many researchers have developed solutions for computing the battery size for a microgrid, in coordination with

intermittent renewable resources [105]–[111]. Naturally, a key part of this analysis is an estimate for the daily and hourly electric demand to be supplied. In a typical distribution grid, the electric demand must be met at all times, and load shedding must be left as the last resort. However, for a microgrid, the requirements may be less strict. If a microgrid is designed to temporarily operate in an islanded and decoupled mode, it may be acceptable to shed some of the noncritical loads, otherwise, the required sizes of BESS and other energy resources may end up being too large to be cost-effective or practical. Design and operation of micronets can be done in a similar fashion. Many researchers have proposed solutions for optimal operation or planning of the water distribution network. The variability of water demand affects the operation schedule of pumps, which in turn as affect the cost of operation. Solutions have been proposed in the literature for optimal pump scheduling to minimize operation cost [112]–[114] and finding optimal sizes of tanks and pumps [115], [116]. WWTPs may also need to be utilized to meet the growing need of water for some communities [117], [118], especially in arid regions. Studies have been reported on optimizing the operation of WWTP [119], [120].

Most modern microgrids are designed with sustainability in mind, hence mostly using renewable energy sources such as PV and small-scale wind turbines. However, the intermittency of these energy resources can at times affect the reliability of the microgrid [121], [122]. Adding a CES system such as a battery can alleviate the uncertainty of microgrid operation by providing backup power when the primary energy source is unavailable [123]. Although CES can help improve the quality of power, its overall cost is significant compared to the zero fuel cost of renewable generators [124]. Another way to mitigate the variability of renewables is to use DR [125]. With DR, loads can be controlled (shed or shifted to a different time) such that power generation matches the power demand at any given time. Similarly, there are pump scheduling

techniques proposed in the literature to reduce their energy footprint [43]–[45]. Many researchers have focused on operation of microgrids with stochastic energy resources [128]. Authors in [129] developed a two-stage stochastic model to estimate a day-ahead optimal strategy for dispatching distributed units considering variability of renewable energy resources. Similarly, authors in [29],[30] formulated a two-stage stochastic programming problem to incorporate uncertainty in load and PV forecast. Authors in [132] developed a stochastic mixed-integer programming model to identify the optimal size of power system components considering variability in wind and PV system.

However, regardless of the number and sizes of energy resources within a microgrid, the resource is typically limited. This is in particular crucial when access to the main grid is not readily available, either due to disturbances not being cleared or due to physical damages in the aftermath of natural disasters. In this case, use of deferrable loads can provide a balance between generation and demand [133], at least over shorter time horizons.

Similarly, the traditional water system can be divided into micro-nets where the communities could use localized sourcing of water, e.g. localized surface water, groundwater wells, rainwater harvesting, or greywater reuse, instead of pumping water from sometimes hundreds of miles away. The community could have more control of the source of the water and the pipeline network. Plus, any repair and maintenance issues could be resolved faster than in case of large-scale networks. This can be highly beneficial for isolated communities where the major water network is either not available or is not in operation due to natural disasters for instance. In conventional water distribution networks, one or more centralized water reservoirs supply water to demand points via a network of pipes, pumps, pressure reducing valves (PRVs), and tanks. Because of changing

climate and increased number of extreme weather conditions around the world, the water availability and quality is declining every day [50]. In addition, extreme weather conditions such as droughts, hurricanes, and flooding events and other disasters such as wildfires and earthquakes threaten the availability of freshwater quantity and quality. Finally, manmade hazards such as chemical spills and contamination can potentially add another layer of threat (albeit temporary) to traditional water networks [134], [135]. When the water network is divided into (potentially) self-contained micro-nets, they can improve the resilience of the water network during events mentioned above.

In the recent years, there has been extensive research related to the interdependency of energy and water networks and improving the efficiency of both systems [136]–[138]. Some have looked into optimal design of water distribution network in terms of pipes, pumps, and tanks in the network [139]–[141]. Others have tried to model exiting water distribution networks and optimize their operation schedule, especially in the presence of dynamic electricity pricing [112], [142], [143]. In most of these studies, assumptions have been made that sufficient water supply from the traditional water sources is available. However, it is very possible that this condition does not hold true. In CHAPTER 4 and CHAPTER 6 of this thesis, a neighborhood is considered for which the operations of water and energy networks are co-optimized. Here, it is assumed that access to external water resources is not guaranteed. As such, in addition to implementing electrical demand response in the form of demand shifting or load curtailment to reduce overall energy consumption [127], [144], it has been assumed that water demand also needs to be regulated. It is also assumed that the remote community is equipped with a WWTP where wastewater from residential houses is collected and treated, and the resultant clean water is pumped to a community storage tank for future use. Although some amount of wastewater is typically discharged as

untreated effluent, this approach allows the community to minimize the amount of water needed from external sources. Therefore, the model proposed here is a combined microgrid-micro-net that tries to co-optimize the operation of both systems.

2.5 Stochastic and Multi-Objective Optimization

Stochastic optimization or stochastic programming (SP) models are mathematical optimization formulations in which optimization decisions need to be made under uncertainty. The deterministic programs are formulated with parameters that are assumed to be known with certainty, whereas SP models deal with non-deterministic variables, which is more realistic in the real-world problems. Consider a combined power and water distribution network of a remote and isolated community where the residents rely on renewable energy sources like PV, wind and battery storage for daily electrical power needs as well as wastewater treatment for water reuse. Both power and water systems have uncertainty associated with them, which could be related to uncertain water demand, uncertain energy consumption, and natural variations in power generation from renewable resources. In order to reliably meet the energy and water demand of the community it is therefore important to model such uncertainties. In SP the uncertainty of input parameters is specified either by using their probability distributions using a scenario-based approach. In this thesis a scenario-based approach has been implemented.

Multi-objective optimization or multi-objective programming problem is used in multiple criteria decision-making. The multi-objective optimization deals with optimization problems involving two or more objective functions to be optimized simultaneously. The objective functions are generally interdependent. One example of multi-objective optimization in case of power systems is maximizing energy served (minimizing load loss) and minimizing operation cost

generation. Similarly, minimizing the traveling cost of vehicles and maximum cover of distance in shipping industry is another example of multi-objective optimization multiple objectives. There are different techniques to solve multi-objective optimization problem including goal programming, lexicographic method, global criterion method, and inverted utility function method. A goal programming method called Chebyshev Goal Programming (CGP) technique has been used in this thesis to solve the multi-objective formulation.

CHAPTER 3

OPTIMAL ENERGY MANAGEMENT IN DECENTRALIZED MUNICIPAL WASTEWATER TREATMENT PLANTS

In this chapter, an optimal control strategy is proposed for a decentralized wastewater treatment facility utilizing a SBMBR. To optimize the energy demand of the SBMBR, a MINLP model is developed for the aeration and membrane permeation processes. The proposed formulation focuses on the operation times and speeds of air blowers, which affect the concentration of DO, and the ASB speed and permeation rate, which impact the TMP of the membranes. The DO and TMP are some of the most important parameters for wastewater treatment and as such, need to be maintained within permissible ranges at all times. The MINLP model is solved as a moving window and generates optimal set-points for aeration and permeation. Although the model is developed for a particular case study, it is easily generalizable to other similar WWTP.

3.1 Description of the System

A demonstration-scale SBMBR at the Colorado School of Mines, Golden, CO is used to treat domestic wastewater of the student housing complex. The facility treats approximately 30 m^3 per day of wastewater collected from the 250 apartment-units of a student housing cluster near Mines campus. In the SBMBR, air blowers supply DO to the initial biological treatment units for the conversion and removal of carbon, phosphorous, and nitrogen; and this aeration stage accounts for a major portion of the facility's energy demand. After aeration and mixing, the treated water and biological solids mixture is pumped into MTs where a filtration process takes place. Pumps

pull a vacuum to separate the liquid-solid mixture and to keep the liquid-solid mixture from concentrating on the membranes, ASB aerates the outside of the membrane. Air blowers and pumps controlled with variable frequency drives (VFDs) have been used in the facility for aeration, filtration, and permeation processes. Figure 3-1 illustrates the schematic diagram of the SBMBR system implemented at Mines.

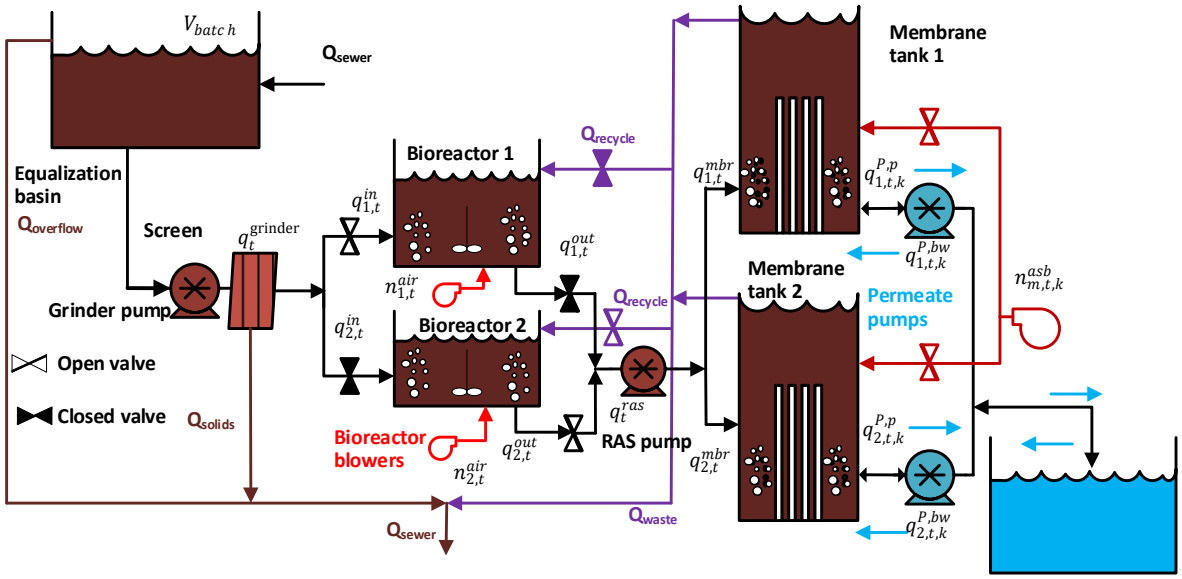

Figure 3-1 Schematic diagram of the SBMBR system at Mines. A batch of wastewater to be processed is collected in equalization basin which is then supplied to BRs via grinder pump at the beginning of each BR cycle. After mixing and aeration process in the BRs for chemical and biological treatment, the mixed aerated fluid is pumped into MTs via a RAS pump. The permeate pumps pull the treated water through the submerged membranes leaving behind the solid component of the fluid in the MTs.

3.2 Bioreactor Operation

As indicated in Figure 3-1, a batch of wastewater from an equalization basin is pumped into one of two BRs by a grinder pump. This phase of filling a BR with a batch of raw wastewater (~324 gallons) is referred to as the mix-fill phase because a mixer in the BR mixes the fluid as it is filling the BR for an even distribution of carbon and nutrients. Once the BR is filled, an air

blower in the BR (G-BH1 Side channel blower, Gardner, Denver, CO) alternates between on and off modes to provide a variety of aeration conditions (i.e., controls DO concentrations), which facilitate the microbial transformation of different contaminants (e.g., organic compounds, ammonia, nitrate). When the blower is off, the mixer is on to prevent settling. This phase is known as the react phase. Together, the mix-fill and react-fill phases take half of the total cycle time, the remaining period is called react-draw. During react-draw phase, the mixed and aerated biologically active solid-liquid mixture (also known as activated sludge) is pumped into the MT through the RAS pump (81 1/2A52-B centrifugal pump, Gorman-Rupp, Mansfield, OH as given in APPENDIX A). As the first BR is going through the react-draw phase, the second BR is filled with raw wastewater and undergoes the mix-fill and react-fill phases as described above. The cycle repeats throughout the day to process multiple batches of sewage. Figure 3-2 illustrates the various phases. The second BR goes through the same cycle with one hour of time shift, i.e. as the first BR starts pumping water into the MT, the second BR starts the mix-fill phase.

3.3 Membrane Tank Operation

When the activated sludge is pumped into the two MTs by the RAS pump, a portion of it is filtered through the two membrane cassettes (Puron®, KMS, Wilmington, MA) by two permeate pumps (H12 Reversible Gear Pump, Liquiflo, Garwood, NJ as given in APPENDIX A) and clean permeate water is transferred into a 100 gal. permeate tank. As the permeate pumps pull water through the membranes by vacuum, pressure across the membrane increases due to biomass accumulation on the surface of the membrane fiber. Every 4 minutes each permeate pump reverses flow to clean the membrane in backwash mode, where permeate is drawn from the permeate tank by the respective permeate pump for 25 seconds. During this reverse flow period, air scouring is

used at the maximum air flow to ensure dispersal of any accumulated solids on the surface of the membrane. The detached solids and remaining activated sludge are then returned to the BRs by gravity via a spillway (RAS trough). Only one MT can be backflushed at a given time to ensure constant production of treated water. The react-draw phase takes approximately 60 minutes and both MTs are involved in processing the activated sludge. Once the one-hour cycle is completed, the activated sludge from the second BR start being pumped into the two MTs.

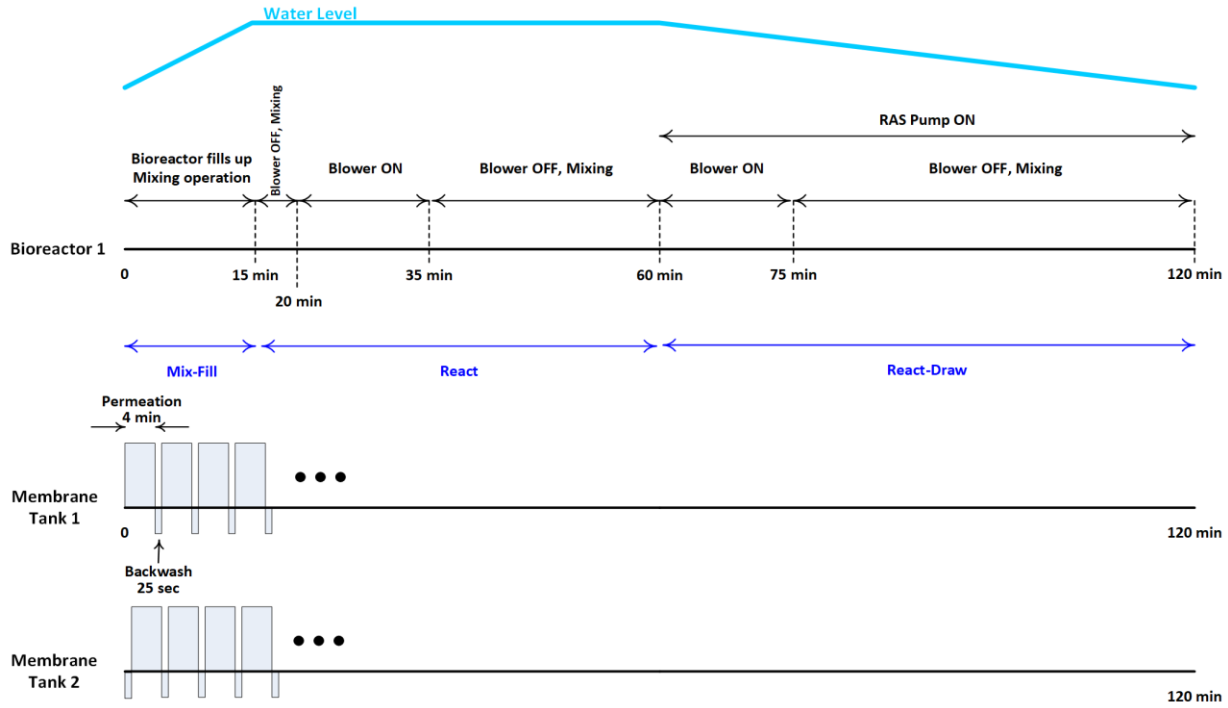

Figure 3-2 Time diagram of the SBMBR operation. This diagram details the existing schedule of electromechanical components used in bioreactor 1 and both MTs. Operation of bioreactor 2 follows the same time diagram, except that it is time shifted by one hour.

3.4 Methodology

The focus of this chapter is to model and optimize the operation of electromechanical components used in SBMBR system. A data-driven approach has been used in the problem formulation to optimize the water treatment process. The problem is formulated as minimizing the

energy consumption of all pumps and blowers in the BR and MT and minimizing the deviation of DO and TMP from the desired values over the time horizon of the problem. By modeling the key parameters such as DO and TMP, the required speed of blowers and pumps can be determined as a part of an energy optimization control strategy—to identify the most efficient operating conditions. A case study is presented for a project.

In this case study, water inflows and outflows in BR and MT are modeled using physics-based relationship of hydraulics. An AR integrated moving average exogenous (ARIMAX) model described in [145] is implemented using the Econometric Modeler App in Matlab [146] to estimate the concentration of DO in BR and TMP in MT. A historical time series dataset of DO, blower speed, TMP, and ASB speed has been used to estimate the weight parameters of the ARIMAX model. This model provides a linear relationship between input and output variables which is then used in the optimization model to compute decision variables. However, the overall mathematical model is nonlinear in nature. The MINLP optimization model is solved using the LINDOGLOBAL solver in General Algebraic Modeling System (GAMS) [147].

3.5 Mathematical Model Formulation

This research focuses on the operation of the BRs and MTs and their corresponding inflows and outflows. The idea of this research to find out an optimal control strategy for all the electromechanical components used in the SBMBR system such that total energy consumption of those component is as minimal as possible while maintaining all system requirements. In order to investigate energy consumption of the system to process one batch of activated sludge, the optimization model is solved over a two-hour window during which one BR undergoes mixing and aeration, while the other one has its activated sludge pumped into the MT. The 2-hour window

consists of multiple time steps corresponding to the operation cycles of the aeration and mixing as listed in Table 3-1. The duration of each time step Δ_t is chosen by the user.

Table 3-1 Time duration of different processes during react-draw

Process	Time
React-draw phase	60 minutes
RAS pump	Continuous operation
MT ASB	Continuous operation
BR air blower	30 minutes
BR mixer	90 minutes; mixer is OFF when blower is ON
Permeation	4 minutes
Backwash	25 seconds

For the MT, the total time horizon is divided into t number of time steps and each time step has 2 sub-steps represented by index k. The sub-steps represent either permeation or backwash modes of operation within a single time step. Since both membranes cannot have backflush at the same time, the following sequence was assumed for the two tanks. It should be noted that both MTs can have permeation at the same time; however, backwash occurs at different times in each MT. In the following Table 3-2, duration for Permeation and Backwash is different, 4 minutes and 25 seconds, respectively.

Table 3-2 Permeation and backwash sequence in the MTs

Tank (*m*)	Sub-step (*k*)	Mode of operation
1	1	Permeation
	2	Backwash
2	1	Backwash
	2	Permeation

3.5.1 Bioreactor Operation

3.5.1.1 Objective Function

The problem is formulated as minimizing the energy consumption of all pumps and blowers in the BRs as well as minimizing the deviation of DO from the desired concentration levels during the aerobic phase, over the time horizon of the problem:

$$\min \sum_{t\in \mathrm{T}} \left((P_t^{\mathrm{grinder}} + P_t^{\mathrm{ras}}) + \sum_{b=1}^{2} (P_{b,t}^{\mathrm{air}} + P_{b,t}^{\mathrm{mixer}}) \right) \cdot \frac{\Delta_t^{\mathrm{br}}}{60} + M \cdot \sum_{b} \sum_{t\in \mathrm{T}_a} | o_{b,t} - O_{\mathrm{des}} | \qquad (3.1)$$

Where, $P_t^{grinder}$, P_t^{ras}, $P_{b,t}^{air}$, and $P_{b,t}^{mixer}$ are power consumption of grinder pump, RAS pump, air blower in BR *b*, and mixer in BR *b* during time t, respectively. The big M represents a sufficiently large number in the optimization model. $o_{b,t}$ and O_{des} represent instantaneous and desired value of DO in the BR b, respectively. The above objective function will be minimized subject to the constraints described in section 3.5.1.2.

3.5.1.2 Constraints

3.5.1.2.1 Bioreactor Inflow and Outflow

Water flows from the grinder pump to the BR and is provided to the MT through the RAS pump. Without loss of generality, it is assumed here that BR 1 is receiving inflow from the grinder and outflow through RAS (constraints (3.2) and (3.3)) while BR 2 is processing a different batch of fluid which is not a part of V_{batch}. Since both BRs have identical operation cycles, but are independent of one another, it is assumed here that BR 2 has no inflow and outflow (constraint (3.4)). The total volume through the grinder pump equal to the batch volume that needs to be processed (constraints (3.5)). The RAS pump pumps out the activated sludge into MTs continuously over time T (V_{ras}) and portion of the V_{ras} is discharged back into BR 1 from spillway and some portion of the V_{ras} gets filtered through membranes and flows out of the MTs as given in constraint (3.6). Note that multiplying the flow rate by the number of seconds in a time step Δ_t^{br} provides the volume of inflow or outflow during that time step. It is assumed that the bioreactor fills up in ~15 minutes, which corresponds to 3-time steps (constraint (3.7)) and RAS pump delivers flow in MT during react-draw phase after 60 minutes, which corresponds to time step 13 and onwards (constraint (3.8)). Constraints ((3.9) and (3.10)) ensure the continuity of the flow until the volume requirement V_{batch} is met, i.e. if the inflow or outflow becomes zero at a time step, it cannot increase to a nonzero value in the subsequent time steps. In other words, these constraints ensure that pumps do not change speed abruptly for every time step. The inflow and outflow will affect the volumes of water in the bioreactors (constraint (3.11)). Finally, minimum and maximum water height levels always need to be maintained (constraint (3.12)).

$$\forall t : q_{1,t}^{\text{in}} = q_t^{\text{grinder}} \tag{3.2}$$

$$\forall t : q_{1,t}^{\text{out}} = q_t^{\text{ras}} \tag{3.3}$$

$$\forall t : q_{2,t}^{\text{out}} = q_{2,t}^{\text{in}} = 0 \tag{3.4}$$

$$\sum_{t \in \text{T}} (q_t^{\text{grinder}} \cdot \Delta_t^{\text{br}} \times 60) = V_{\text{batch}} \tag{3.5}$$

$$\begin{aligned} &\sum_{t \in \text{T}} (q_t^{\text{ras}} \cdot \Delta_t^{\text{br}} \times 60) = V_{ras} \\ &\forall b : V_{ras} = \sum_{t \in \text{T}} (q_{b,t}^{\text{bf}} \cdot \Delta_t^{\text{br}} \times 60) + \sum_{m=1}^{2} V_m^p \\ &\forall m : 0.1 \cdot V_{ras} \le V_m^p \le 0.167 \cdot V_{ras} \\ &V_{ras} \ge V_{batch} \end{aligned} \tag{3.6}$$

$$\forall t > 3 : q_t^{\text{grinder}} = 0 \tag{3.7}$$

$$\forall t < 13 : q_t^{\text{ras}} = 0 \tag{3.8}$$

$$\forall t : q_t^{\text{grinder}} \le q_{t-1}^{\text{grinder}} \tag{3.9}$$

$$\forall t > 13 : q_t^{\text{ras}} \le q_{t-1}^{\text{ras}} \tag{3.10}$$

$$\forall t, \forall b : v_{b,t} = v_{b,t-1} + q^{\text{in}}_{b,t} \cdot \Delta^{\text{br}}_{t} \times 60 + q^{\text{bf}}_{b,t} \cdot \Delta^{\text{br}}_{t} \times 60 - q^{\text{out}}_{b,t} \cdot \Delta^{\text{br}}_{t} \times 60 \quad (3.11)$$

$$\forall t, \forall b : A \cdot h_{\min} \leq v_{b,t} \leq A \cdot h_{\max} \quad (3.12)$$

3.5.1.2.2 Bioreactor Mixers and Blowers

During the operation of the bioreactors, whenever blowers are not used, the mixers will be operational (constraint (3.13)). Blowers do not operate when the corresponding tank is filling up (constraints (3.14) and (3.15)). In addition, blowers are off during the anoxic/anaerobic phases (constraint (3.16)). The DO concentration is estimated here using an ARIMAX (5,0,5) model based on its own past values as well as the current values of the blower speed (constraint (3.17)). The ARIMAX (5,0,5) model has been selected through trial and error by assessing model specific performance metrics including the residual sum of squares (RSS), Akaike Information Criterion (AIC), and Bayesian Information Criterion (BIC) values, as well as the impact on the overall optimization solution. Parameters a, c, and e are the coefficients of the ARIMAX function and ε indicates the error terms. Coefficient $a_{b,i}$'s represent weights for the past values of DO in BR b, coefficient c is a speed multiplier, and $e_{b,j}$'s are weights of the past values of error between the actual and predicted DO. Constraint (3.18) ensures that the speeds of pumps and mixer are less than or equal to their rated values.

$$\forall t, \forall b : \beta^{\text{mixer}}_{b,t} + \beta^{\text{air}}_{b,t} = 1 \quad (3.13)$$

$$\forall t, \forall b : \{q^{\text{in}}_{b,t} > 0 \Rightarrow \beta^{\text{air}}_{b,t} = 0\} \rightarrow q^{\text{in}}_{b,t} \leq (1 - \beta^{\text{air}}_{b,t}) \cdot M \quad (3.14)$$

$$\forall t, \forall b : n_{b,t}^{\text{air}} \leq n_{\text{rated}}^{\text{air}} \cdot \beta_{b,t}^{\text{air}} \tag{3.15}$$

$$\forall t \in T - T_a : \beta_{b,t}^{\text{air}} = 0 \tag{3.16}$$

$$\forall t \in T_a, \forall b : \frac{o_{b,t}}{0.002} = \sum_{i=1}^{p} \frac{a_{b,i}}{0.002} \cdot o_{b,t-i} + \frac{c_b}{3450} \cdot n_{b,t}^{\text{air}} + \sum_{j=1}^{q} e_{b,j} \cdot \varepsilon_{b,t-j} \tag{3.17}$$

$$\begin{aligned} n_t^{\text{grinder}} &\leq n_{rated}^{\text{grinder}} \\ n_{b,t}^{\text{air}} &\leq n_{rated}^{\text{air}} \\ n_{b,t}^{\text{mixer}} &= n_{rated}^{\text{mixer}} \\ n_t^{\text{ras}} &\leq n_{rated}^{\text{ras}} \end{aligned} \tag{3.18}$$

3.5.1.2.3 Power Consumption

For grinder and RAS pumps, power consumption is assumed to be a function of the operational speed (constraints (3.19) and (3.20)). In addition, the operational speed is assumed to be linearly related to the flow rate (constraints (3.21) and (3.22)). Mixers in both bioreactors run at full speed. Hence, their power consumption will be the rated value when they are on and zero when they are off (constraint (3.23)). Conversely, blowers are controlled using VFDs to allow for changing their speed (constraint (3.24)) [148].

$$\forall t : P_t^{\text{grinder}} = \frac{P_{\text{rated}}^{\text{grinder}}}{(n_{\text{rated}}^{\text{grinder}})^3} (n_t^{\text{grinder}})^3 \tag{3.19}$$

$$\forall t : P_t^{\text{ras}} = \frac{P_{\text{rated}}^{\text{ras}}}{(n_{\text{rated}}^{\text{ras}})^3}(n_t^{\text{ras}})^3 \tag{3.20}$$

$$\forall t : q_t^{\text{grinder}} = \frac{q_{\text{rated}}^{\text{grinder}}}{n_{\text{rated}}^{\text{grinder}}} n_t^{\text{grinder}} \tag{3.21}$$

$$\forall t : q_t^{\text{ras}} = \frac{q_{\text{rated}}^{\text{ras}}}{n_{\text{rated}}^{\text{ras}}} n_t^{\text{ras}} \tag{3.22}$$

$$\forall t, \forall b : P_{b,t}^{\text{mixer}} = \frac{P_{\text{rated}}^{\text{mixer}}}{(n_{\text{rated}}^{\text{mixer}})^3}(n_{b,t}^{\text{mixer}})^3 \cdot \beta_{b,t}^{\text{mixer}} \tag{3.23}$$

$$\forall t, \forall b : P_{b,t}^{\text{air}} = \frac{P_{\text{rated}}^{\text{air}}}{(n_{\text{rated}}^{\text{air}})^3}(n_{b,t}^{\text{air}})^3 \cdot \beta_{b,t}^{\text{air}} \tag{3.24}$$

3.5.2 Membrane Tank Operation

3.5.2.1 Objective Function

The optimization model is formulated as minimizing two terms: the energy consumption of the permeate pumps and the ASB over the time horizon of the model, as well as deviation of actual permeation rate from the estimated permeation rate for a given batch. The estimated permeation (flow) rate is calculated by diving the batch volume by the total number of seconds within the one-hour react-draw phase.

$$\min \begin{Bmatrix} \left(\sum_{t \in \mathrm{T}} P_t^{\mathrm{ras}} .\Delta_t^{\mathrm{mbr}} + P_t^{\mathrm{asb,p}} .\Delta_t^{\mathrm{p}} + P_t^{\mathrm{asb,bw}} .\Delta_t^{\mathrm{bw}} + \sum_{m=1}^{2} (P_{m,t}^{\mathrm{P,p}} .\Delta_t^{\mathrm{p}} + P_{m,t}^{\mathrm{P,bw}} .\Delta_t^{\mathrm{bw}}) \right) \cdot \frac{1}{60} \\ +M \cdot \sum_{t \in T} \left| q_{1,t,1}^{P,p} + q_{2,t,2}^{P,p} - \frac{V_{batch}}{3600} \right| \end{Bmatrix} \quad (3.25)$$

Where, P_t^{ras} is power consumption of RAS pump during time t. $P_t^{asb,p}$ and $P_t^{asb,bw}$ represent power consumption of ASB during permeation and backwash mode at time t, respectively. Similarly, $P_{b,t}{}^{P,p}$ and $P_{b,t}{}^{P,bw}$ represent power consumption of permeate pumps during permeation and backwash at time t, respectively. The big M represents a sufficiently large number in the optimization model. The $q^{P,p}{}_{m,t,k}$ represents permeate pump flow rate in membrane tank m, during time t, sub time k and V_{batch} represent batch volume of activated sludge that needs to be processed. The above objective function will be minimized subject to the constraints described in section 3.5.2.2.

3.5.2.2 Constraints

3.5.2.2.1 Membrane Tank Inflow and Outflow

After the react-fill phase is completed in each bioreactor, the processed wastewater is pumped into the two MTs via RAS pump. The volume of wastewater that is pumped through RAS pump over time horizon T is related to its flow rate (constraint (3.26)). Both MTs get filled up by a single RAS pump (constraint (3.27)). While the activated sludge pumped into the bottom of a MT, permeation and backwash cycles take place, and the remaining fluid is discharged back into BRs over a spillway. There is a lower limit at which the activated sludge height must be maintained in order to maintain the TMP across the membranes (constraint (3.28)). Water permeates through the membranes and is stored in a tank for backwash before being discharged. In the current system,

total time for the react-draw phase is 60 minutes, which means that the estimated permeation flow rate from each permeate pump would be according to (3.29) but no more than its rated flow rate (constraint (3.29)). It should be noted that in (3.29) MT 1 (m = 1) is in permeation mode during sub-step 1 (k = 1) while MT 2 (m = 2) permeates water during sub-step 2 (k = 2). This is because although both MTs can permeate at the same time, only one tank can be backflushed at a time due to insufficient air scouring available from a single blower. These are reflected in constraints ((3.30) and (3.31)). As given in the Table 3-1, each membrane tank will have backflush after every permeation sub-time-step and about 5–10% of the permeated water in previous permeation period would be back fed into the membranes for a short period of time (constraint (3.32)).

$$\begin{aligned} &\sum_{t\in T} 60 q_t^{\text{ras}} \cdot \Delta_t^{\text{mbr}} = V_{\text{ras}} \\ &\forall t : q_t^{\text{ras}} \le q_{\text{rated}}^{\text{ras}} \end{aligned} \tag{3.26}$$

$$\forall t : \sum_{m=1}^{2} q_{m,t}^{\text{mbr}} = q_t^{\text{ras}} \tag{3.27}$$

$$\begin{aligned} &\forall m,t : h_{m,t}^{\text{mbr}} = h_{base}^{\text{mbr}} + 60 \frac{\left(q_{m,t}^{\text{mbr}} \cdot \Delta_t^{\text{mbr}} - \sum_{k=1}^{2} q_{m,t,k}^{\text{P,p}} \cdot \Delta_t^{\text{p}} + \sum_{k=1}^{2} q_{m,t,k}^{\text{P,bw}} \cdot \Delta_t^{\text{bw}} \right)}{A^{\text{tank}}} \\ &\forall m,t : h_{\min} \le h_{m,t}^{\text{mbr}} \end{aligned} \tag{3.28}$$

$$\forall t : q_{1,t,1}^{\text{P,p}} \le q_{\text{rated}}^{\text{P}},\ q_{2,t,2}^{\text{P,p}} \le q_{\text{rated}}^{\text{P}} \tag{3.29}$$

$$\forall t : q^{\mathrm{P,p}}_{1,t,2} = 0$$
$$\forall t : q^{\mathrm{P,p}}_{2,t,1} = 0 \tag{3.30}$$

$$\forall t : q^{\mathrm{P,bw}}_{1,t,1} = 0$$
$$\forall t : q^{\mathrm{P,bw}}_{2,t,2} = 0 \tag{3.31}$$

$$\forall t : \frac{0.05 \times q^{\mathrm{P,p}}_{1,t,1} \cdot \Delta^{\mathrm{p}}_{t}}{\Delta^{\mathrm{bw}}_{t}} \leq q^{\mathrm{P,bw}}_{1,t,2} \leq \frac{0.1 \times q^{\mathrm{P,p}}_{1,t,1} \cdot \Delta^{\mathrm{p}}_{t}}{\Delta^{\mathrm{bw}}_{t}}$$
$$\forall t : \frac{0.05 \times q^{\mathrm{P,p}}_{2,t-1,2} \cdot \Delta^{\mathrm{p}}_{t}}{\Delta^{\mathrm{bw}}_{t}} \leq q^{\mathrm{P,bw}}_{2,t,1} \leq \frac{0.1 \times q^{\mathrm{P,p}}_{1,t-1,2} \cdot \Delta^{\mathrm{p}}_{t}}{\Delta^{\mathrm{bw}}_{t}} \tag{3.32}$$

3.5.2.2.2 Membranes

A time step would be the sum of permeate time and backwash time (constraint (3.33)). The wastewater is filtered through membranes ultrafiltration membranes. In the current system vacuum is applied on the permeate side of the ultrafiltration membranes to produce clean water. The vacuum applied is the TMP, which is the pressure between the feed (activated sludge) and permeate (clean water). The TMP increases proportionally to the increase in water production. A contributing factor is the suspended solid concentration of the feed solid-liquid mixture; as the permeate flow increases, there is a larger concentration of solids on the feed-membrane interface. To reduce the concentration effect, the feed flow to the MT is maintained above a certain level. Standard MBR operational guidance suggests that the MT feed flowrate should be 3 to 5 times the permeate flow rate through that MT (constraint (3.34)). The TMP is modeled as an ARIMAX function of past TMP observations and the current values of the permeate pump speed and ASB speed (constraint (3.35)). Similar to the previous section, this model has been chosen based on the

values of the RSS, AIC, and BIC of different models as well as the impact of the models on the overall optimization solution. An ARIMAX (4, 0, 0) model[1] was eventually developed with parameters ϕ, μ, θ, ω and σ. Coefficients ϕ_i's represent weights of the past values of TMP, μ's are the weights for the past errors between the actual and predicted TMP, and coefficients θ, σ and ω are multipliers for permeate pump speed, ASB speed, and MT inflow, respectively. TMP has to be maintained below a maximum limit during the normal operation of the membranes (constraint (3.36)). If TMP is too high, membrane damage can occur. Thus, there is an upper TMP limit that will trigger a system shutdown in the event of high TMP. As explained above, during the backwash period, the air scour is used at the maximum air flow; however, its speed can vary at other times (constraints (3.37) and (3.38)). Similarly, the speed of permeate pumps is limited by their rated speed (constraint (3.39)).

$$\forall m, \forall t : \Delta_t^{\text{mbr}} = \Delta_t^{\text{p}} + \Delta_t^{\text{bw}} = 4 + 25/60 \tag{3.33}$$

$$\begin{aligned} &\forall t : 3 \cdot q_{1,t,1}^{\text{P,p}} \le q_{m,t}^{\text{mbr}} \le 5 \cdot q_{1,t,1}^{\text{P,p}} \\ &\forall t : 3 \cdot q_{2,t,2}^{\text{P,p}} \le q_{m,t}^{\text{mbr}} \le 5 \cdot q_{2,t,2}^{\text{P,p}} \end{aligned} \tag{3.34}$$

$$\begin{aligned} &\forall t : \frac{\text{TMP}_{1,t,1}}{11032} = \sum_{i=1}^{p} \frac{\phi_{1,i}}{11032} \cdot \text{TMP}_{1,t-i,1} + \sum_{j=1}^{q} \mu_{1,j} \cdot \varepsilon_{1,t-j,1} + \frac{\theta_1}{1755} \cdot n_{1,t,1}^{\text{P,p}} + \frac{\sigma_1}{1755} \cdot n_{1,t,1}^{\text{asb}} + \frac{\omega_1}{0.0011} \cdot q_{1,t}^{\text{mbr}} \\ &\forall t : \frac{\text{TMP}_{2,t,2}}{15168} = \sum_{i=1}^{p} \frac{\phi_{2,i}}{15168} \cdot \text{TMP}_{2,t-i,2} + \sum_{j=1}^{q} \mu_{2,j} \cdot \varepsilon_{2,t-j,2} + \frac{\theta_2}{1755} \cdot n_{2,t,2}^{\text{P,p}} + \frac{\sigma_2}{1755} \cdot n_{2,t,2}^{\text{asb}} + \frac{\omega_2}{0.0010} \cdot q_{2,t}^{\text{mbr}} \end{aligned} \tag{3.35}$$

[1] ARIMAX(p, 0, 0) is the same as a ARX(p) model, i.e. there is no differencing or a moving average. However, the term ARIMAX is used here for consistency.

$$\forall t: \begin{cases} \mathrm{TMP}_{1,t,1} \le \mathrm{TMP}^{\max} \\ \mathrm{TMP}_{2,t,2} \le \mathrm{TMP}^{\max} \end{cases} \tag{3.36}$$

$$\forall t: \begin{cases} n_{1,t,2}^{\mathrm{asb}} = n_{\mathrm{rated}}^{\mathrm{asb}} \\ n_{2,t,1}^{\mathrm{asb}} = n_{\mathrm{rated}}^{\mathrm{asb}} \end{cases} \tag{3.37}$$

$$\forall t: \begin{cases} n_{1,t,1}^{\mathrm{asb}} \le n_{\mathrm{rated}}^{\mathrm{asb}} \\ n_{2,t,2}^{\mathrm{asb}} \le n_{\mathrm{rated}}^{\mathrm{asb}} \end{cases} \tag{3.38}$$

$$\forall m, \forall t, \forall k: \begin{cases} n_{m,t,k}^{\mathrm{P,p}} \le n_{\mathrm{rated}}^{\mathrm{p}} \\ n_{m,t,k}^{\mathrm{P,bw}} \le n_{\mathrm{rated}}^{\mathrm{p}} \end{cases} \tag{3.39}$$

3.5.2.2.3 Power Consumption

For ASB and permeate pumps, the operational speed is assumed to be linearly related to the flow rate (constraints (3.40) and (3.41)). The power consumption in pumps and blower is assumed to be a function of their operational speed (constraints (3.42)–(3.45)), e.g., power consumed by permeate pumps at time step *t* would be equal to the sum of power consumption of pumps in tanks 1 and 2 both operating at their permeation speed.

$$\forall m, \forall t, \forall k: q_{m,t,k}^{\mathrm{P,p}} = \frac{q_{\mathrm{rated}}^{\mathrm{p}}}{n_{\mathrm{rated}}^{\mathrm{p}}} n_{m,t,k}^{\mathrm{P,p}} \tag{3.40}$$

$$\forall m, \forall t, \forall k : q_{m,t,k}^{\mathrm{P,bw}} = \frac{q_{\mathrm{rated}}^{\mathrm{p}}}{n_{\mathrm{rated}}^{\mathrm{p}}} n_{m,t,k}^{\mathrm{P,bw}} \tag{3.41}$$

$$\forall t : P_t^{\mathrm{P,p}} = \frac{P_{\mathrm{rated}}^{\mathrm{p}}}{(n_{\mathrm{rated}}^{\mathrm{p}})^3} (n_{1,t,1}^{\mathrm{P,p}})^3 + \frac{P_{\mathrm{rated}}^{\mathrm{p}}}{(n_{\mathrm{rated}}^{\mathrm{p}})^3} (n_{2,t,2}^{\mathrm{P,p}})^3 \tag{3.42}$$

$$\forall t : P_t^{\mathrm{P,bw}} = \frac{P_{\mathrm{rated}}^{\mathrm{p}}}{(n_{\mathrm{rated}}^{\mathrm{p}})^3} (n_{1,t,2}^{\mathrm{P,bw}})^3 + \frac{P_{\mathrm{rated}}^{\mathrm{p}}}{(n_{\mathrm{rated}}^{\mathrm{p}})^3} (n_{2,t,1}^{\mathrm{P,bw}})^3 \tag{3.43}$$

$$\forall t : P_t^{\mathrm{asb,p}} = \frac{P_{\mathrm{rated}}^{\mathrm{asb}}}{(n_{\mathrm{rated}}^{\mathrm{asb}})^3} (n_{1,t,1}^{\mathrm{asb}})^3 + \frac{P_{\mathrm{rated}}^{\mathrm{asb}}}{(n_{\mathrm{rated}}^{\mathrm{asb}})^3} (n_{2,t,2}^{\mathrm{asb}})^3 \tag{3.44}$$

$$\forall t : P_t^{\mathrm{asb,bw}} = \frac{P_{\mathrm{rated}}^{\mathrm{asb}}}{(n_{\mathrm{rated}}^{\mathrm{asb}})^3} (n_{1,t,2}^{\mathrm{asb}})^3 + \frac{P_{\mathrm{rated}}^{\mathrm{asb}}}{(n_{\mathrm{rated}}^{\mathrm{asb}})^3} (n_{2,t,1}^{\mathrm{asb}})^3 \tag{3.45}$$

$$\forall t : q_t^{\mathrm{ras}} = \frac{q_{\mathrm{rated}}^{\mathrm{ras}}}{n_{\mathrm{rated}}^{\mathrm{ras}}} n_t^{\mathrm{ras}} \tag{3.46}$$

$$\forall t : P_t^{\mathrm{ras}} = \frac{P_{\mathrm{rated}}^{\mathrm{ras}}}{(n_{\mathrm{rated}}^{\mathrm{ras}})^3} (n_t^{\mathrm{ras}})^3 \tag{3.47}$$

3.6 Case Study

In this section, the proposed formulation in section 3 has been implemented and solved for the SBMBR at the Colorado School of Mines (Mines), Golden, CO. The results of the ARIMAX modeling is presented first, followed by the outcome of the optimal energy dispatch solution.

3.6.1 ARIMAX Modeling

ARIMAX models have been developed for estimating both DO and TMP. The parameters for the first model are presented in Table 3-3. Although the model is considered as one with an exogenous input (speed of air blower in BR), the corresponding coefficient is very small (even considering the fact that the speed is in rpm units), which means that the DO level at any point in time can be estimated using the past values. Figure 3-3 illustrates the results of the DO estimation against the actual values.

Table 3-3 ARIMAX model parameters for estimating DO

Index *i*	**AR terms (a_i)**	**MA terms (e_i)**	**Exogenous (c)**
1	1.3066	–0.6313	
2	–1.2918	0.8891	
3	1	–0.6048	0.227
4	–0.557	0.4172	
5	0.2065	–0.2513	

*Parameters are the same for both BRs. Here, index *b* is dropped for simplicity.

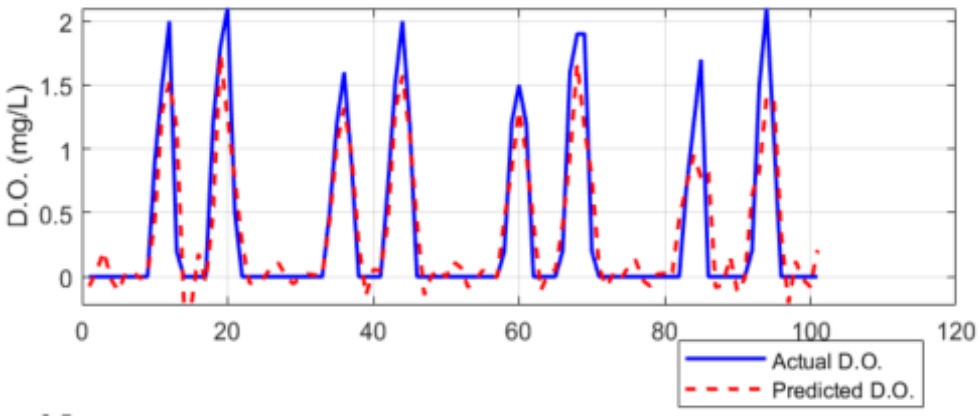

Figure 3-3 ARIMAX model fit of DO in BR1 (blue graph is the actual DO)

The same approach has been used for estimating the TMP. The relevant coefficients and the resulting waveforms are shown in Table 3-4 and Figure 3-4, respectively.

Table 3-4 ARIMAX model parameters for estimating TMP

MT 1		**MT 2**	
Parameter	Value	Parameter	Value
$\emptyset_1$	0.2642	π_1	0.267
$\emptyset_2$	–0.1393	π_2	–0.1285
$\emptyset_3$	0.0368	π_3	0.0259
$\emptyset_4$	–0.0533	π_4	–0.0361
$\boldsymbol{\theta_1}$	0.0016	θ_2	0.0018
$\boldsymbol{\sigma_1}$	0.3911	σ_2	1.2331
$\boldsymbol{\omega_1}$	0.0058	ω_2	–0.0388
$\boldsymbol{\mu_{1,j}}$	$\forall j$: 0	$\mu_{2,j}$	$\forall j$: 0

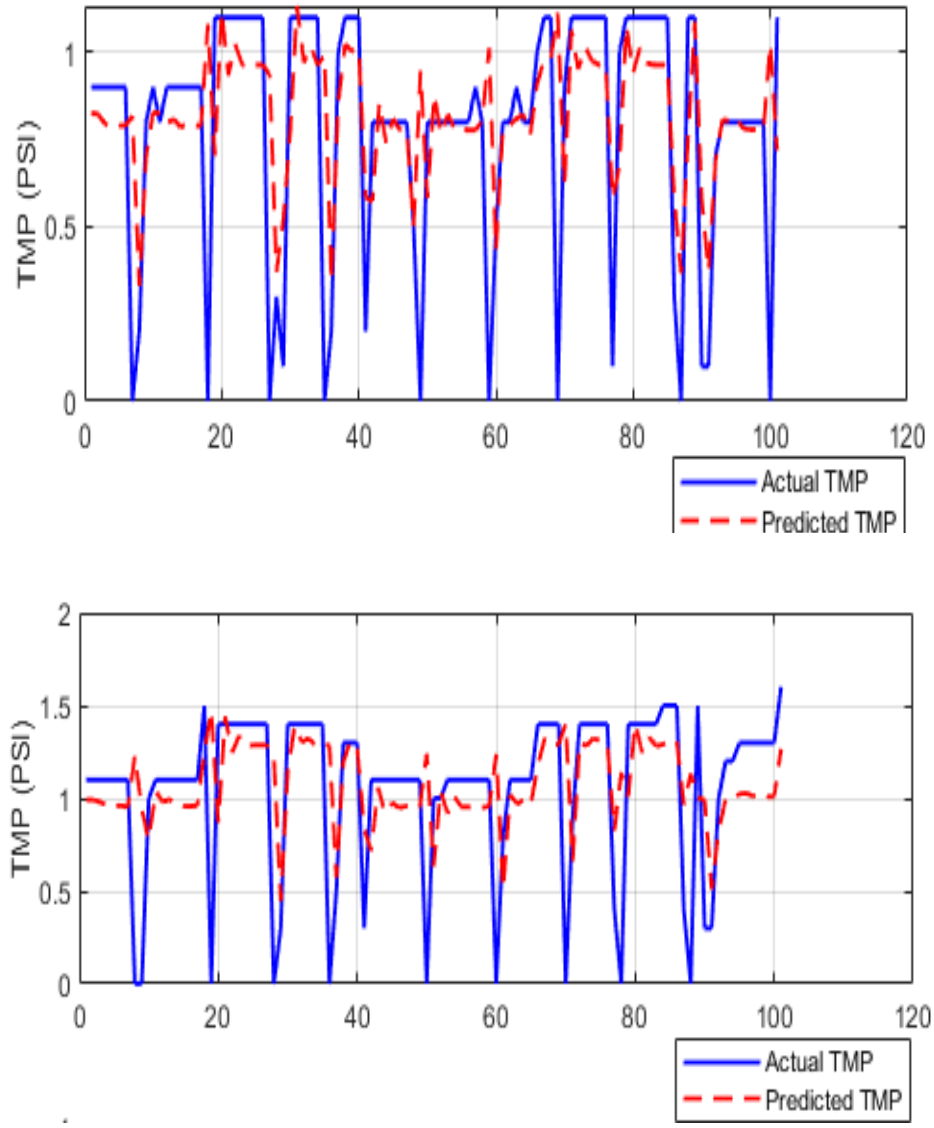

Figure 3-4 ARIMAX model fit of TMP in MT: (top) Tank 1, (bottom) Tank 2

3.6.2 Input data

The input data used in the optimization has been listed in Table 3-5.

Table 3-5 BR and MT parameters

Parameter	Value	Parameter	Value
$\boldsymbol{A^{br}}$	6.32 m^2 (68 sq. ft.)	A^{tank}	2.38 m^2 (1.7 m ×1.4 m)
$\boldsymbol{\Delta_t^{br}}$	5 minutes	Δ_t^p	4 minutes
$\boldsymbol{h_{max}^{br}}$	1.722 m (5.65 ft.)	Δ_t^{bw}	25 seconds
$\boldsymbol{h_{min}^{br}}$	1.524 m (5.0 ft.)	Δ_t^{mbr}	4 min. 25 seconds
$\boldsymbol{n_{rated}^{air}}$	3,450 rpm	h_{min}^{mbr}	3.08 m (10 ft.)
$\boldsymbol{n_{rated}^{grinder}}$	3,270 rpm	M	10000
$\boldsymbol{n_{rated}^{mixer}}$	1,160 rpm	n_{rated}^{asb}	1,755 rpm
$\boldsymbol{n_{rated}^{ras}}$	1,755 rpm	n_{rated}^{p}	1,755 rpm
$\boldsymbol{O_{des}}$	0.002 kg/m^3 (2.0 mg/l)	P_{rated}^{asb}	1.3 kW
$\boldsymbol{P_{rated}^{air}}$	2.55 kW	P_{rated}^{p}	0.7457 kW
$\boldsymbol{P_{rated}^{mixer}}$	0.7457 kW	q_{rated}^{p}	0.0044 (69.74 GPM)
$\boldsymbol{P_{rated}^{grinder}}$	2 kW	q_{rated}^{ras}	0.0044 m^3/s (69.74 GPM)
$\boldsymbol{P_{rated}^{ras}}$	1.1 kW	TMP^{max}	48263.3 Pa (7 psi)
$\boldsymbol{q_{rated}^{grinder}}$	0.0027 m^3/s (42.8 GPM)	V_{batch}	1.226 m^3 (324 gallons)

3.6.3 Results and Discussion

3.6.3.1 Bioreactor Results

The optimization problem in section 3.2 is solved using the LINDOGLOBAL solver in GAMS. Using a computer with Intel Xeon(R) E3-1240 3.50 GHz CPU and 16GB RAM. The optimization model was run multiple times and the solution converged all time in less than a second. The results are depicted in Figure 3-5 and Figure 3-6. The time sequence in the solution matches the existing time diagram of the SBMBR system provided in Figure 3-2. Bioreactor 1 filled with 1.226 m^3 (324 gallons) of activated sludge in the first 15 minutes (from time step 1–3) by the grinder pump at a speed of approximate 1740 rpm (50.43% of rated speed), while the mixer mixes the fluid at its full capacity (at rated speed) during the first 20 minutes (time steps 1–4) as shown in Figure 3-5.

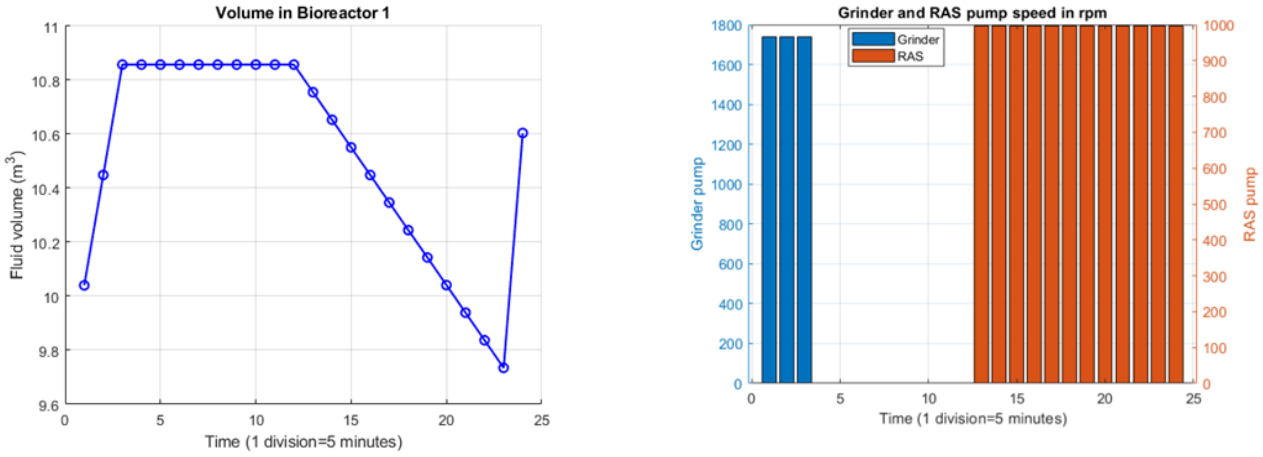

(a) (b)

Figure 3-5. (a) Flow into and out of a BR and (b) speed of grinder and RAS pumps. BR 1 is being filled during time steps 1–3, as indicated by the increasing fluid volume. During this time, the grinder pump operates at a speed of 1,740 rpm as shown in (b). RAS pump continuously operates during time steps 13–24 to pump out the fluid into the MT, as indicated by the change in water volume in (a).

The increased volume at time step 24 indicates that there is an incoming flow into the BR from the grinder pump. The increase in RAS pump speed from 0 to 996 rpm (56.78% of maximum rated speed) in Figure 5-7 (b) indicates that the RAS pump is running during time steps 13-24, as expected. After the non-aerated fill-mix and mixing phase, the aeration system starts delivering oxygen into the BR from time steps 5 to 7. Depending on the last DO observation, the proposed ARIMAX model suggests a required blower speed to meet the 2.0 mg/L DO concentration. For example, when DO concentration from time steps 1–4 is zero, it is suggested to run the blower at full capacity (3450 rpm, 100% rated speed) in order to achieve the target. Once the oxygen concentration is greater than zero it is possible to meet oxygen demand even at reduced speeds as indicated by the reduced blower speed of 2,434 rpm (70.50% of rated) during time step 7. Since there is an inverse relationship between the current DO concentration and its own past values as indicated by the negative coefficients $a_{1,2}$ and $a_{1,4}$ in Table 3-3, it is possible that DO might not stay at 2.0 for the entire time even if blower runs at rated capacity. The 100% blower speed during time step 6 demonstrates this. The aerated water is then mixed completely during time steps 8–12 before it is pumped out into MT from time step 13–24. During this time, another aerobic phase takes place from time steps 13–15 in order to maintain the DO concentration in the BR while the water is being pumped out. This aerobic phase is the same as the one during time steps 5–7. This process is illustrated in Figure 3-6.

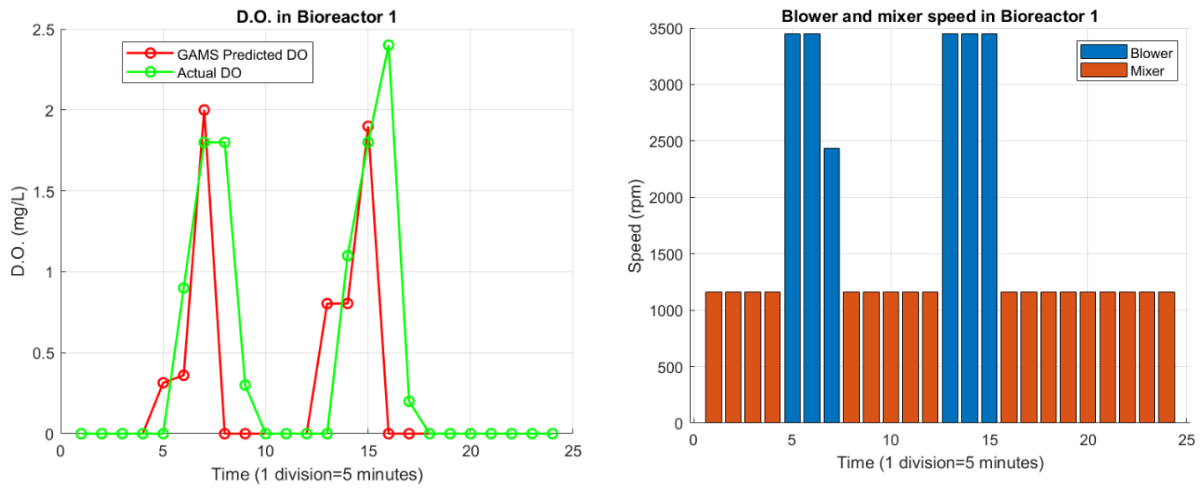

(a) (b)

Figure 3-6. (a) DO level in BR 1 and (b) mixer and blower operation in BR1. The mixer mixes the fluid as it is filling from time steps 1–3 and continues until time step 4 as indicated by the 1, 160 rpm mixer speed in (b). Air blower runs from time steps 5–7 (and during time steps 13–15) at different speeds trying to maintain the DO. As expected, alternate cycle of mixer and blower is given in (b).

3.6.3.2 MT Results

The optimization problem in this section is solved using the same computer specifics as mentioned in section 3.6.3.1, the problem converges in less than a second on average. The solution to the optimization model provides a control strategy for the permeate pumps and the ASB used in the MTs. The results are shown in (*a*) shows the flow rate into the MT. The variations in flow rates are due to variations in the optimal permeation and backwash phases, which are necessary for the MT operation. For example, in Figure 3-8, tank 1 starts permeating from time step 1 sub-step 1, while tank 2 remains idle during that time period. During the same time step 1 but sub-step 2, tank 1 goes through backwash whereas tank 2 is permeating the fluid. This pattern continues during other time steps. It should be noted that the TMP in both tanks is less than the maximum permissible level of 7 PSI at all time as shown in (*b*). Figure 3-8 (*a*) and (*b*) show permeation and

backwash from time steps 1–13 and sub-steps 1 and 2. As expected, tanks 1 and 2 do not go through the backwash mode at the same time.

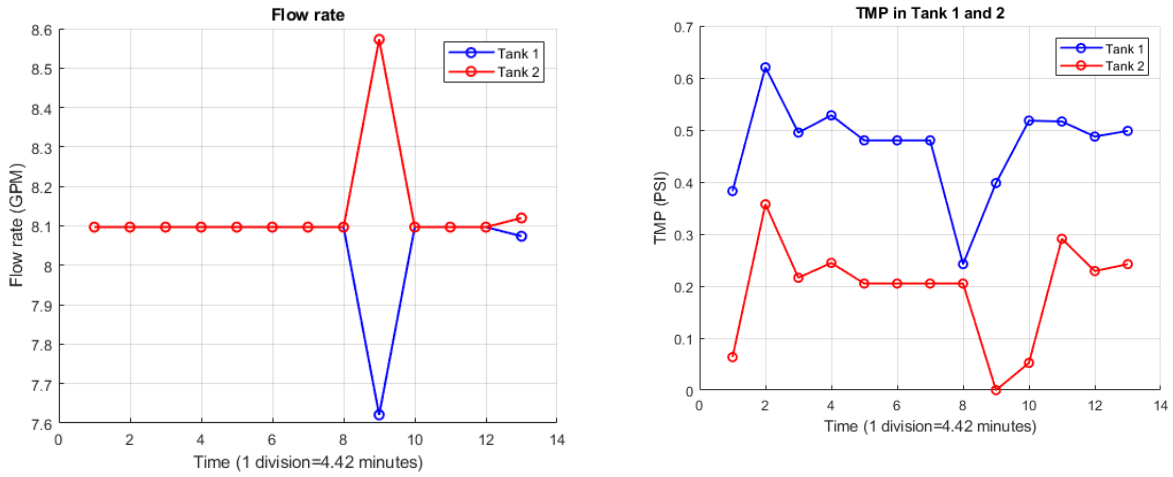

(a) (b)

Figure 3-7. (a) MT inflow and (b) TMP in the tanks. Variations in MT inflow rate in (a) is due to the variation in optimal permeation and backwash required in the corresponding MT. TMP is under maximum allowable TMP of 7 PSI all the time as shown in (b).

Table 3-6 provides a comparison of energy consumption for the base case (as the system has been normally run) and for the dispatch strategy provided by the optimization model. The results show that the total energy consumption level is lower when the system is operated based on the proposed optimal strategy than the base case. This is also true for all individual components, except for the ASB. However, this is compensated for when the total energy footprint is considered. The RAS pump and the permeation pumps have relatively smaller energy footprint because they operate continuously at very low speed (approximately 56.78% and 12% of rated, respectively) and pressure. The BR blower operated at 100% of rated speed for some time steps and the optimization model reduces the blower speed when the DO level in BR reaches to 2.0 mg/L limit, which helps reduce energy footprint of the blower. This is because power consumption of blower

is proportional to cubic power of its speed, which helps lower power consumption when the speed is reduced.

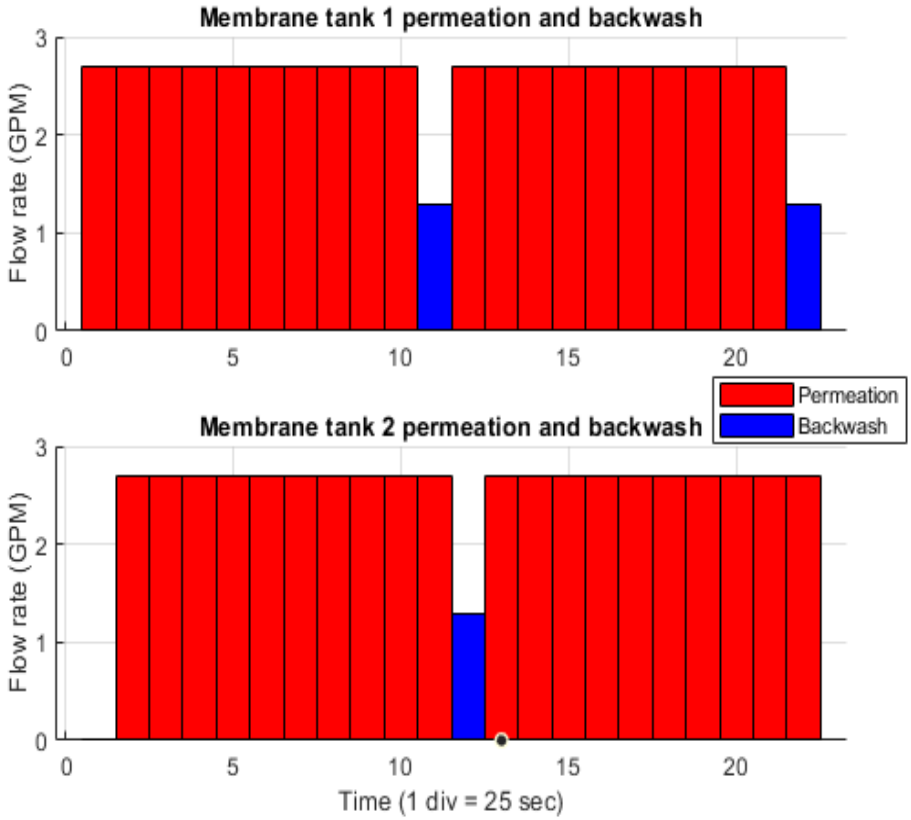

Figure 3-8. Permeation and backwash in both tanks plotted in one graph. Both MTs are allowed to have permeation at the same time; however, backwash occurs at different times in each MT. This is because during the backwash mode, a higher pressure is needed to detach the solids from the fiber and the ASB can only provide enough pressure to one MT at a time. However, air flow from the ASB is enough for both MTs during permeation mode. Time in x-axis represents 4 minutes (red bars) for permeation and 25 seconds (blue bars) for backwash. However, these are not shown to scale. The complete schedule for a 1-hour time frame of react-draw is plotted in Figure 3-9.

Both MTs are allowed to have permeation at the same time; however, backwash occurs at different times in each MT. This is because during backwash mode higher pressure is needed to detach the solids from the fiber and the ASB can only provide sufficient pressure to one MT at a time. However, air flow from the ASB is sufficient for both MTs during permeation mode. Time

in x-axis represents 4 minutes (red bars) for permeation and 25 seconds (blue bars) for backwash for 2-time steps but it is not in exact scale. All time step over 1-hour period of react-draw is plotted in Figure 3-9.

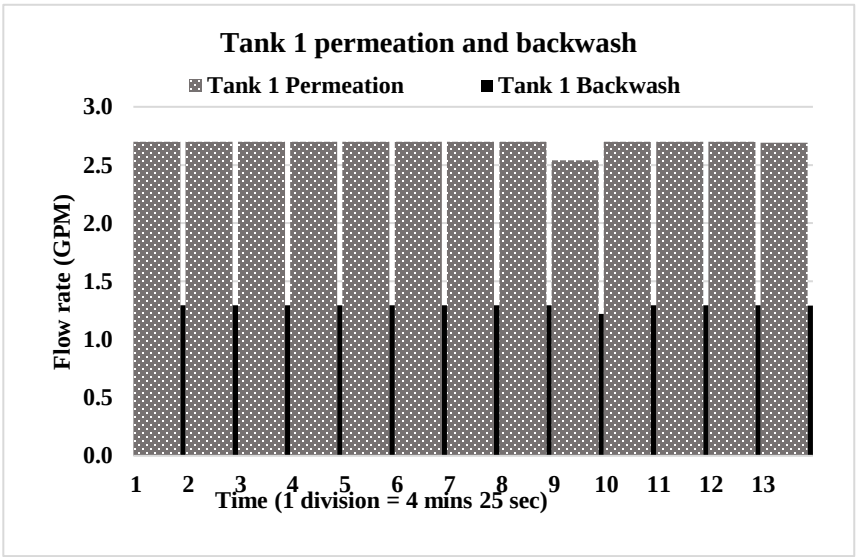

(a)

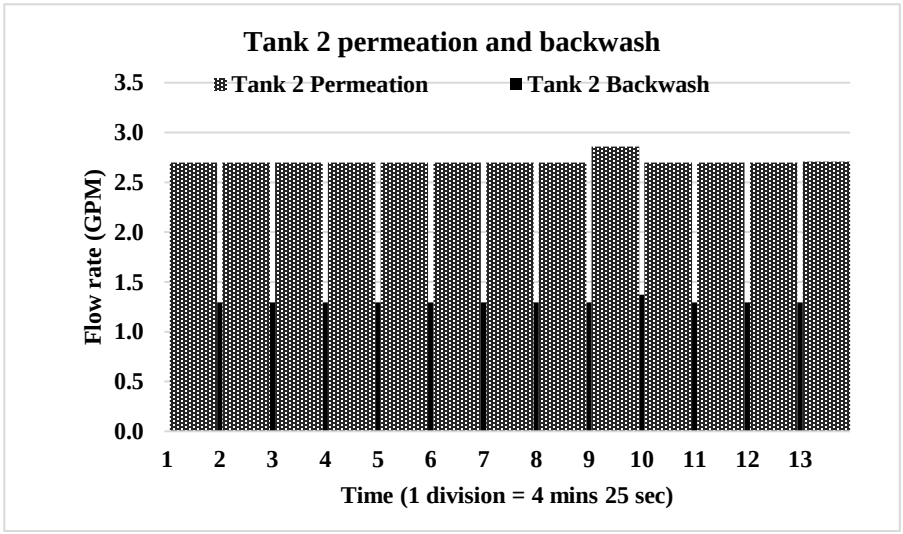

(b)

Figure 3-9. Complete permeation and backwash cycles in MT 1 (a) and MT 2 (b). Alternate permeation and backwash modes of operation in both MTs are shown for the entire react-draw phase. Total volume of clean water pumped out of the permeation pumps and stored in a storage tank is approximately 280 gallons which is about 86.4% of the raw wastewater supplied to the system.

Similarly, low speed operation of RAS pump and permeation pumps to achieve the required flow rates (RAS pump flowrate and permeation flow rate) helps lower energy footprint of these components in the system. RAS pump operates for 1 hour to fill the MT and maintain TMP as well as to provide flow for required permeation rate. Because the volume processed by RAS pump depends on both flow rate and operation time, for a given batch of activated sludge, a react-draw period of shorter than 1 hour would have increased RAS pump speed, which would in turn result in higher power consumption for the pump. The same concept applies to permeate pumps. It is important to note that even though backfill from MT to BR uses gravity and requires no energy consumption, in order to supply additional backfill activated sludge the RAS pump would need to work more just to circulate the activated sludge between BR and MT. This is discouraged by the optimization model, and RAS pump speed is maintained at a constant low speed as expected. The BR blowers and the mixers have the highest energy footprints in the system. Figure 3-10 (a) and (b) highlight the difference in energy consumption between the base case and the optimal dispatch strategy, and the percentage energy footprint of each component in the system, respectively.

Table 3-6 Energy consumption of the electromechanical components

Component	Energy consumption to process one batch (kWh)	
	Actual	Optimization
Grinder pump	0.10	0.064
Blower	0.94	1.14
Mixer**	1.12	1.12
RAS pump	1.38	0.32
ASB	1.49	0.23
Permeate pumps	0.53	0.37
Total	5.56	3.24

**Actual kWh for mixer was not available. Since mixer runs at rated speed whenever it operates (no VFD control), the actual kWh is assumed to be same as the optimized kWh.

From the values presented in Table 3-6, it can be inferred that the control strategy presented by the optimization model reduces the total energy footprint of the system by 2.32 kWh per batch of wastewater, which is approximately 42% less than the base case energy consumption. This is equivalent to savings of 7.16 kWh per 1000 gallons or 7.16 MWh per million gallons.

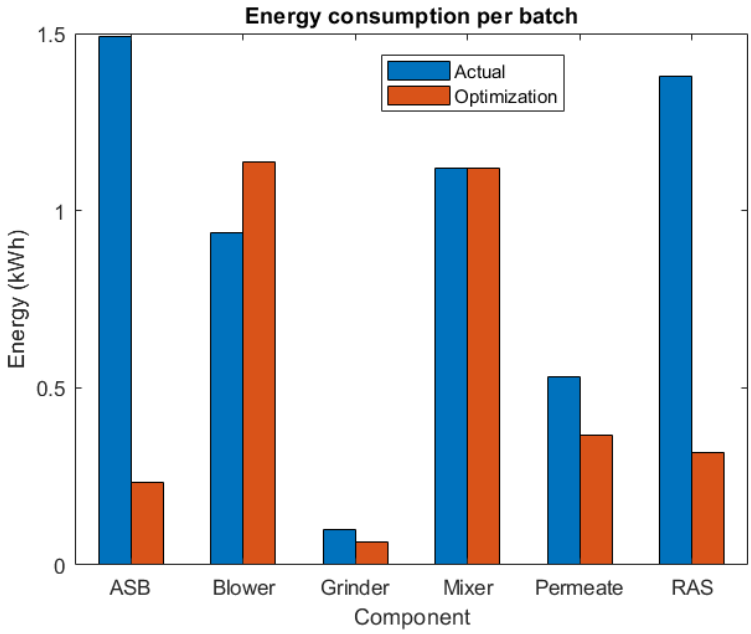

(a)

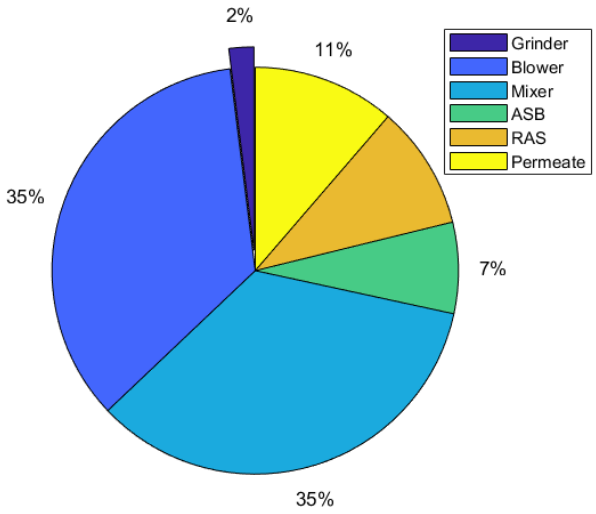

(b)

Figure 3-10 Energy consumption comparison from actual system data and optimization results. (a) Shows difference in actual kWh data vs optimization results for electromechanical components used in the system. (b) Shows percentage contribution of energy consumption

3.7 Conclusion

This paper presents an optimal control strategy for aeration and permeation in an SBMBR system. The energy optimization model has been formulated as a mixed-integer nonlinear programming problem and is solved using the GAMS software for a decentralized wastewater treatment facility. For a given batch of fluid and user defined time steps, this solution provides the set of optimal operation schedules and speeds for the blowers, mixers, and other pumps, in a way that the energy consumption in the system is minimal while desired levels of DO concentration and TMP are maintained. In order to model the dynamics of the SBMBR system, a data-driven modeling approach is used to estimate some of the largest energy-consuming parameters of the system such as the DO in the BRs and the TMP in the MTs. It has been shown that by implementing the proposed methodology and by using historical time series data from available sensors in WWTP, the near future (i.e., next time interval) values of critical biochemical parameters can be estimated, and the electromechanical components can be controlled in order to improve overall system performance and minimize the energy footprint. Comparing the energy footprint obtained from the optimal operation strategy with that of the base case (i.e., how the system is currently running to maintain operational constraints) demonstrates that by applying the former, the SBMBR system can operate at approximately 58% of the actual energy consumption. The reduction in energy consumption is obtained by controlling the speeds of various pumps in the system, including BR blowers, grinder pump, RAS pump, air-scour blower, and permeation pumps.

The case study presented here uses a user defined time step size of 5 minutes in the BRs and 4 minutes and 25 seconds in the MTs in order to minimize the solution time by limiting the number

of decision variables in the problem. However, this is not necessary and more granular time steps can be adopted, at the expense of longer solution times.

CHAPTER 4

ENERGY AND WATER CO-OPTIMIZATION FOR THE RESILIENT NEIGHBORHOOD OF FUTURE

Electrical microgrids are small scale energy systems that can operate in both grid connected as well as standalone mode. The capability to island from the grid during disturbances and continue supplying the loads locally helps improve the reliability and resilience of the network. The concept can be extended to water micro-nets that, if necessary, can disconnect from the main water distribution network and utilize locally available water resources. This concept can be implemented for the communities where the traditional centralized municipal water distribution network is either not available due to geographical or cost limitations, or is temporarily out of service as a result of natural or manmade disasters such as earthquake, water contamination, flooding, etc. This chapter proposes a framework and a solution for co-optimization of energy and water networks for a neighborhood of residential units, with the goal of maximizing sustainability, i.e. utilizing local energy and water resources as much as possible. It is assumed that DER along with demand response are employed to meet energy demands, while a WWTP built in the community is used to treat and recycle wastewater. The objective of this chapter is to demonstrate mathematically how a self-contained community can schedule available energy and water resources optimally so that both energy and water demands are met with minimal external support. The problem is modeled as a multi-objective mixed-integer nonlinear programming model. A case study is presented as proof of concept.

4.1 Problem Formulation

4.1.1 Assumptions

This problem considers a self-contained neighborhood with limited energy and water resources that tries to address its energy and water needs in a sustainable manner and with the least help from the outside world. This could be for instance due to being geographically far from the main grid and/or water network, or due to unusual circumstances such as natural disasters that may have rendered the main grid and/or water network temporarily unavailable. The neighborhood is assumed to consist of multiple houses connected to a single distribution bus.

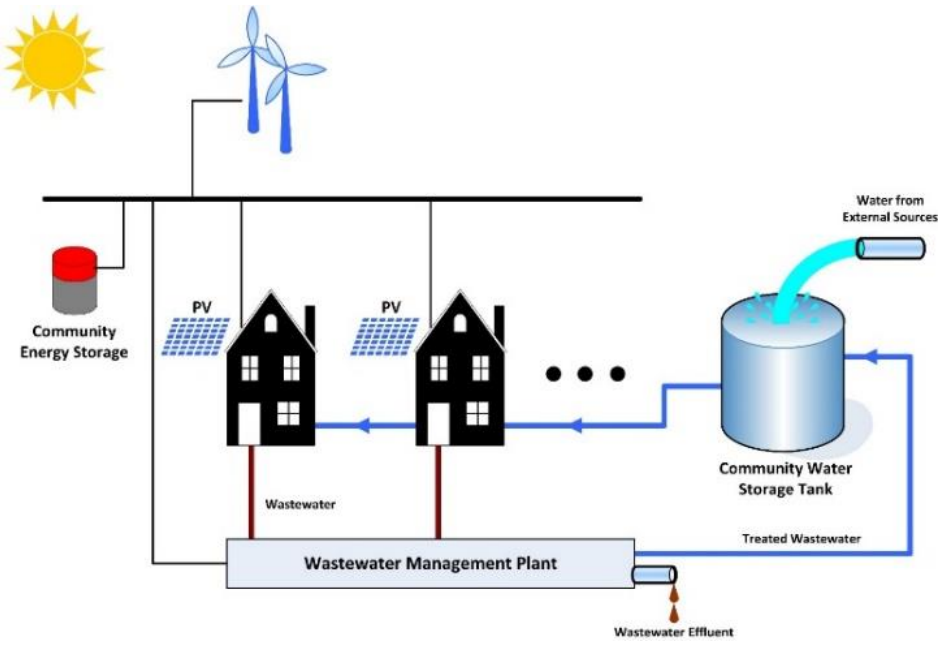

Figure 4-1 Schematic diagram of the system under study

The goal of this chapter is to propose a model that optimizes the collective operation of a combined microgrid and micro-net. It is assumed here that:

- The microgrid is equipped with a community energy storage system (CES) (a battery in this case), a small-scale wind turbine, and rooftop PVs for individual residential units,
- The system is equipped with an internal water distribution network that supplies water to houses from a local water storage tank,
- Intake to the water storage tank (ST) is through two means: water purchased and delivered by water tankers (or perhaps coming from the main water distribution network), or treated potable water provided by the local WWTP,
- The system is geographically small, which means power flow and losses in the microgrid as well as water flow losses in the water distribution network can be safely ignored,
- Community ST is located at a higher elevation than the individual houses, which means that water can flow to individual customers due to gravity. However, the treated wastewater needs to be pumped to the reservoir.

4.1.2 Objective Functions

4.1.2.1 Minimizing the Amount of Load Shed and Shift

The first objective is to ensure that, as much as possible, individual demands are met at the desired levels and at their desired times. Houses with higher number of residents will get precedence. Equation (4.1) denotes the number of shiftable loads that are supplied at the intended time, which needs to be maximized.

$$O_1 = \max_{v_{i,\tau,t}} \sum_{i \in N} \sum_{\substack{t \in T \\ \tau = t}} o_i \cdot v_{i,\tau,t} \tag{4.1}$$

4.1.2.2 Minimizing External Water Purchases

It is assumed that the goal of this community is to be self-contained and self-sufficient as much as possible. As such, the amount of water provided to the community from external sources should be minimized.

$$O_2 = \min_{q_t^{s,\text{in}}} \sum_{t \in \mathrm{T}} \Delta \cdot q_t^{s,\text{in}} \tag{4.2}$$

4.1.2.3 Minimizing the Usage of Battery System

Batteries have a limited lifetime, which is typically modeled in terms of the number of deep discharge cycles. To prolong the life of the battery, it is desired to discharge it as little as possible. This has been modeled as a cost function as shown in (4.3).

$$O_3 = \min_{P_t^{B,d}} \sum_{t \in \mathrm{T}} c^{\mathrm{B}} \frac{P_t^{\mathrm{B},d}}{P^{\mathrm{B,max}}} \tag{4.3}$$

4.1.3 Constraints

The problem is solved subject to the following constraints:

4.1.3.1 Power Balance:

Total power provided by the generation resources equals the total demand. It should be noted that since the system spans a small geographical area, power losses have not been considered. However, this is not necessary and actual power flow equations can be incorporated into the problem formulation.

$$\forall t \in \mathrm{T} : P_t^{\mathrm{W}} + P_t^{\mathrm{B},d} - P_t^{\mathrm{B},c} = \sum_{i \in \mathrm{N}} (P_{i,t}^{d} - P_{i,t}^{\mathrm{PV}}) + P_t^{ww} \tag{4.4}$$

$$\forall i \in \mathrm{N}, \forall t \in \mathrm{T} : P_{i,t}^{d} = P_{i,t}^{d,\mathrm{NSH}} + \sum_{\tau=1}^{t} v_{i,\tau,t} P_{i,\tau}^{d,\mathrm{SH}} \tag{4.5}$$

4.1.3.2 Demand Shiftable Loads

Demand shifting is a form of demand response. Since it may potentially introduce inconvenience for the customers, its application should be regulated. The constraints listed here limit the number of demand shifting instances. Equation (4.6) ensures that a shiftable load can only be shifted to one future time step, and not multiple time steps. Note that because of using an inequality, the load may be shed instead of being shifted to a future time step. This indicates a different category of demand response. In addition, ((4.7) limits the number of times during the dispatch period that a customer may experience demand shifting. It should be noted that for a shiftable load at time t, $v_{i,t,t} = 1$ indicates that the load will not be shifted to a future time step. In addition, it is assumed here that demand shifting is not performed partially and if scheduled, the entire load will be shifted to a future time step.

$$\forall i \in \mathrm{N}, \forall \tau \in \mathrm{T} : \sum_{t=\tau}^{\mathrm{T}} v_{i,\tau,t} \leq 1 \tag{4.6}$$

$$\forall i \in \mathrm{N} : \sum_{t=1}^{\mathrm{T}} v_{i,t,t} \geq \mathrm{T} - \mathrm{TSH} \tag{4.7}$$

4.1.3.3 Battery Constraints:

The battery can be either charging or discharging at any point in time, but not both (see (4.8)). Also, battery state-of-charge (SOC) constraints are represented by (4.9) and (4.10):

$$\forall t \in \mathrm{T} : u_t^{\mathrm{B},c} + u_t^{\mathrm{B},d} \leq 1 \tag{4.8}$$

$$\forall t \in \mathrm{T}: \mathrm{SOC}_t = (1-\gamma) \cdot \mathrm{SOC}_{t-1} + \frac{P_t^{\mathrm{B},c} \eta^c}{P_i^{\mathrm{B,max}}} - \frac{P_t^{\mathrm{B},d}}{\eta^d P^{\mathrm{B,max}}} \tag{4.9}$$

$$\forall t \in \mathrm{T} : \mathrm{SOC}^{\min} \leq \mathrm{SOC}_t \leq \mathrm{SOC}^{\max} \tag{4.10}$$

4.1.3.4 Power Generation Constraints:

Power provided by the wind turbine and the PV panels depend on the average wind speed and the solar irradiance, respectively (see (4.11)-(4.12)). For simplicity, and without loss of generality, it is assumed here that all houses receive the same level of irradiance. The amount of power charged or discharged by the battery is bound by its maximum power (see (4.13)-((4.14)).

$$\forall t \in \mathrm{T} : P_t^{\mathrm{W}} = \frac{0.5 \cdot \alpha \cdot \rho_a \cdot A \cdot w_t^3}{1000} \tag{4.11}$$

$$\forall i \in \mathrm{N}, \forall t \in \mathrm{T} : P_{i,t}^{\mathrm{PV}} = P_i^{\mathrm{PV,STC}} \frac{\Phi_{i,t}}{\Phi^{\mathrm{STC}}} \tag{4.12}$$

$$\forall t \in \mathrm{T} : 0 \leq P_t^{\mathrm{B},d} \leq P^{\mathrm{B,max}} u_{i,t}^{\mathrm{B},d} \tag{4.13}$$

$$\forall t \in \mathrm{T} : 0 \leq P_t^{\mathrm{B},c} \leq P^{\mathrm{B,max}} u_t^{\mathrm{B},c} \tag{4.14}$$

4.1.3.5 Water Demand Constraints:

Total flow provided from the community storage tank should equal the demand (see (4.15)). The volume of water in the storage tank is determined based on the amount of inflow to and outflow from it (see ((4.16)). This value should be within the acceptable range as shown in (4.17). For each customer, the amount of water provided during one dispatch period should be enough to ensure basic needs (see (4.18)).

$$\forall t \in \mathrm{T} : \sum_{i \in \mathrm{N}} q_{i,t}^{d} = q_{t}^{s,\mathrm{out}} \tag{4.15}$$

$$\forall t \in \mathrm{T} : V_{t}^{s} = V_{t-1}^{s} + q_{t}^{\mathrm{s,in}} \cdot \Delta + q_{t}^{\mathrm{ww,out}} \cdot \Delta - q_{t}^{\mathrm{s,out}} \cdot \Delta \tag{4.16}$$

$$\forall t \in \mathrm{T} : V^{s,\min} \leq V_{t}^{s} \leq V^{s,\max} \tag{4.17}$$

$$\forall i \in \mathrm{N} : \sum_{t \in \mathrm{T}} q_{i,t}^{d} \geq q^{\min} \cdot \frac{\sum_{t \in \mathrm{T}} o_{i,t}}{T} \tag{4.18}$$

4.1.3.6 Wastewater Management Constraints:

Water discharged from the customers collects at the WWTP. Without loss of generality, this is assumed to be the inflow for the next time step (see (4.19)). The volume of wastewater in the WWTP is determined based on the amount of inflow to and outflow from it (see (4.20)). This value should be within the acceptable range as shown in (4.21). The amount of power consumed for treating the wastewater and pumping it to the reservoir is assumed to be proportional to the volume

of wastewater treated, as shown in ((4.22). Finally, constraint (4.23) limits the flow rate through pipes.

$$\forall t \in \mathrm{T} : \sum_{i \in \mathrm{N}} q_{i,t}^{d} = k^{ww} q_{t+1}^{ww,\mathrm{in}} \tag{4.19}$$

$$\forall t \in \mathrm{T} : V_t^{ww} = V_{t-1}^{ww} + q_t^{ww,\mathrm{in}} \cdot \Delta - q_t^{ww,\mathrm{out}} \cdot \Delta - q_t^{ww,\mathrm{eff}} \cdot \Delta \tag{4.20}$$

$$\forall t \in \mathrm{T} : V^{ww,\min} \le V_t^{ww} \le V^{ww,\max} \tag{4.21}$$

$$\forall t \in \mathrm{T} : P_t^{ww} = \Delta \cdot (p^{ww} + p^{\mathrm{pump}}) \cdot q_t^{ww,\mathrm{out}} \tag{4.22}$$

$$\forall i \in \mathrm{N}, \mathrm{t} \in T : q_{i,t}^{d} \le q^{\max} \tag{4.23}$$

4.2 Solution Methodology

CGP has been used in this chapter to solve the multi-objective optimization problem because the CGP tries to achieve a good balance between all goals as opposed to other GP approaches that either prioritize some goals over others (Lexicographic GP) or choose a set of weight variables that make the model subjective (Weighted GP) [149]. To achieve Pareto optimality, the methodology discussed in [149]–[151] has been adopted, where a small percentage (ε_q = 0.05 for all goals) of each original objective function to the CGP function.

$$\min Z = \lambda + \sum_{q=1}^{3} \varepsilon_q \frac{O_q}{b_q} \tag{4.24}$$

Subject to:

$$\forall q : \frac{p_q}{b_q} \leq \lambda \tag{4.25}$$

$$\begin{aligned} O_1 + p_1 &\geq b_1 \\ O_2 - p_2 &\leq b_2 \\ O_3 - p_3 &\leq b_3 \end{aligned} \tag{4.26}$$

$$\forall q : p_q \geq 0 \tag{4.27}$$

In these equations p_1 is positive deviation (or under-satisfaction deficiency variable), whereas p_2 and p_3 are negative deviation (or over-satisfaction deficiency variables) from targets defined for goals q = 1, 2, 3. Variable λ is a new auxiliary decision variable that combines all the goals together. The objective in this combined model is to simultaneously optimize all objective functions so that their respective deviations from their target values are minimized.

4.3 Case Study

4.3.1 System Data

In this study, a residential neighborhood consisting of 10 households is considered. For demonstration purposes, the model is solved for a 24-hour period and a time step of one hour for

the city of Sacramento, CA. The energy consumption level has been considered based on the average power consumption over 10 days in the month of July (July 18–27) available from US DOE TMY3 dataset [152]. This data set represents average hourly profile of 8760 hours in a year based off of long-term historical (at least 10 years) data. A household energy consumption is assumed to consist of a portion that can be shifted to another time and another portion which is not shiftable. The maximum allowable number of times during the 24-hour dispatch period that a customer may experience demand shifting (TSH) is assumed to be 2. General lighting loads, cooking and microwave, and the refrigerator are considered non-shiftable because changing their operation time could adversely impact convenience of people in the household. An additional 1 kW of power is added to the non-shiftable loads to cover any critical electrical appliances in the house that is missing from the above list, such as heating, cooling, or the water heater. However, loads such as the dishwasher, washer and dryer, and all TVs are assumed shiftable. These assumptions are made for demonstration purposes and do not affect the generality of the solution. Occupancy level at the residence can affect the power consumption of both shiftable and non-shiftable loads as indicated in Residential Energy Consumption Survey (RECS) data [153]. Hence, different occupancy profiles (one occupant through five occupants) have been assumed for the 10 houses in the community so that there is a diversity in power consumption of the houses. Appendix B presents total daily electrical demands of the entire community with shiftable and non-shiftable loads. The occupancy profiles assumed in the community for this loading are given in Figure 4-5.

The power of the water pump needed to lift water from the WWTP to the ST is computed using the calculation given in Appendix B. From this calculation, the energy consumption for the pump (p^{pump}) is approximately 0.21 kWh/m^3. Similarly, power consumption to treat 1 m^3 of wastewater at the WWTP (p^{ww}) is assumed to be 0.81 kWh/m^3 [85], [154], [155]. According to the

US EPA [156] and USGS data [157], about 80-85% of water inflow to residential households is released to the sewer system. This range is used to estimate the water inflow to the WWTP, so the value for k^{ww} is considered to be 1.17 here. The size of ST and WWTP is assumed to be 50 m^3 (13,208 gallons) for the community. It is assumed that the ST is filled up with water at the beginning of the time horizon so that there is a water source for water demand of the community.

The average solar irradiance and wind speed data are taken from the National Solar Radiation Data Base available at [158], [159] for the city of Sacramento during the time period July 18–27. Other data used are: Φ^{STC}=1000 W/m^2, α=0.593, SOC^{min}=30%, SOC^{max} =100%, for battery, γ=0.0025, c^B=\$28.5, η^c and η^d =0.8, and hourly occupancy profile readers are referred to see the paper [151]. $P_i^{PV,STC}$ values of 5–10 kW have been assigned to reflect the residential PV sizes of the customers [160]. A single wind turbine of diameter approximately 13.8 meters (600 m^2 swept area) is considered for this study. The air density ρ_a is assumed to be 1.25 kg/m^3. The CES size is assumed to be 100kW so that it can accommodate the entire consumption of the community including the WWTP and pump in case of no power from PV or wind. It is assumed here that the water distribution system is already in place and maximum flow rate in the pipe network is 0.0007 m^3/s per house (or approximately 11 gallons per minute (GPM) based on the assumption of maximum of 2.2 GPM for 5 faucets in the house located in bathrooms, kitchen, shower, and laundry area as per the US EPA's standard [161]) at 41 m head (approximately 60 pound per square inch (PSI)).

4.3.2 Simulation Results

The multi-objective function (4.24) is solved subject to constraints (4.4)-(4.23) and ((4.25)-((4.27) using the GAMS/ LINDOGLOBAL solver on an Intel Core i5 2.70 GHz CPU and 12.0

GB RAM computer. The optimization model was run multiple times and the solution converged all time in less than a second. Individual objective functions are first solved subject to their relevant constraints. This provides the true optima for each single objective. The goal (target) values for the objective functions are then set as a percentage of the true optima (by assuming a 10% tradeoff with respect to the single objective optima). These targets are then incorporated into ((4.25) and (4.26) for the multi-objective problem. Table 4-1 summarizes these values. The results indicate that in order to achieve all three objectives at the same time the community would have to shed or shift some loads (see Figure 4-6), purchase no external water for that day, and pay $4.35 for battery discharging cost. By comparing the MO values with their SO counterparts, the multi-objective problem can attain (or improve) the targets set for O_1 and O_2, but not O_3. This behavior is normal, since the multi-objective problem tries to find the Pareto optimal solution, which has no guarantee to achieve all single objective optima.

Table 4-1 Objective function values

Objective Function	**SO Values**	**Goal (Target) Values**	**MO Values**
O_1	383.95	345.55	366.97
O_2 (m^3)	0	0	0
O_3 ($)	2.64	2.9	4.35

SO: single objective optimization, MO: multi-objective optimization

Figure 4-2 illustrates the total generation and demand over the 24-hour dispatch period. It has been observed that the WWTP plant operates during times 4 through 16 since the formulation is utilizing the available PV and wind power during that time. The batteries are charged during

this time period as well so that they can be discharged when PV or wind system are not capable of meeting all demands by themselves, for example during time period 19 to 20.

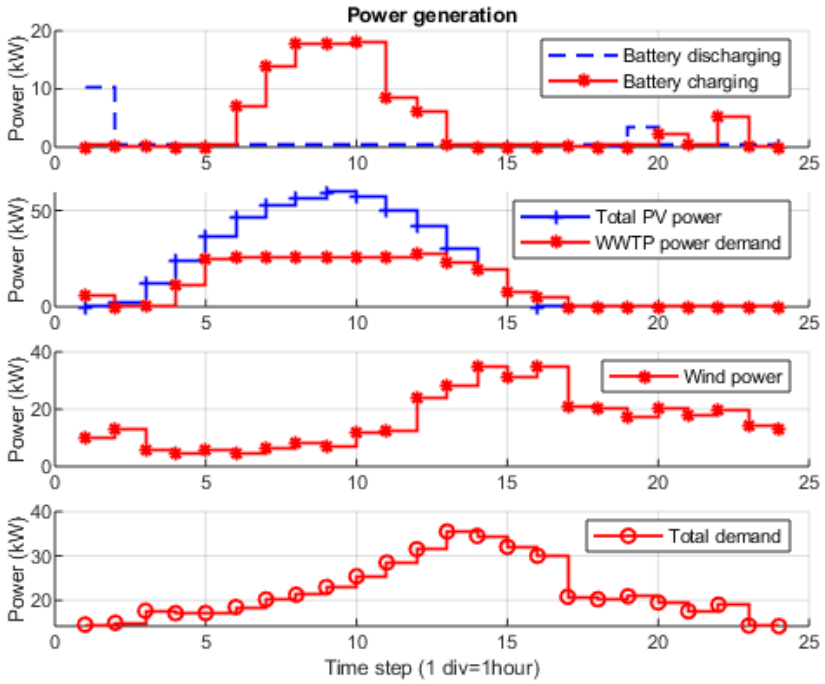

Figure 4-2 Total power generation and demand over the course of the 24-hour dispatch period

Figure 4-3 shows inflow and outflow rates in the ST and WWTP tanks. As expected, some fraction of the outflow from the ST during time t becomes the inflow to the WWTP for time t+1. This wastewater is then treated at the WWTP and pumped back to the ST for future use by the residents.

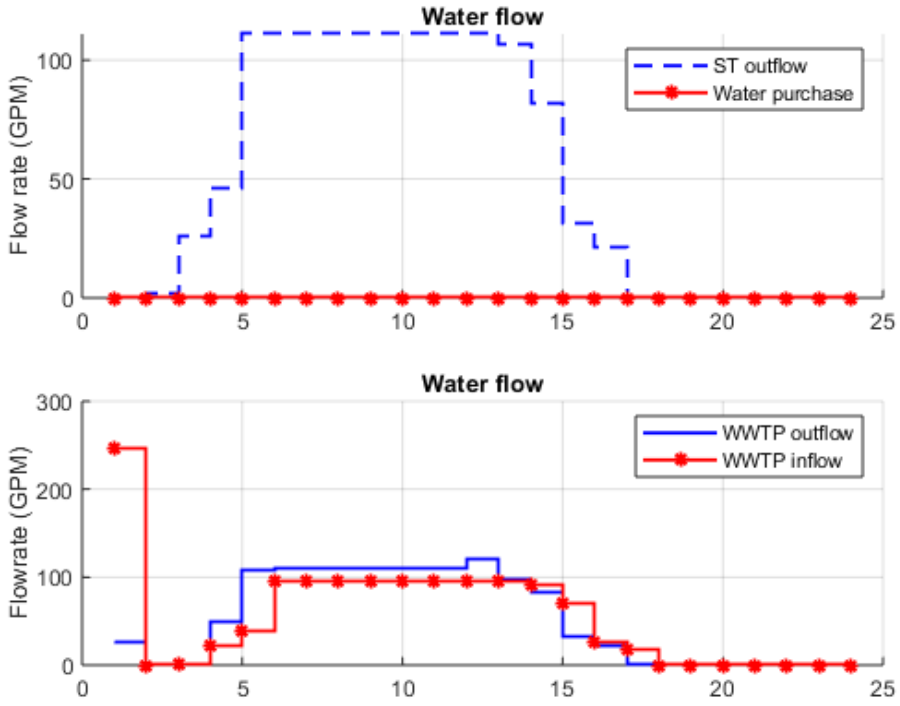

Figure 4-3 Water inflow and outflow rates over the course of the 24-hour dispatch period.

Depending on the power available from the wind turbine and the PV units, and the charging level of the battery at each point in time, load shifting and/or curtailment may become necessary in order to maintain the stability of the system (see Figure 4-4). No loads are shifted during times 1, 3–16, and 19–24. There are 3 shiftable loads shifted from time 2 to time 13 in the community. There is no bar at time 17, which implies that either all shiftable loads in the community at that time are shed or shifted to other times. This can be identified by observing each customer demand pattern. For example, in Figure 4-4 (a) the load at time 17 is shed for that particular customer while in Figure 4-4 (b), the load at time 17 is shifted to time 20 for another customer. It should be noted that the non-shiftable loads will be supplied as intended, as they are not considered as a part of demand response.

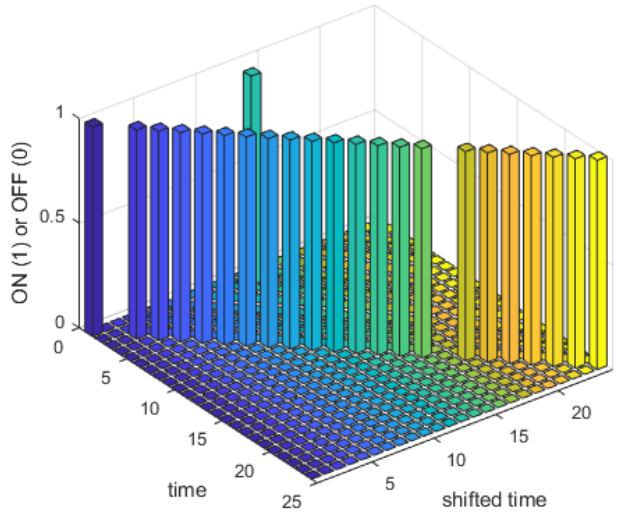

(a)

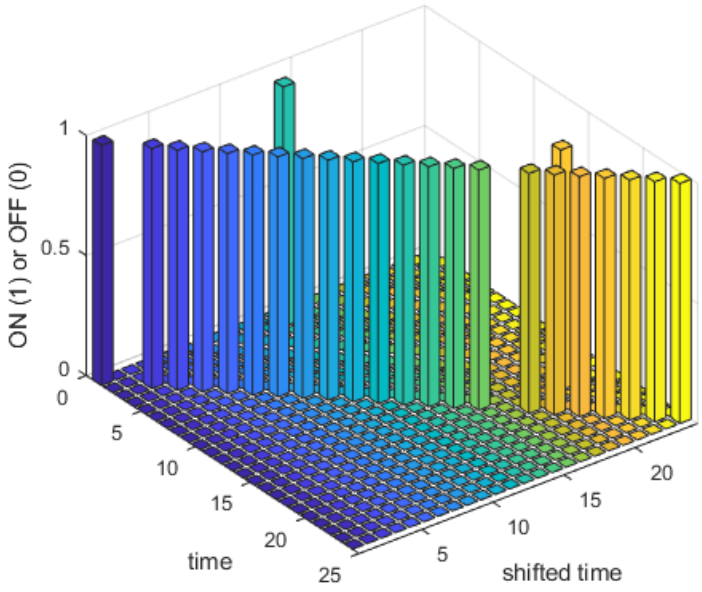

(b)

Figure 4-4 Load shifting and curtailment. Diagonal bars represent loads being met as intended for every time step (i.e. at the desired point in time), whereas off-diagonal bars represent loads being shifted to a future point in time. (a) Example of a house with low occupancy (b) example of a house with high occupancy.

The following Figure 4-5 and Figure 4-6 show load profile of the shiftable loads in the highest and lowest occupancy houses and total load profile after the formulation in the entire community respectively. For highest occupancy houses, load from time 2 is shifted to time 13 and from time 17 to 21 while for the lowest occupancy house load is shed during times 17 and 18. This is because the formulation prioritizes the higher occupancy in DR response. Figure 4-6 shows overall shifting and shedding load profile of the community.

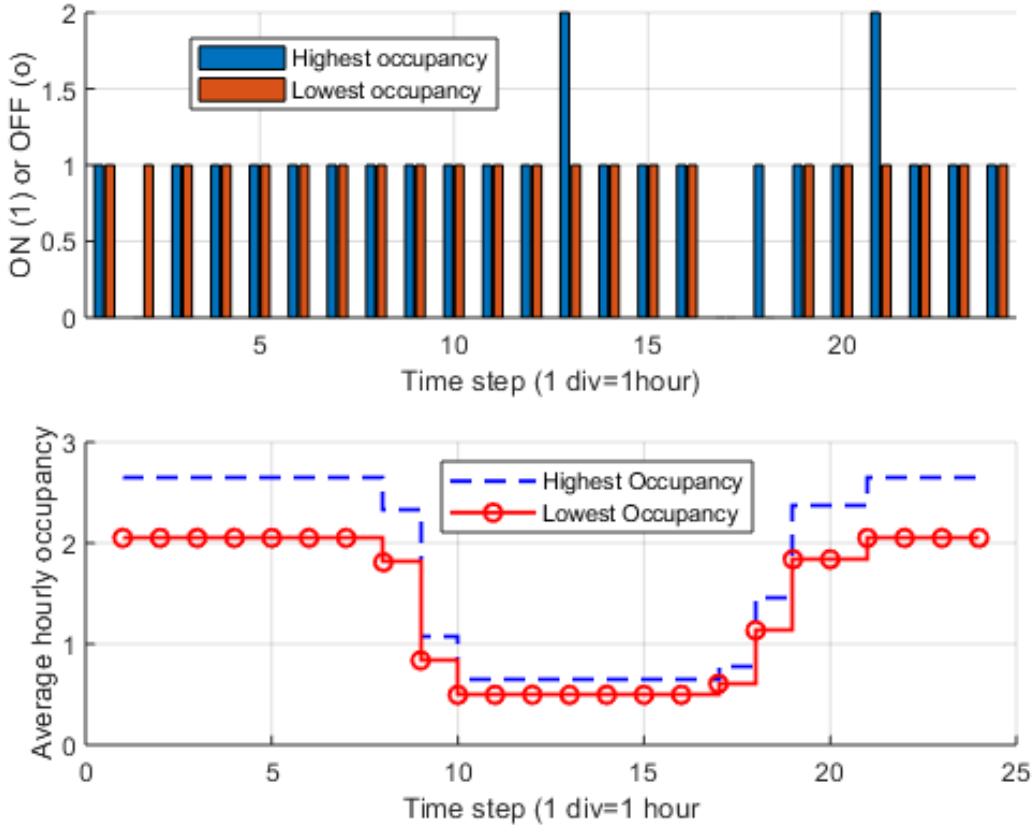

Figure 4-5 Occupancy and load shifting. The Y-axis in the upper graph shows whether the shiftable load at time t is ON (1) or OFF (0). The formulation is able to prioritize the occupancy level in the house as intended. Highest occupancy house has smaller number of load shedding compared to lowest occupancy level

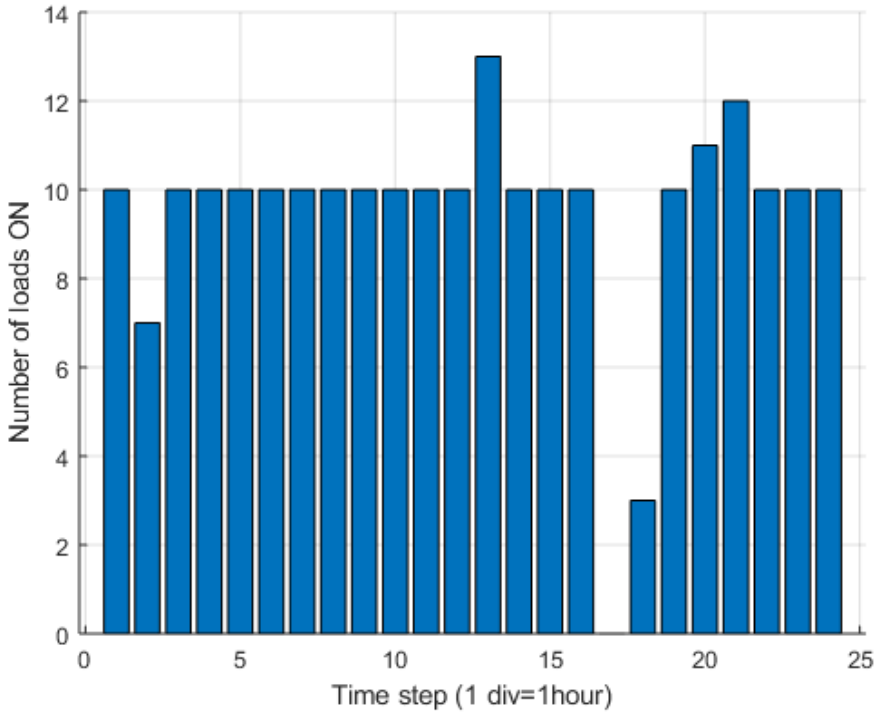

Figure 4-6 Total numbers of loads served (or ON) at each time. If $v_{i,t,t}$ is 1 for all customers at time t, then total numbers of load served would be 10. If $v_{i,t,t}$ is less than 10 that represents that there was at least one customer during time t whose load was shed or shifted to another time

4.3.3 Impact of Uncertainties

In this study a known set of data for solar irradiance, wind speed, customer energy and water demand, and occupancy levels is considered. This makes the model deterministic. To account for uncertainties one can imagine that the 24-hour dispatch can be run as a sliding window, taking all actual input data for the present time (as here-and-now) as well as estimates for the future time steps (as wait-and-see [162]) which is implemented in CHAPTER 6. Another approach could be to allocate certain reserve margins both for energy and water supplies in order to accommodate for deviations from expected values. This can be easily done by adjusting constraints (4.4) and (4.15).

4.4 Conclusions

This chapter demonstrates an optimal operational strategy for water and energy systems in a self-contained community. The case study presented shows how such a community can plan its operation to meet its daily water and energy needs with minimal external support. A load shifting and load shedding demand response technique has been implemented to ensure that there always exists a balance between generation and demand of electrical energy. A battery-based community energy storage system is used to accommodate some of the variability in energy generation from PV and wind resources. It is important to note that this case study represents a deterministic scenario for energy demand, energy generation, and water demand. However, in reality, all these parameters have variability from time to time. The stochastic modeling presented in CHAPTER 6 considers the variability of wind and PV generation, variability in power demand and variability in water demand of the community. Various scenarios are studies to understand the impacts of different generation and load scenarios in the system.

CHAPTER 5

COMMUNITY RESILIENCE AGAINST NATURAL DISASTERS USING COMBINED MICROGRID-MICRONET SYSTEMS

In this chapter, a multi-objective mixed integer nonlinear programming (MMINLP) model has been presented to design a combined water and energy system for a remote community such that it can be operated fully independent from external support. An optimal size of energy resources like wind, PV, battery system and size of water ST are obtained using a multi-objective mixed integer nonlinear programming model. In this study it is considered that the isolated microgrid does not have any possibility of purchasing power from external source. The electrical demand of residential customers in the community and electrical demand in water network needs to be supplied by the microgrid system. There is a possibility of load shedding in the microgrid in case power generation is no sufficient to meet the load. The microgrid and micronet are considered to be isolated from the main power grid and water network, respectively. The renewable energy resources like PV and wind have been selected for the generators because these generators have been widely used around the world and they provide environmental benefits over conventional power generators. Since these primary generators (PV and wind) change their output based on the availability of solar irradiance and wind velocity, a battery storage system is proposed to offset the variability from primary renewable generators. Similarly, a water ST will store clean water from WWTP and external purchase (like purchased from water tankers, if necessary) to serve the water need of the community. Two design options are presented. First option considers that the excess generation from the primary resources is curtailed when demand is less in the system. This requires

smaller BESS in the network. The second design option considers capturing maximum power possible which requires a larger BESS. CGP is used to solve the multi-objective MINLP.

5.1 Background

It is desired to optimally design a combined microgrid-micronet to enable its standalone operation should the main networks to which it is connected (i.e., power grid and/or the water distribution network) be damaged and become nonoperational due an external event. Sustainability is a cornerstone of the proposed approach, both from an economic perspective (i.e., lowering the cost of purchasing power or water from outside world) as well as practicality (i.e., road access to the community may have been lost due to the natural disaster). While this is intended for temporary situations, for instance until the repairs to the main grid or the water network are completed, it can be envisioned that such models may be deployed for remote communities in arid regions. The focus of the design problem addressed in this work is on determining the optimal sizes of energy resources (i.e., wind turbine, PV, and BESS) and water storage tank for the community. This is done while considering the typical demand profiles for both water and energy, considered under worst case conditions. BESS is intended to absorb the excess generation from wind and solar resource to later use them when the energy resource is not available. Finally, while electric load shedding is considered to be a possible option for maintaining the stability of the microgrid, it is desired to minimize its use. The rest of the chapter is organized as follow. Section 5.2 presents the proposed approach and the mathematical model. Section 0 presents the solution methodology adopted and the input parameters necessary to solve the mathematical model. In section 5.4 of this chapter, a case study is analyzed for proof-of-concept purposes and the relevant findings are discussed.

5.2 Problem Formulation

5.2.1 Preliminaries and Assumptions

A small-scale residential community is considered, which is exposed to natural hazards. It is assumed that the severity of potential hazards is such that the main power grid and/or the water network from which the community is supplied may become temporarily unavailable. To improve resilience, it is desired to operate the community network as a combination of an electric microgrid and a water micronet. The main objective in this chapter is to propose an optimal resource allocation strategy for this microgrid/micronet. The ultimate goal is to be able to, as much as possible, supply all energy and water needs with the lowest capital investment. It is assumed that the community may be equipped with a community BESS, a community PV solar panel system, and a small-scale wind turbine to address local energy needs. Further, its local water network consists of a water storage tank and a WWTP that allows for (partial) water reuse. In this chapter two design options are considered. First, without loss of generality, curtailment of wind and PV is allowed in case of excess generation than power demand. In the second design option, a maximum power point tracking (MPPT) system is implemented which considers storing maximum available power from PV or wind at any time. In MPPT system, a DC-DC converter checks the output of wind and PV system and adjust the generators output voltage such that battery can be charged at maximum current possible. In this case, the excess generation will be stored into a battery system so that the power can be utilized when there is less power generation from wind and PV. Second design option also considers external water purchase is available if needed same as design the first design option.

In both of the design options it is assumed that no external energy resources are available (for instance, connection to the main grid); however, purchasing water from external resources is an option, although not desired. The latter assumption is made since water losses are inevitable and as a result, operating as a fully closed micronet is not practical. Utilizing technologies such as rainwater catchment systems is another option but is considered out of scope in this thesis. It is also assumed that the daily profiles of average (or perhaps worst-case) power consumption, average water demand, average wind speed, and average solar irradiance are known. Lastly, the microgrid is equipped with means for load curtailment to address any mismatch between generation and demand.

5.2.2 Mathematical Model

The design problem is formulated in the form of a constrained multi-objective optimization model as outlined below. The sizes of the energy and water resources are determined in such a way that the demand profiles (power and water) are met with the least amount of load curtailment. Often, to ensure a robust design capable of handling various uncertainties, the average consumption profiles are converted into worst-case conditions. We do not distinguish between the two because the choice of average versus worst-case condition does not affect the generality of the problem.

5.2.3 Objective Function

At the high level, it is desired to minimize the cost of the system (hence, the sizes of the energy and water resources) while ensuring an acceptable quality of service. The optimization model is formulated in the form of a multi-objective one, where the Pareto optimal solution is

sought through a goal programming approach. There are six objective functions to be optimized, as outlined below.

$$\min\left\{P^{\mathrm{BT,max}},\ P^{\mathrm{PV,STC}},\sum_{x\in\mathrm{X}}\mathrm{u}_x^{\mathrm{LWT}}+\sum_{y\in\mathrm{Y}}\mathrm{u}_y^{\mathrm{swt}},\ \mathrm{V}^{\mathrm{ST,max}},\ V^{\mathrm{w}},\ \sum_{t\in\mathrm{T}}\left(P_t^{\mathrm{des}}-\sum_{i\in\mathrm{C}}P_{i,t}\right)_+\right\} \tag{5.1}$$

The first four terms represent the size of the battery system, the size of the PV solar panel the size of the wind system (modeled as total number of wind generators that are online), and the size of the storage tank, respectively. The fifth term denotes hourly water purchases from outside sources, and the last term is used to ensure that, as much as possible, electric demand is met at the desired levels.

5.2.4 Constraints

The multi-objective optimization problem in (5.1) is solved subject to the constraints listed below.

5.2.4.1 Power Balance

This chapter studies two modes of operation in the microgrid. One is power curtailment mode of operation which is to allow power curtailment from wind and PV in case of excess generation in the system. In order to achieve curtailment mode of operation, at each time-step during the dispatch period T, power provided by the generation resources must be greater or equal to the total demand, as given in (5.2). Another mode of operation is to run the system at maximum power or MPPT mode of operation. In order to achieve MPPT mode of operation, at each time-step during the dispatch period T, power provided by the generation resources must be equal to

the total demand, as given in (5.3). Power generation from wind generators depends on wind velocity and swept area of wind turbine rotor [see (5.4)and (5.5)]. In addition, the status of wind turbines (online or offline) will determine total wind power generated at any time *t*. Total power generation from wind system is given in (5.6). Similarly, power generation from PV system depends on solar irradiance available [see (5.7)]. Equations (5.8)- (5.9) indicate the operational constraints of the battery. At any point in time, the battery can be either charging or discharging, but not both [see (5.8)]. The upper bound for charge/discharge power is limited by the installed capacity of the battery, as indicated in (5.9)(5.11)-(5.10). The state-of-charge of the battery at any point in time depends on its value at the previous time step, adjusted based on the amount of charge or discharge at that point in time [see (5.11)], and its value must always lie within the acceptable lower and upper limits [see (5.12)]. Further, it has been assumed that at the first time-step, i.e., beginning of the dispatch period, the battery is charged to its lowest permissible level, as in (5.13).

$$\forall t \in \mathrm{T} : P_t^{\mathrm{WT}} + P_t^{\mathrm{PV}} + P_t^{\mathrm{BT},d} \geq \sum_{i \in \mathrm{C}} P_{i,t} + P_t^{\mathrm{ww}} + P_t^{\mathrm{BT},c} \tag{5.2}$$

$$\forall t \in \mathrm{T} : P_t^{\mathrm{WT}} + P_t^{\mathrm{PV}} + P_t^{\mathrm{BT},d} - P_t^{\mathrm{BT},c} = \sum_{i \in \mathrm{C}} P_{i,t} + P_t^{\mathrm{ww}} \tag{5.3}$$

$$\forall x \in \mathrm{X}, \forall t \in \mathrm{T} : P_{x,t}^{\mathrm{LWT}} = \frac{1}{2} \frac{\alpha \cdot \rho_a \cdot \mathrm{A}^{\mathrm{LWT}} \cdot w_t^3}{1000} \cdot u_x^{\mathrm{LWT}} \leq P^{\mathrm{LWT,max}} \tag{5.4}$$

$$\forall y \in \mathrm{Y}, \forall t \in \mathrm{T} : P_{y,t}^{\mathrm{swt}} = \frac{1}{2} \frac{\alpha \cdot \rho_a \cdot \mathrm{A}^{\mathrm{swt}} \cdot w_t^3}{1000} \cdot u_y^{\mathrm{swt}} \leq P^{\mathrm{swt,max}} \tag{5.5}$$

$$\forall t \in \mathrm{T} : P_t^{\mathrm{WT}} = \sum_{x \in \mathrm{X}} P_{x,t}^{\mathrm{LWT}} + \sum_{y \in \mathrm{Y}} P_{y,t}^{\mathrm{swt}} \tag{5.6}$$

$$\forall t \in \mathrm{T} : P_t^{\mathrm{PV}} = P^{\mathrm{PV,cap}} \frac{\Phi_t}{\Phi^{\mathrm{STC}}} \leq P^{\mathrm{PV,cap}} \leq P^{\mathrm{PV,max}} \tag{5.7}$$

$$\forall \boldsymbol{t} \in \mathbf{T} : \boldsymbol{u}_t^{\mathrm{BT},c} + \boldsymbol{u}_t^{\mathrm{BT},d} \leq \mathbf{1} \tag{5.8}$$

$$\forall t \in \mathrm{T} : 0 \leq P_t^{\mathrm{BT},d} \leq P^{\mathrm{BT,cap}} \cdot u_t^{\mathrm{BT},d} \leq P^{\mathrm{BT,max}} \cdot u_t^{\mathrm{BT},d} \tag{5.9}$$

$$\forall t \in \mathrm{T} : 0 \leq P_t^{\mathrm{BT},c} \leq P^{\mathrm{BT,cap}} \cdot u_t^{\mathrm{BT},c} \leq P^{\mathrm{BT,max}} \cdot u_t^{\mathrm{BT},c} \tag{5.10}$$

$$\forall t \in T : \mathrm{SOC}_t = (1-\gamma) \cdot \mathrm{SOC}_{t-1} + \frac{P_t^{\mathrm{BT},c} \eta^c}{P^{\mathrm{BT,cap}}} - \frac{P_t^{\mathrm{BT},d}}{\eta^d P^{\mathrm{BT,cap}}} \tag{5.11}$$

$$\forall t \in \mathrm{T} : \mathrm{SOC}^{\min} \leq \mathrm{SOC}_t \leq \mathrm{SOC}^{\max} \tag{5.12}$$

$$\mathrm{SOC}_{\circ} = \mathrm{SOC}^{\min} \tag{5.13}$$

5.2.4.2 Demand Shedding

Load curtailment is performed to ensure that balance between generation and demand is always met and that the microgrid remains stable in the sense of frequency. This is necessary because sudden changes in electric demand are a natural part of any power system, and if not mitigated, can be more detrimental for smaller scale networks such as microgrids. Naturally, reducing demand beyond desired levels introduces inconvenience for the consumers, which is why its application must be regulated. The last objective function in (5.1) tries to achieve this at the microgrid-level. However, in addition to this, consumer equity requires that no subset of users is disproportionately affected by load curtailment. This is achieved by constraints (5.14)-(5.16). A

consumer will be experiencing load shedding if the generation in system is smaller than the demand at that point in time. But the number of times during which each user experiences this must be limited [see (5.14)]. Moreover, the total amount of load shed experienced by each consumer during a dispatch period should not exceed a certain percentage of its overall desired demand during that same period [see (5.15)]. Finally, constraint (5.16)ensures that actual demand supplied to a consumer is not more than its desired demand. Also, when load shedding is not required for a consumer, constraint (5.16)prevents the formulation from incorrectly assigning more power demand than their desired level in case the total power generation in the microgrid exceeds the total system demand. In other words, constrain (5.16) will divert excess power to the battery system for charging purpose.

$$\forall i \in \mathrm{C} : \sum_{t=1}^{\mathrm{T}} v_{i,t} \leq \mathrm{N}_{\mathrm{sh}} \tag{5.14}$$

$$\forall i \in \mathrm{C} : \sum_{t=1}^{\mathrm{T}} (P_{i,t}^{\mathrm{des}} - P_{i,t})_{+} \leq k_{\mathrm{sh}} \cdot \sum_{t=1}^{\mathrm{T}} P_{i,t}^{\mathrm{des}} \tag{5.15}$$

$$\forall i \in \mathrm{C}, \forall t \in \mathrm{T} : P_{i,t} = P_{i,t}^{\mathrm{des}} \cdot (1 - v_{i,t}) \tag{5.16}$$

5.2.4.3 Water Demand

At any point in time, the total amount of water flow provided by the storage tank to the community should equal the total water demand, which is a sum of individual consumers' demands. Without loss of generality, it is assumed that at the beginning of the dispatch period, the tank is at $V^{\mathrm{ST,min}}$. The community has the option of purchasing water from external resources, although this is not desired and must be minimized [see (5.1)]. Water demand is supplied by the

outflow from the storage tank [see (5.17)]. Flow through pipes feeding users is limited by the maximum allowable rate, as indicated in (5.18). Equation (5.19)presents initial water volume in ST considering minimum available water in the ST and the possible input from external sources. Equation (5.20)presents the water flow balance of the tank for the study period, which depends on the starting volume, and the inflow/outflow to/from the tank. The volume of water in the tank should never exceed the installed capacity of the tank which should be always lower or upper reservoir limits [see (5.21)]. It is assumed that the tank is located at a higher elevation than the community, so water can naturally flow without a need for a pump. This assumption does not affect the generality of the problem, i.e., if the tank is located at a lower elevation, power consumption of pumps that are needed to transfer water to individual houses must be incorporated into (5.2)and/or (5.3).

$$\forall t \in \mathrm{T} : \sum_{i \in \mathrm{C}} q_{i,t} = q_t^{\mathrm{ST,out}} \tag{5.17}$$

$$\forall i \in \mathrm{N}, \forall t \in \mathrm{T} : q_{i,t} \leq q^{\max} \tag{5.18}$$

$$V_{\circ}^{\mathrm{ST}} = V^{\mathrm{ST,min}} + V^{\mathrm{w}} \tag{5.19}$$

$$\forall t \in \mathrm{T} : V_t^{\mathrm{ST}} = V_{t-1}^{\mathrm{ST}} + q_t^{\mathrm{p,out}} \cdot \Delta - q_t^{\mathrm{ST,out}} \cdot \Delta \tag{5.20}$$

$$\forall t \in \mathrm{T} : V^{\mathrm{ST,min}} \leq V_t^{\mathrm{ST}} \leq V^{\mathrm{ST,cap}} \leq V^{\mathrm{ST,max}} \tag{5.21}$$

5.2.4.4 Wastewater Treatment Plant

It is assumed that the WWTP can treat the incoming batch of water during one time-step, i.e., one hour. This has been chosen for demonstration purposes only and does not affect the generality of the problem. A certain fraction of water discharged from the consumers is collected at the WWTP to be treated, i.e., not all the water is recycled [see (5.22)]. Equation (5.23) represents the initial volume in the WWTP. The volume of wastewater in the WWTP is determined based on the amount of inflow to and outflow from it [see (5.24)] and cannot exceed its capacity, as indicated in (5.25).The amount of power consumed for treating the wastewater and pumping it to the reservoir is assumed to be proportional to the volume of wastewater treated, as shown in (5.26). Similar to before, it has been considered that the WWTP resides at a lower elevation than the storage tank.

$$\forall t \in \mathrm{T} : q_t^{\mathrm{ww,in}} = k_{\mathrm{ww}} \cdot \sum_{i \in \mathrm{C}} q_{i,t} \tag{5.22}$$

$$V_{\circ}^{\mathrm{ww}} = V^{\mathrm{ww,min}} \tag{5.23}$$

$$\forall t \in T : V_t^{\mathrm{ww}} = V_{t-1}^{\mathrm{ww}} + q_t^{\mathrm{ww,in}} \cdot \Delta - q_t^{\mathrm{ww,out}} \cdot \Delta - q_t^{\mathrm{ww,eff}} \cdot \Delta \tag{5.24}$$

$$\forall t \in \mathrm{T} : V^{\mathrm{ww,min}} \leq V_t^{\mathrm{ww}} \leq V^{\mathrm{ww,max}} \tag{5.25}$$

$$\forall t \in \mathrm{T} : P_t^{\mathrm{ww}} = (p^{\mathrm{ww}} + p^{\mathrm{pump}}) \cdot q_t^{\mathrm{ww,out}} \cdot \Delta \tag{5.26}$$

5.3 Solution Methodology

5.3.1 Estimation of Electrical Power Demand

The first step is to identify the loads that the generator is going to serve. Load data for residential customers were taken from [163]. This dataset contains hourly load profile data for residential buildings in all Typical Meteorological Year (TMY3) locations in the United States and provides one year of hourly data that best represents median weather conditions over a multiyear period for a particular location. For this study, the city of Golden CO was selected as the case study. The residential load is based on the Residential Energy Consumption Survey (RECS) data for different building types by location. Assuming a community consisting of 10 residential units, load data for ten residential consumers were selected as input parameters to the formulation. The hourly plot is shown in Figure 5-1.

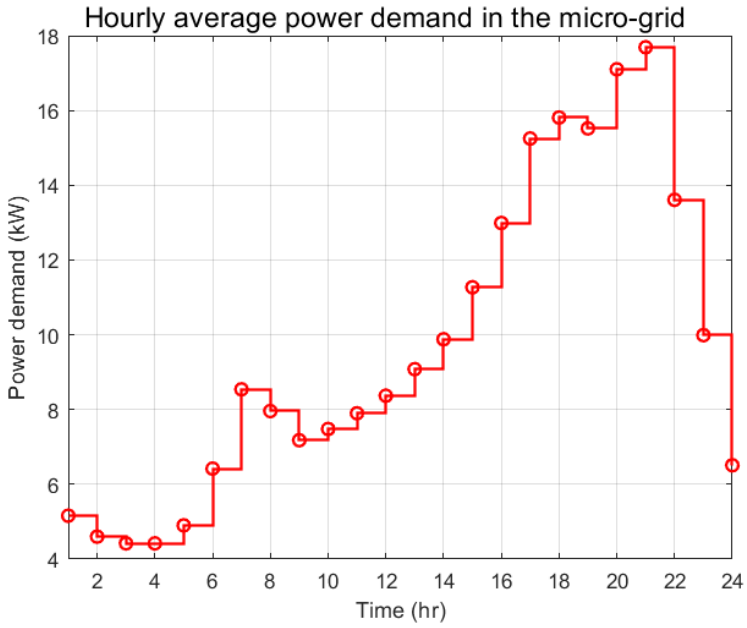

(a)

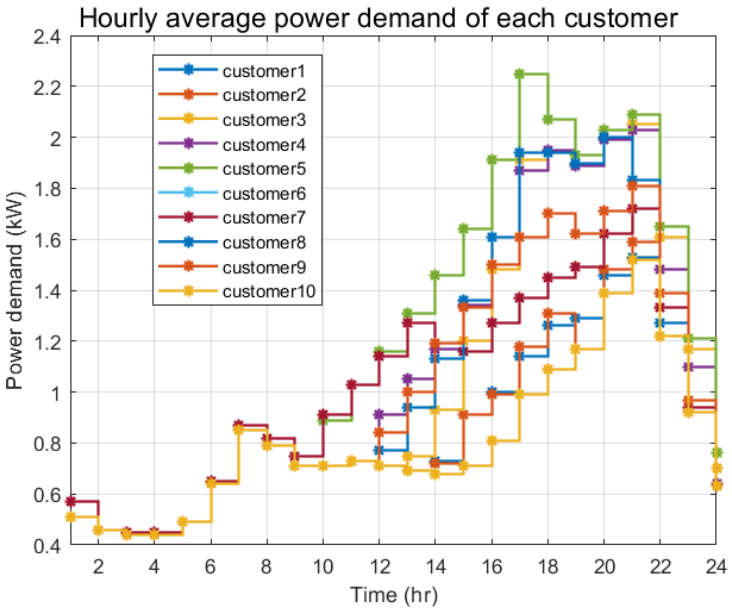

(b)

Figure 5-1 Average hourly demand (kW) in the micro-grid of 10 customers (a) and individual load profiles (b). The time scale 1 through 24 represents the 24-time steps used in this study.

To estimate the electric demand at the WWTP, historical data on power consumption of different electromechanical components in a typical WWTP are used to estimate total load. The data used represents the average demand (in kW) for various electromechanical components that is being utilized in the Mines Park WWTP located in Golden, CO. The system processes one batch of wastewater (1.22 m^3) in two hours. The grinder pump is used to fill the bioreactors with incoming wastewater from the residential households. The bioreactors are like the water storage tanks that are used to store clean water, but they are equipped with electromechanical devices like air blower and mixer to treat the incoming wastewater. Once the wastewater is in the bioreactor the blower will supply oxygen to the wastewater and mixer will stir the fluid so that biochemical reaction can occur the system and the fluid is ready is to be filtered in a separate tank (also known as membrane tank). The RAS pump will pump out the wastewater from bioreactor to membrane tank where small membrane will filter the waste in fluid with the help of air scour blower pump.

Clean water will be pumped out of the WWTP via permeate pumps. The following Table 5-1 shows power consumption of these devices to treat the wastewater.

Table 5-1 Energy consumption of the electromechanical components in the WWTP to treat one batch of wastewater (1.22 m^3) over two hours

Component	Energy in kWh
Grinder pump	0.10
Blower	1.14
Mixer	1.12
RAS pump	1.38
Air Scour Blower (ASB)	1.49
Permeate pumps	0.53
Total	5.55

The total demand (in kW) of the community is one of the critical information to estimate size of generators. From Table 5-1, 5.55 kWh energy is utilized to treat 1.22 cubic meter of wastewater in 2 hours which is equivalent to 4.55 kWh to treat 1 cubic meter in 2 hours.

5.3.2 Solar Irradiance and Wind Speed

Data related to solar irradiance and wind speed impacts the sizes of the PV system and wind turbine necessary to supply the demand. NREL provides this data for Golden, CO [159], [164] (see Figure 5-2). The size of the PV system is estimated based on the standard available sizes of PV panels in the market. It is assumed that the community can install up to a total of 1,000 solar

panels at 250-350W capacity each (under standard test conditions). These individual panels measure 1.5 m by 1 m in size. Considering average roof size of 185 m^2 (2,000 sq. ft.) for typical residential house in the US [165] or 92.5 m^2 (1, 000 sq. ft.) for one roof and 1.5 m^2 (16 sq. ft.) for one solar panel, one house can install approximately 62 panels producing approximately 18.6 kW (using 300 W per panel). This is equivalent to 186 kW of PV capacity for 10 customers in the community. This indicates that the community will have an additional solar garden of approximately 64 kW. For a smaller roof size houses the community solar garden will be larger and for larger residential house with garage the average roof size can go over 130 m^2 (1,400 sq. ft.) per roof and such houses can generate more than 24 kW of PV per house. At the upper bound, this would be equivalent to 25 kW of solar power per residential customer. Wind power is the other source of energy for the community, especially since highest wind speeds typically occur during evening times when solar power may not be available. The size of the possible wind turbine is estimated based on the average wind speeds available in the study area. A wind energy conversion system of size 300 kW for a 31 m diameter wind turbine [166] is assumed to be the highest capacity that the community can install. In this paper two design options are studied considering the different wind turbine sizes. One design case considers that the community has two wind turbines of the same capacity (300 kW max capacity with 31 m rotor diameter). Another design options considers that the community has one larger wind turbine (300 kW max capacity and 31 m diameter) and 40 additional smaller wind turbines (5.5 kW max capacity with 4.3 m rotor diameter [167]). Depending on the energy need for a given time the turbines will be turned on or off to maintain load generation balance in the microgrid.

Both PV and wind power generators depend on energy resources, i.e., solar irradiance and wind, that are intermittent in nature and undergo variations throughout the day. When there is

insufficient energy available from these sources to supply the demand, a BESS would have to be used to ensure power balance in the microgrid. Community energy storage solutions come in different forms and sizes. For this study, a maximum possible capacity of 200 kW is assumed for the BESS.

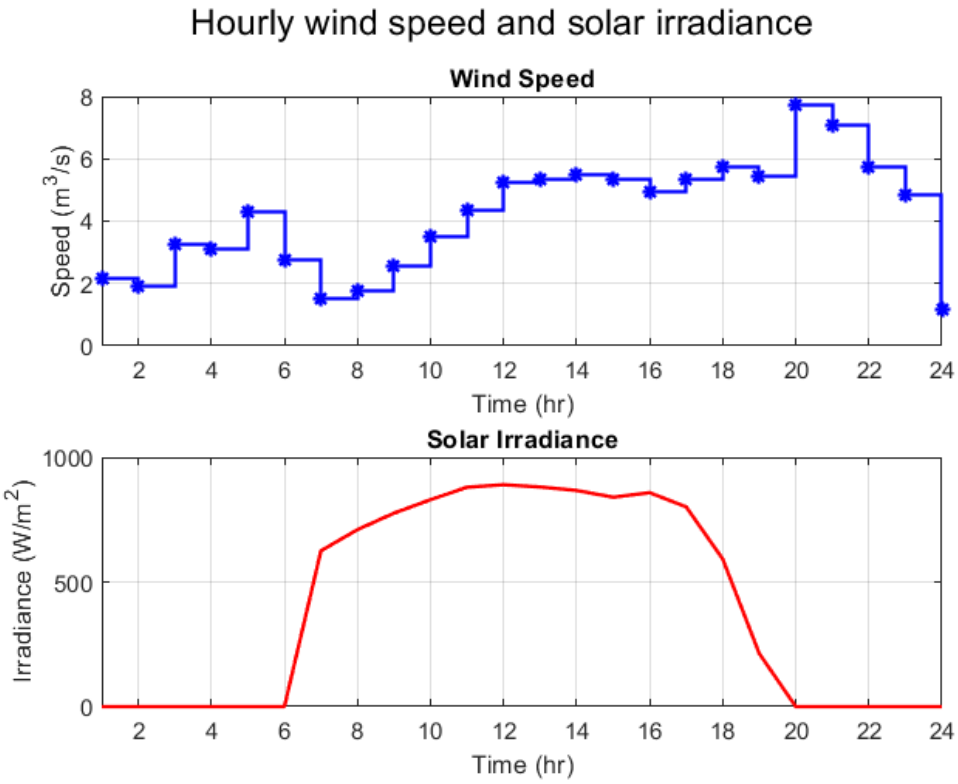

Figure 5-2 Wind speed and solar irradiance available in the study area.

5.3.3 Water Demand of the Community

Water demand for the households is estimated based on the hourly occupancy profile of each household and average water consumption per person. It is assumed here that the occupancy levels are known or can be derived from historical data available from the community. The water demand for each user is estimated to be 0.37 m^3 (100 gallons) of water per day as provided by U.S. Geological Survey (USGS) [168]. The average hourly occupancy profile and water consumption

level of residential customers is given in the plots below. The daily profile considered in this study is illustrated in Figure 5-3. Naturally, this is for demonstration purposes only and the shape and values of the water profile do not affect the generality of the problem.

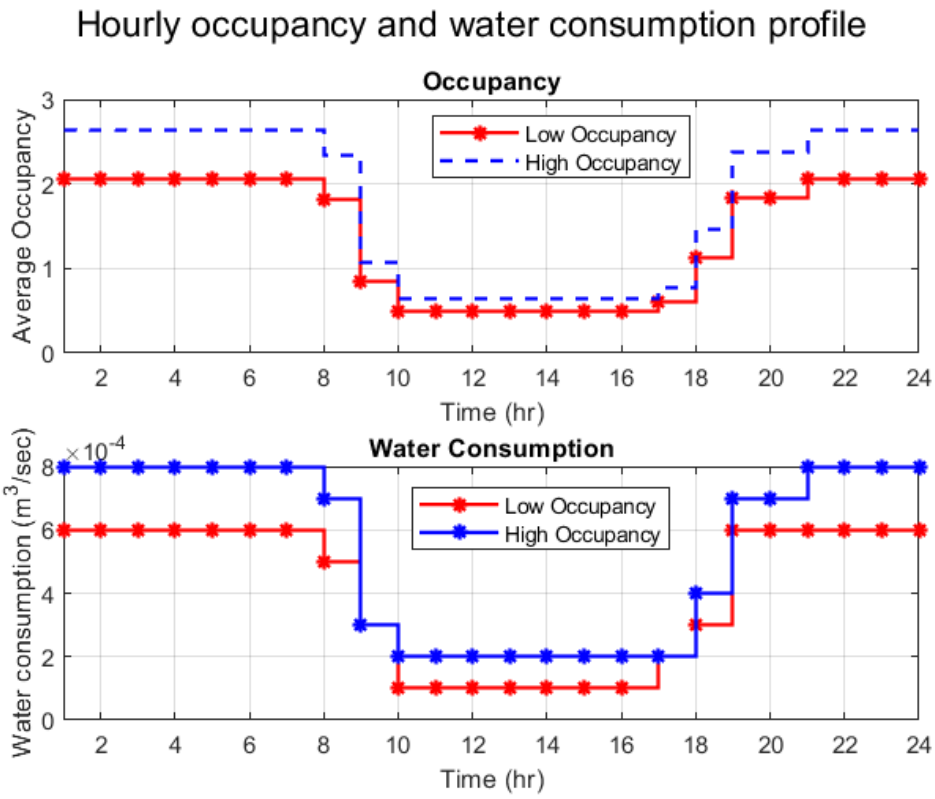

Figure 5-3 Hourly average occupancy and water demand of the households in the community.

The size of water pump required at the WWTP is estimated using the following equation [169]:

$$P_t = \frac{\rho \cdot g \cdot q_t^{ww,out} \cdot H}{\eta} \tag{5.27}$$

It is assumed here that the water distribution system is already in place and able to supply an average flow rate of 0.0007 m^3/s per house (or approximately 11 gallons per minute (GPM), which is estimated based on the assumption of a maximum of 2.2 GPM for 5 faucets in the house located in bathrooms, kitchen, shower, and laundry area as per the US EPA's standard [161]) at 41 m water head (approximately 60 pound per square inch (PSI) or 414 kPa water pressure). Hence, the total head from WWTP and storage tank needs to be at least 41 m (or 60 PSI pressure difference). With these parameter values, a pump system with a power rating of 4.022 kW (5.39 hp) is chosen. This implies that the pump would consume 0.21 kWh per unit volume of water lift at that pressure. This number is close to 0.19 kWh/m^3 requirement of water pumping provided in [170].

5.3.4 Solution Methodology

The optimization model proposed in this chapter is a multi-objective one. A traditional approach in solving such problems has been to combine all individual objective functions into a single aggregate one to be optimized. The problem with this approach is that it is easy for one objective to dominate others. Some address this issue by weighing the objective functions proportionately so as to make them comparable in size and/or to intentionally prioritize one or more over the others. However, this would be a subjective approach. The above issues are exacerbated when some of the objectives are contradictory to the others, as is the case in the model presented in (5.1). Under such circumstances, it is crucial to ensure that all objective functions are treated equally and that no single objective dominates others.

In this thesis we adopt the CGP, to solve the multi-objective model. As the first step, we define goals (targets) to be met for each individual objective function. These goals are usually

derived from solving the single objective optimization models (as explained in the next section). We then allow objective functions to deviate from the goal (target) by defining deficiency variables. In the rare condition that the model manages to achieve all predetermined goals, it stops improving the solution further. To avoid this and to ensure that Pareto optimality is achieved, the methodology discussed in [149], [150] has been adopted, where a small percentage of each original objective function (ε_q = 0.005 in this study) is added to the CGP aggregate function so that the model continues to improve the objectives even if the user-defined goals (targets) are met. The CGP problem can be expressed as follows. In this model, objectives O_1 through O_6 are the size of the battery, the size of the PV system, the swept area of the wind turbine rotor, the size of the storage tank, the amount of water to be purchased from outside sources, and the amount of load shed, respectively [see (5.1) for more details].

$$\min Z = \lambda + \sum_{q=1}^{6} \varepsilon_q \frac{O_q}{b_q} \tag{5.28}$$

Subject to:

$$\forall q : \frac{p_q}{b_q} \leq \lambda \tag{5.29}$$

$$O_q - p_q \leq b_q \tag{5.30}$$

$$\forall q : p_q \geq 0 \tag{5.31}$$

In these equations p_q's are deficiency variables that allow objectives to deviate from the user defined goals (targets) b_q [see (5.30)]. However, the amount of the deviation must be minimized, as indicated in (5.29). Variable λ is an auxiliary decision variable that provides an upper bound on the normalized deficiency variables. The objective in this combined model is to simultaneously optimize all objective functions so that their respective deviations from their target values are minimized.

5.4 Results and Discussion

In this section, the objective function (5.28) is solved subject to constraints (5.2)- (5.26) and (5.29)- (5.31)for a community consisting of 10 residential units, with electricity and water demand profiles as illustrated in Figure 5-1 and Figure 5-3. It is desired to find the optimal sizes for the PV, the wind turbine, the BESS, and the storage tank while also ensuring water purchases from external sources and load shedding instances are minimized. The proposed multi-objective optimization model is solved using General Algebraic Modeling System (GAMS) software using an Intel® Core™ i7-8750H CPU @ 2.5GHz–2.21GHz computer. The optimization model was run multiple times with an average convergence time of approximately 28 minutes, median convergence time of 28 minutes, and standard deviation of 1.16 minutes. The solution converged during all the sample. In the CGP model adopted in this chapter, each objective function is first solved in isolation, i.e., ignoring other objectives, to find its true optimum value. These values (in most cases, subject to a slight deterioration) are then used as the goals (targets) to be met in the multi-objective setting. In cases such as this study, where the objectives are contradictory to one another, the goals are normally never met.

In this chapter, two design options are considered regarding the energy supply from wind and PV sources. Both design options consider no external support for energy but a minimal water supply from external sources is allowed in both options. The design options are: (a) using two large wind turbines each of capacity 300 kW (swept area of 755 m^2) (b) using 1 large wind turbine of capacity 300 kW (swept area of 755 m^2) and 40 small wind turbines each of capacity 5.5 kW (swept area of 14.5 m^2). The other constraints and size of resources remain same for both design options. In both cases, the community network is expected to solely rely on its own energy resources, i.e., the installed PV, wind, and battery system. Table 5-2 and Table 5-4 list the results of the single objective optimization models for both design options. For each design option, as per the constraints (5.2) and (5.3), the optimization model will maintain either total generation is greater or equal to total demand (5.2)or total generation is equal to total demand (5.3) for every time step. There was no significant difference in the final design results for power curtailment mode or MPPT mode of operation which implies that the community could choose power curtailment (using equation (5.2)) or MPPT (using equation (5.3)) mode of operations as required for the similar amount of financial investment on the water and energy resources. In both design cases, the system is designed for the worst-case scenario. The worst-case scenario is the time step when there is minimum power generation possible from wind and PV. Only PV and wind are primary sources of power the battery system gets power from these resources in order to charge and discharge. Hence for the worst case the battery system discharging is not considered as it may or may not have charged in the previous time steps. The optimization model computes the size of PV and battery to meet the power demand at the worst-case and it also computes the number of wind turbines that need to be online during the worst-case scenario. Once the power generation for

wind generation, PV, and battery is determined for the worst-case the same size will be used for the other time steps.

Each single objective (SO) optima, i.e., cells highlighted in Table 5-2 and Table 5-4, is used as the corresponding goal (target) for the multi-objective model. Also, a 10% deterioration is applied to each value, except for those objectives whose optima are zero. Then the problem is solved to try to achieve the lowest amount of deviation from those goals (targets). Table 5-3 and Table 5-5 summarize the results. In single objective optimization, it is possible to achieve superior solutions for each objective than the corresponding solution achieved under the multi-objective model where it can be seen that all objectives are worse compared to their SO optima, except the O_6 in design option 2. This is expected because the multi-objective model minimizes the overall solution for all objectives.

5.4.1 Case 1: Two larger wind turbines

In this design option, it is considered that the community has two larger wind turbines along with PV and BESS for power supply. As expected, when the community needs to be prepared for the worst-case condition the size of critical resource must be sufficient to meet the energy need of the community. In this case the wind power is most critical resource as the PV system only provides power during day times and battery system only provides power when it charged. The solution given in Table 5-3 indicates that both wind turbines must be online in order to meet the power need all the time. When there is excess generation from the wind the BESS will store power for later use, but if the community decides to curtail power from wind and PV, the BESS is not required to store charge if it is not going to be discharged during the study horizon. In this case study the BESS discharging occurs mainly during time step 24 and hence it needs to be charged

ahead of the time (during time step 20) as given by the charging and discharging times in Figure 5-7. The battery SOC level is also presented in Figure 5-7. In the following table, the six objectives are defined as, O_1: Battery size (kW), O_2: PV size (kW), O_3: Number of wind turbines that are ON, O_4: ST capacity (m^3), O_5: Water purchased (m^3), and O_6: Total load loss (kW).

Table 5-2 Single objective (SO) optimization results when two wind turbines are considered

Minimize	**O_1**	**O_2**	**O_3**	**O_4**	**O_5**	**O_6**	**Number of loads shed**
O_1	6.84	250	2	200	200	5.53	10
O_2	10.60	19.45	2	200	200	9.76	10
O_3	0.07	250	2	200	200	5.03	10
O_4	10.64	250	2	141.32	141.32	5.36	10
O_5	10.71	250	2	200	141.32	5.36	10
O_6	10.60	20.11	2	200	200	3.37	7

Table 5-3 SO and multi-objective (MO) values for the proposed model considering two wind turbines

Objective Function	**SO Optima**	**Goal (Target) Values**	**MO Optima**
O_1	6.84	7.52	9.24
O_2	19.45	21.40	25.54
O_3	2.00	3	2.00
O_4	141.32	155.45	190.86
O_5	141.32	155.45	190.86
O_6	3.37	3.71	4.13

From Figure 5-4, it can be seen that at nighttime, power from wind (and battery) are the only two sources for the community. Also, wind power is curtailed during time steps 12 through 15, 18, and 20 since the power generation is more than the demand at that time. The BESS system is fully charged during time steps 20-23 to supply power for the future time step 24. As shown in Table 5-3, battery storage of 9.24 kW, PV capacity of 25.54 kW, and two wind generators each of capacity 300kW and rotor swept area of 755 m^2 have been chosen by the model to meet the demand with minimum load shedding as possible . Figure 5-5 depicts the hourly water inflows and outflows associated with ST and WWTP. As the community consumes water for daily activities, the volume of water in ST and WWTP undergo variations. As per the solution in Table 5-3, a storage tank of size 190.86 m^3 (approximately 50,420 gallons) is required to meet the water demand in the community over a 24-hour period. In addition, the community needs to purchase 190.86 m^3 of water for each day in order to adjust the balance. With this design the community will see total of 4.13 kW load loss for the study period.

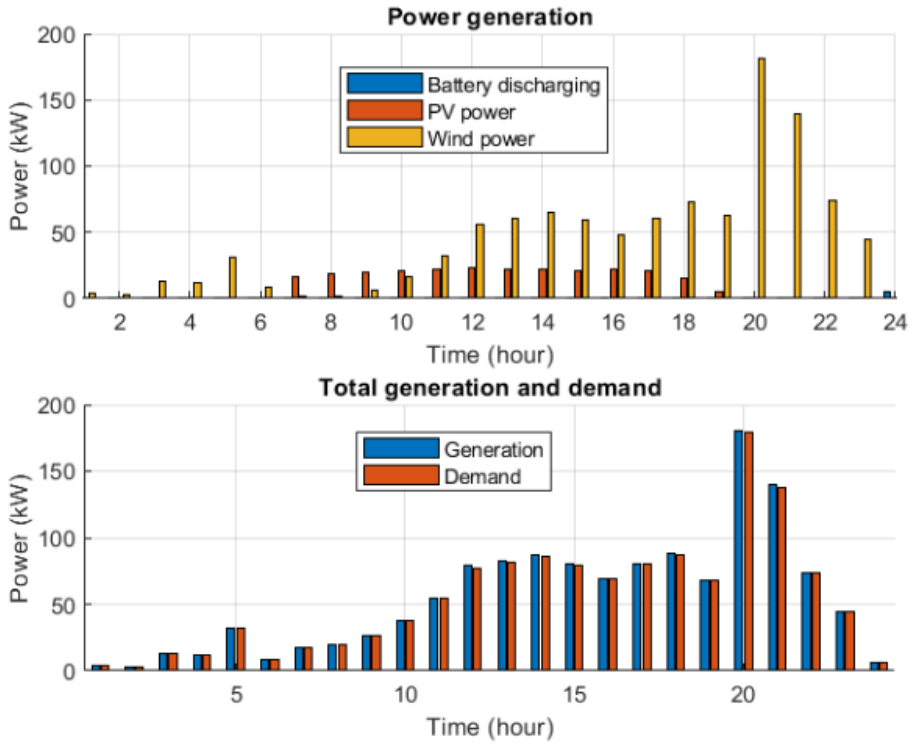

Figure 5-4 Hourly power generation from wind, PV, and CES considering two wind turbines and power curtailment is allowed. Higher generation than load in the bottom graphs shows indicates power curtailment. Hourly power demand of the community and WWTP load shows how demand is changing over the time period.

As per Figure 5-7 there is an increased power demand (more than 50 kW) for the WWTP during time 12 to 22 which is because the WWTP system is treating the water and pumping it into ST so that the water need of the future time steps can be supplied. The decrease in WWTP level during time steps 12 through 18 and 20 through 23 and increase in water level in ST during these times shows the pump operation to supply water need of the community.

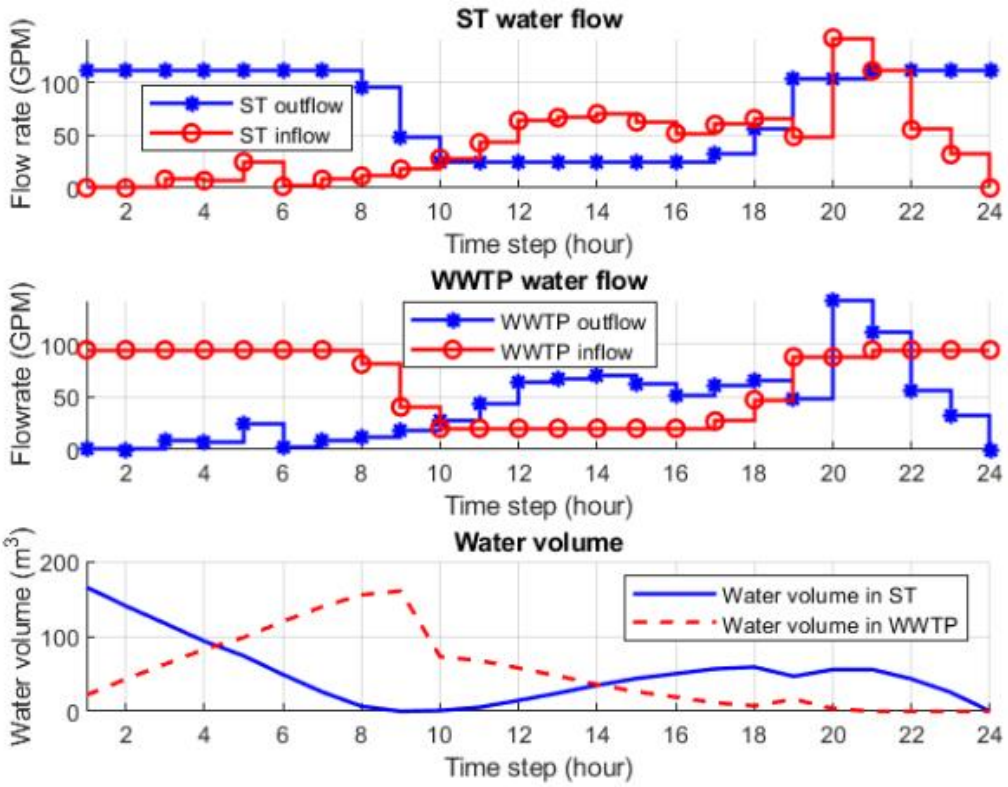

Figure 5-5 Storage tank and WWTP inflow outflow considering external water purchase. Volume of water in ST and WWTP is changing as the water demand is changing for the study period. Since there is higher power generation from wind during time steps 20-22, the WWTP and pumping systems are operating heavily during this time to maintain load generation balance.

There is a small or no power consumption during other time steps by the WWTP because the ST supplies clean water to the community via gravity (without a need of external pumping). Because of this the size of ST must be large enough to store sufficient water for a longer period of time. In other hand, the WWTP must be able to treat the wastewater and pump out clean water in shorter period of time which requires more energy consumption.

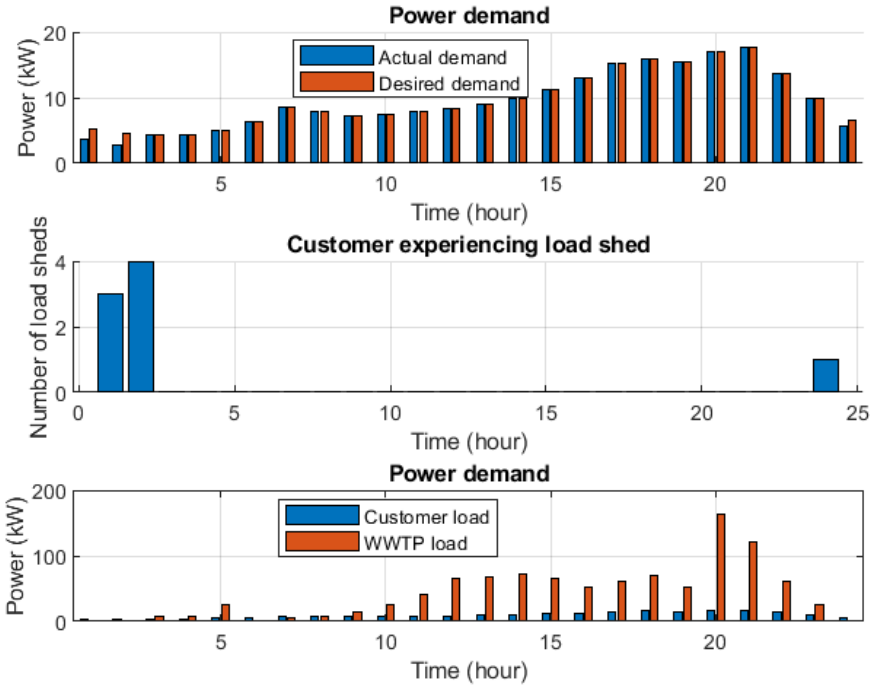

Figure 5-6 Total power generation and demand in the system. Power generation is sufficient to meet power demand for all time-steps except time steps 1, 2, and 24 during which there is load shedding experienced by 3, 4, and 1 consumer, respectively. Power demand from WWTP increases later in the study period to balance higher wind power generation.

As per the design criteria each customer is allowed to experience load shedding for only 1 time in the study period (or only for 1 hour in a day). Which means total of 10 load shedding in the study period. As given in Figure 5-6, three customers experience load shedding during time 1, four customers experience load shedding during time 2, and one customer experiences load shedding during time 24, making total of 8 load sheds in the study period. This load shedding occurred because the power generation was less than the demand during those times and as per the design criteria the load shedding is allowed as long as one customer experiences maximum of 1 hour of load shedding in the day.

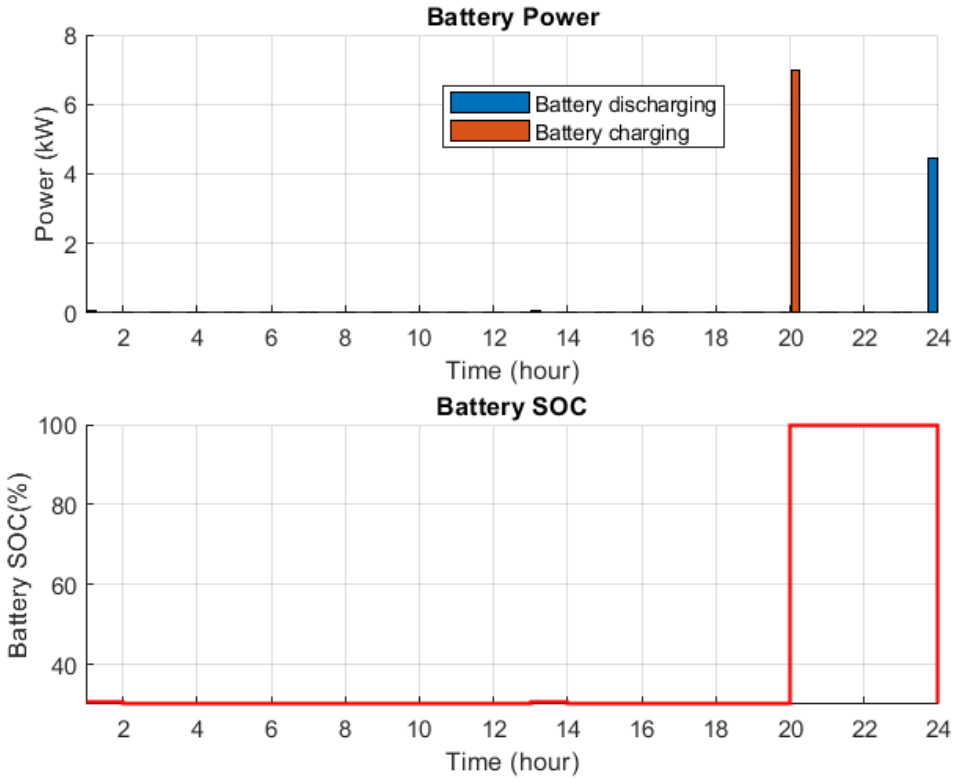

Figure 5-7 Battery charging and discharging status and battery SOC over the study period. When there is larger generation from wind generator the CES gets fully charged as shown during time step 20. During time step 24, the CES system supplies the load and SOC level goes down to minimum.

This study considers another design option which is to install one larger wind turbine and 40 smaller wind turbines as explained in case 2 below.

5.4.2 Case 2: One larger wind turbine and 40 smaller wind turbines

In this design option, one larger wind turbine is installed for the community along with 4 smaller wind turbines that are installed at each customer's house (making 40 total). Other resource capacity including PV size and BESS size is similar to case 1. Similar to case 1, not considering the option of external power purchase requires a preparedness for the worst-case condition which

means that larger size wind and PV systems are needed in case 2 as well. The power generated from wind and PV system will be stored in the BESS for future use as per the need of the community. If the community decides to curtail power from wind and PV, the BESS is not required to store charge if it is not going to be discharged during the study horizon.

Table 5-4 Single objective (SO) optimization results considering one larger and 40 smaller wind turbines

Minimize	**O_1**	**O_2**	**O_3**	**O_4**	**O_5**	**O_6**	**Number of loads shed**
O_1	9.36	250	40	200	200	5.21	10
O_2	10.72	32.29	40	200	20	6.65	10
O_3	10.86	250	27	200	200	4.91	10
O_4	10.72	250	40	143.13	143.13	5.05	10
O_5	10.72	250	40	200	143.13	5.05	10
O_6	10.76	32.57	40	200	200	4.34	9

**Note: The larger wind turbine is always ON*

Table 5-5 SO and multi-objective (MO) values for the proposed model considering one larger and 40 smaller wind turbines

Objective Function	SO Optima	Goal (Target) Values	MO Optima
O_1	9.36	10.30	9.40
O_2	32.29	35.52	42.41
O_3	27	30	36**
O_4	143.13	157.44	187.98
O_5	143.13	157.44	187.98
O_6	4.3	4.774	5.16

***Note: The larger wind turbine is always ON*

During case 2, the larger wind turbine needs to be online and only 36 smaller wind turbines out of 40 need to remain online in order to meet the power demand of the community for the study period. Which is equivalent to having approximately 200 kW wind power on top the 300 kW from the larger turbine. This is lower in installed capacity of wind than in case 1. As expected, the installed capacity of battery and PV is more in case 2 (as given in Table 5-5) compared to case 1 because of smaller wind power available in the microgrid. As shown in Table 5-5, a battery storage of 9.40 kW, PV of size 42.41 kW, one wind turbine of capacity 300 kW and rotor swept area of 755 m^2, 36 wind turbines of capacity 5.5 kW each with swept area 14.5 m^2 have been chosen by the model to meet the demand with minimum load shedding as possible. With this design the community will see total of 5.16 kW load loss for the study period.

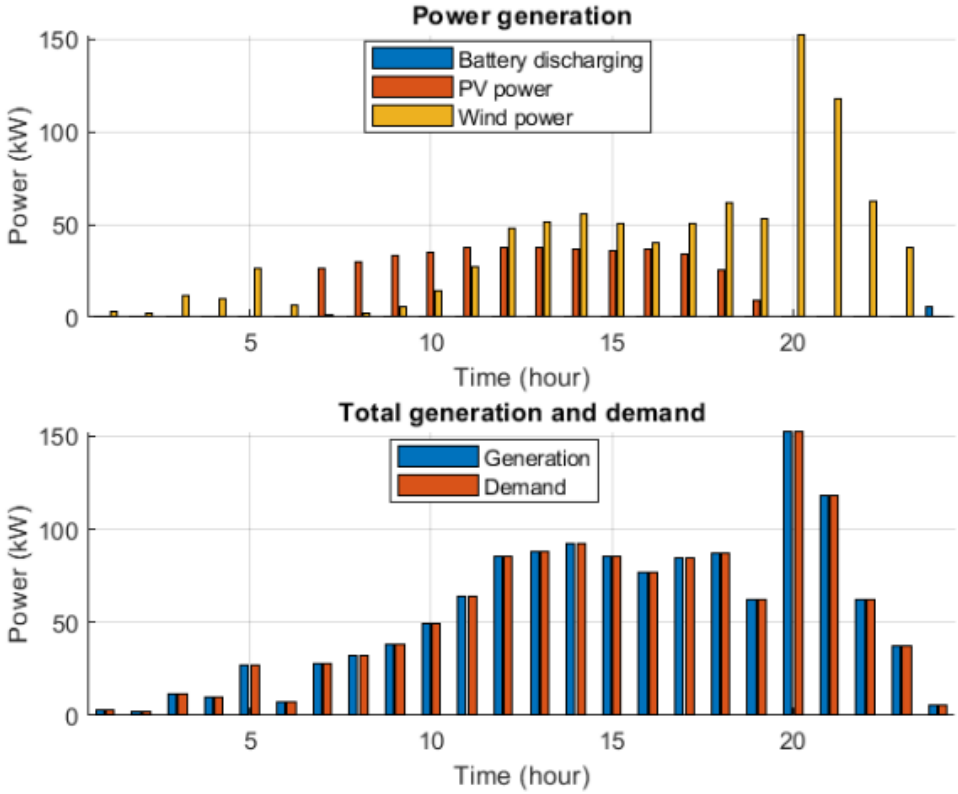

Figure 5-8 Hourly power generation from wind, PV, and CES considering no power purchase from external source. Hourly power demand of the community and WWTP load shows how demand is changing over the time period.

In this case study the BESS charging occurs during time step 23 and discharging occurs during time step 24 which is same as the case 1 and hence number of load shedding are also similar to case 1. As shown in Figure 11, total of 10 customers experience load shedding during the study period: 4 customers during time step 1, 5 customers during time step 2, and 1 customer during time step 24. This is because the PV system cannot provide power early in the morning as there is no solar irradiance available and the BESS is not charged because even with installed capacity of approximately 500 kW of wind the power is not sufficient to meet the community load.

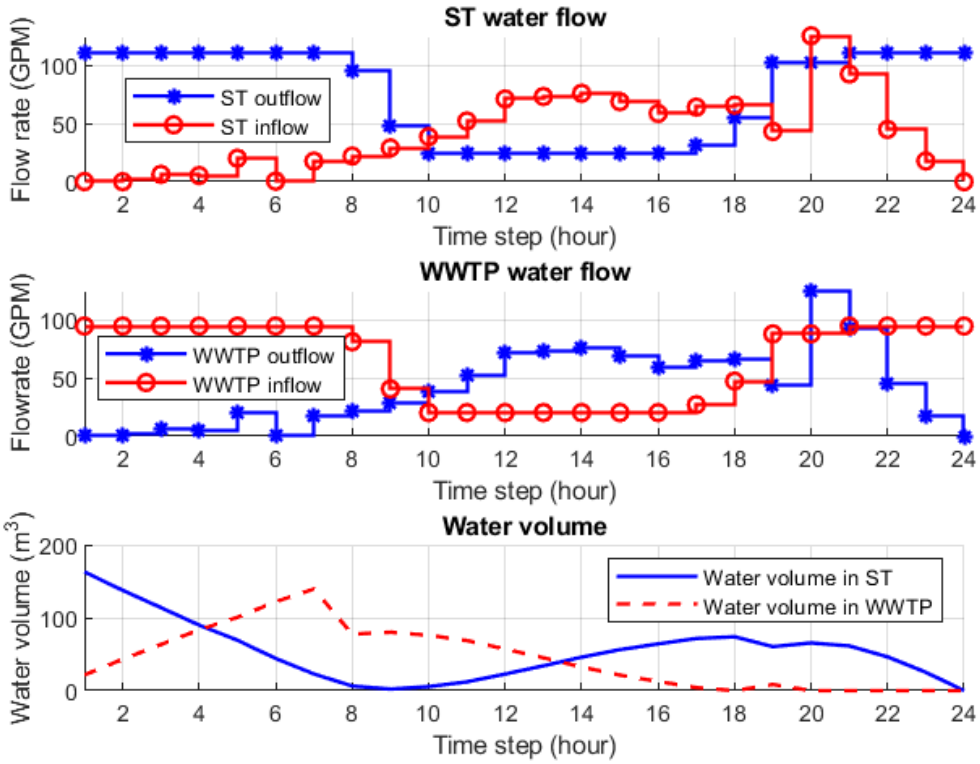

Figure 5-9 Storage tank and WWTP inflow outflow considering external water purchase. Volume of water in ST and WWTP is changing as the water demand is changing for the study period.

Similarly, for time step 24 the stored battery power was only sufficient to supply approximately 5.2 kW of power resulting in load shedding for 1 customer. This load shedding is as per the design criteria which allows one customer experiencing maximum of 1 hour of load shedding in the day. Battery charging and discharging status as well as SOC level at different times in a day is presented in Figure 5-11. As expected, higher the power generation for a given time from primary resources, the CES will store more power and SOC level will rise. When there is no or less power generation from primary resources the CES system will discharge to meet the load as much as possible.

Figure 5-9 depicts the hourly water inflows and outflows associated with ST and WWTP. As the community consumes water for daily activities, the volume of water in ST and WWTP undergo variations. As per the solution in Table 5-5, a storage tank of size 187.98 m^3 (approximately 49,659 gallons) is required to meet the water demand in the community over a 24-hour period. In addition, the community needs to purchase 187.98 m^3 of water for each day in order to adjust the balance.

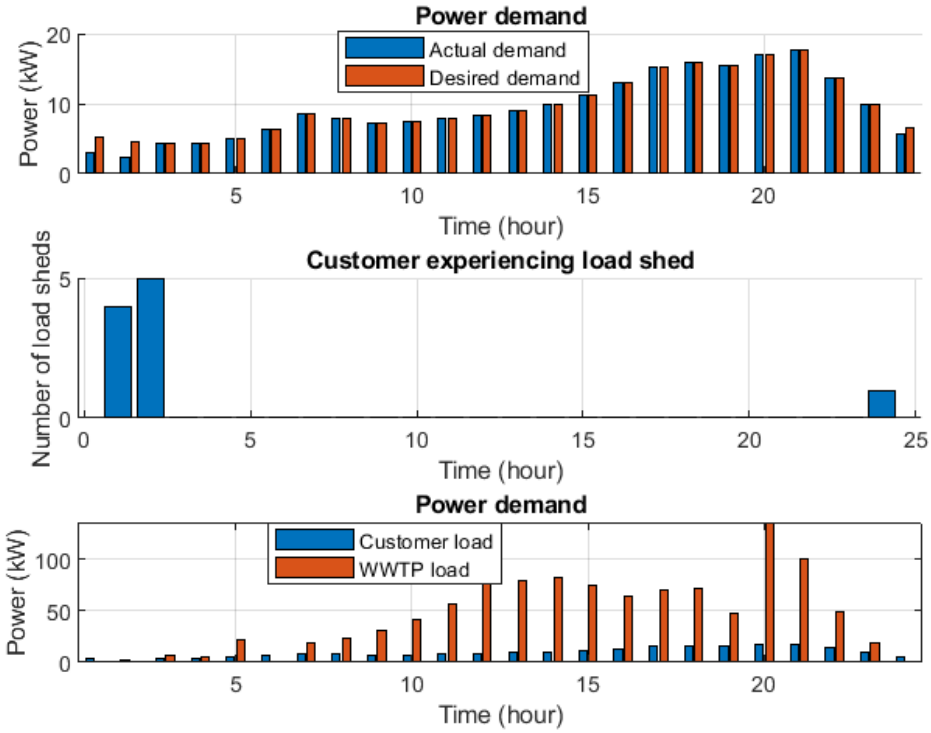

Figure 5-10 Total Power generation and demand in the system. Power generation is sufficient to meet power demand for all time-steps except for time steps 1, 2, and 24 during which there is load shedding experienced by 4 customers, 5 customers, and 1 customer, respectively. Power demand from WWTP increases later in the study period to balance higher wind power generation.

As per Figure 5-10, there is an increased power demand (more than 50 kW) for the WWTP during time 11 through 18, and 20 through 22 which is because the WWTP system is treating the water and pumping it into ST so that the water need of the future time steps can be supplied. The

decrease in WWTP level and increase in WWTP outflow during these times shows the pump operation to supply water need of the community. There is a small or no power consumption by the WWTP at the beginning of the study period because the ST supplies clean water to the community via gravity (without a need of external pumping). Because of this the size of ST must be large enough to store sufficient water for a longer period of time (or the must store the clean water purchased from external source).

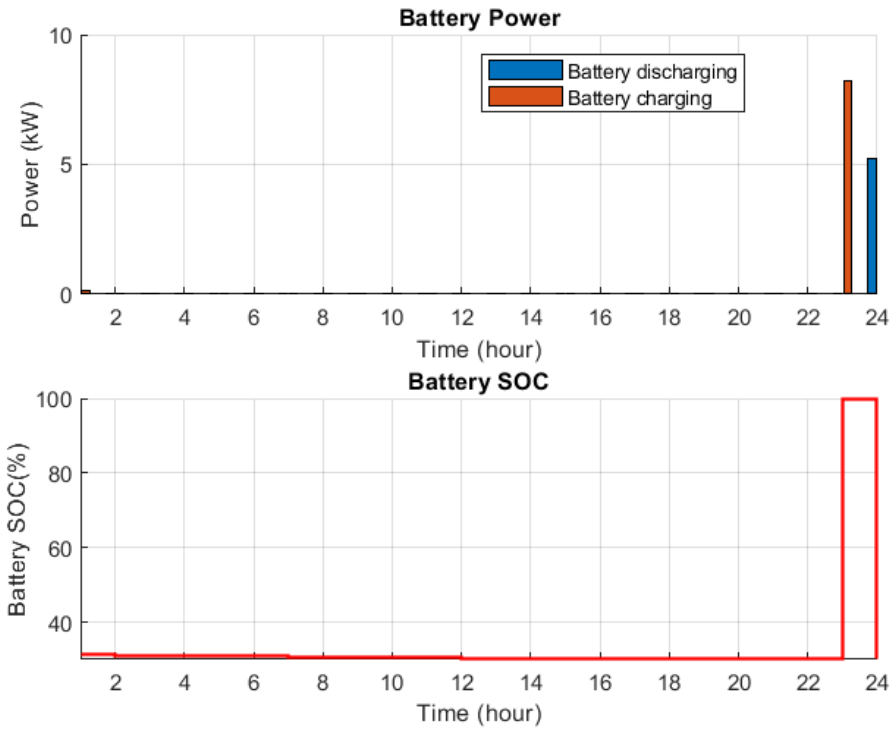

Figure 5-11 Battery charging and discharging status and battery SOC over the study period. When there is larger generation from wind generator the CES gets fully charged as shown during time step 23. During time step 24, the CES system supplies the load and SOC level goes down to minimum.

5.5 Conclusions

In this chapter, MMINLP has been presented for the optimal design of microgrid and micronet systems. The proposed formulation considers combined operation of water and energy

systems for a community that needs to be self-reliant on both resources as much as possible to increase its resiliency against any disturbances that may cause disruption in supply from external sources. The proposed methodology considers isolated mode of operation of the microgrid. From the study results it has been found that the community needs to install at least one wind turbine of capacity 300 kW and rotor diameter of 31 m in order to support the power need in the microgrid. Since one wind turbine is not sufficient to supply the entire load of the community, there is a need to install additional generator. The community has two options to choose from. One option considers installing one additional wind turbine of the same size which would require having to install smaller PV and battery system as suggested by the proposed optimization model. The second design option is to install at least 36 smaller wind turbines of each capacity 5.5 kW and rotor diameter of 4.3 m. The second design option requires larger PV and battery system compared to design option 1 because total installed capacity of wind in design case 2 is lower than the installed wind power in case 1. There would be total of 5.16 kW of load loss in the community and all customers experience load shedding for one hour with design case 2. With design case 1 there would be total load loss of 4.13 kW and 8 out of 10 customers would experience load shedding for one hour in the study period. In both design cases the community could choose to run the system in power curtailment mode or MPPT mode since the investment in resource installation would be similar. In both design options, an optimal size of critical component in the energy and water systems are computed using CGP. An optimal size of battery, PV system, and wind turbines have been obtained for a microgrid system considering average hourly power demand for a day. Similarly, for the water distribution system, an optimal size of a storage tank size and amount of power purchase from external source has been obtained. Size of the pump calculation required to lift the water for the community is also discussed in this paper with the required mathematical

formula. In this study, the community is assumed to be completely off the grid which requires having to build a larger wind generation system, larger PV system, larger ST, and higher amount of water purchase from external source in order to meet the daily need of water and energy. The solution of the optimization model presents the required amount of power that needs to supply from each source all the time in order to run the system smoothly. There is a load shedding suggested by the formulation for certain time and certain customers in order to ensure resilient operation of the system during the entire study period.

CHAPTER 6

OPTIMAL OPERATION OF COMBINED ENERGY AND WATER SYSTEMS FOR COMMUNITY RESILIENCE AGAINST NATURAL DISASTERS

One of the most critical challenges for modern power systems is to reliably supply electricity to its consumers during and in the aftermath of natural disasters. As our dependence on electrical power has increased over the years, long-term power outages can lead to devastating impacts on affected communities. Furthermore, power outages can halt the operation of water treatment plants, leading to shortages in clean water, which is essential during post-disaster recovery. One way to address this is to temporarily reconfigure power and water networks into localized networks, i.e., electric microgrids and water micro-nets, that utilize local resources to supply local demand independently of the main power grid and/or water network. Utilizing DER such as wind and solar and treating wastewater locally for potable reuse can provide the operational flexibility for such systems to operate sustainably. However, due to uncertainties in both renewable energy generation and electric/water consumption, ensuring sustainable operation is a challenging task. In this chapter, an optimal operational strategy is proposed for an islanded microgrid/micro-net, considering the stochastic nature of renewable energy resources, electric demand, and water demand. An energy storage system is modeled to address the uncertainty in power generation and demand, in conjunction with local water storage and wastewater treatment to accommodate variable water demands. A two-stage stochastic programming model is formulated and solved to determine an optimal operation strategy for the combined system.

6.1 Background

This chapter presents a coordinated water and energy operation strategy in an isolated community operating as a combined microgrid/micro-net. It has been assumed that the community is either geographically far away from the main grid or is no longer connected to it due to some disturbances causing an outage. It is shown how the limited energy and water resources can be optimally allocated to address the needs of the community. To address the uncertainty in generation and demand, a stochastic framework is considered. To do this, a two-stage stochastic programming formulation has been proposed which ensures that the demands (both water and power) are met as much as possible, at minimum cost, and with minimum amount of load shedding or shifting. In the first stage of the problem, the solution determines the amount of water to be purchased from the external source at the start of the dispatch period (e.g., a day in advance) and the amount of energy purchased to charge the battery. It is assumed that the community is equipped with a water storage tank and a CES. Then, during the second stage, the purchased resources are utilized to address the demands, while considering the expected probabilities of uncertainties in power generation, water demand, and power demand. Furthermore, load shedding and shifting decisions are considered to assist with the dispatch.

The rest of the chapter is as follows. System description is presented in 6.2, followed by scope of study and contribution of the work in 6.3. Problem formulation is presented in 6.4. A case study is discussed in section 0 for proof-of-concept purposes. Finally, the concluding remarks are presented in section 6.6 of the chapter.

6.2 System Description

This chapter considers a self-contained neighborhood, with limited energy and water resources, that tries to address its energy and water needs in a sustainable manner and with the least help from the outside world. Without loss of generality, the neighborhood is assumed to consist of multiple houses connected to a single bus. Further, it is assumed here that:

- The microgrid consists of an energy storage system (a battery in this case), a small-scale wind turbine, and rooftop PV systems for individual residential units. These generation units have uncertainties as discussed below. The choice of energy resources does not affect the generality of the problem; however, it is intended to show the impacts of uncertainties in available energy.
- Similarly in the water distribution network, a storage tank (ST) is installed to supply water demand of the community.
- The ST receives water through two means: water purchased and delivered by water tankers (or perhaps coming from the main water distribution network), or treated potable water provided by the local WWTP.
- The geographical area served by the water and energy networks is small and power losses in power distribution lines and water losses in the water system can be ignored safely.

The residential customers are at a lower elevation than the elevation of the com-munity ST, which means that water can be supplied to the households naturally due to gravity, which saves energy usage on pumping systems that would otherwise be needed. Similarly, the WWTP is located at a lower elevation than the individual households so that the wastewater from households can flow to the WWTP naturally without a need for pumping. However, the treated clean water

needs to be pumped to the ST, and the WWTP treats the incoming batch of the wastewater over a 2 h time period.

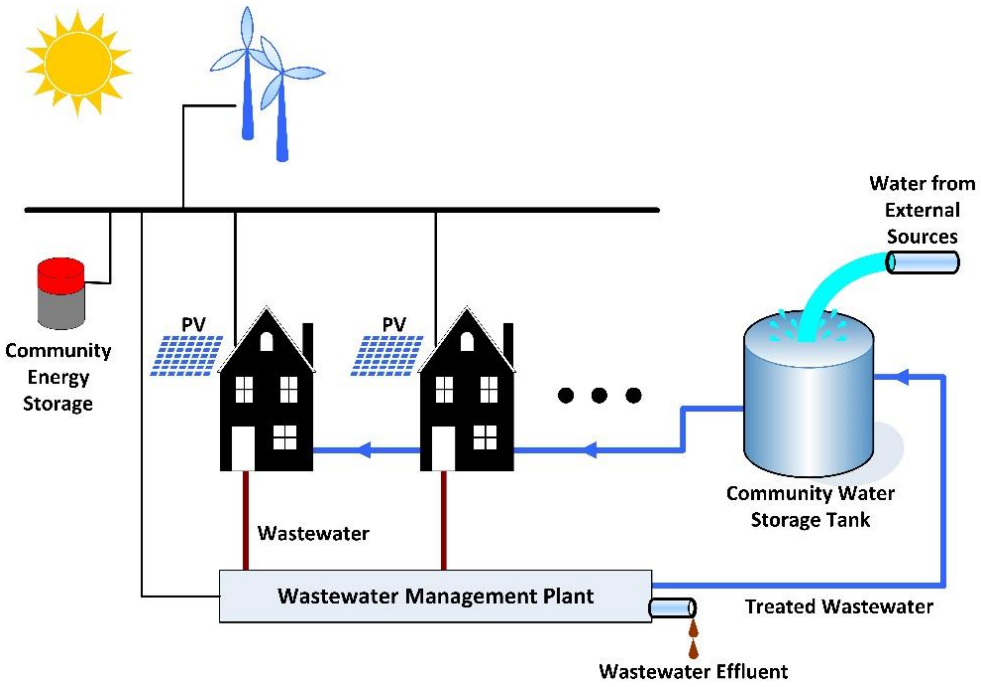

Figure 6-1 Energy and water flow diagram of the community under study. This schematic diagram shows how the energy generators and loads are connected to a microgrid bus. A ST receives water from external sources and supplies water to the community. Wastewater from households is treated in a WWTP and clean water is pumped into ST for reuse.

This chapter presents a stochastic optimization model that optimizes the combined operation of the integrated microgrid/micro-net system, considering the uncertainties associated with power generation, power demand, and water demand.

In order to model the uncertainties, a scenario-based approach is utilized in this chapter. This is adopted because it considers the system uncertainties as random input variables and assigns probabilities to each scenario based on data observations [44]. Without loss of generality, four uncertain parameters are considered, i.e., power de-mand, water demand, wind power generation, and PV power generation, each one having two levels of low and high values for each time-step

to represent hourly variations. These levels could occur based on factors such as the time of day and/or occupancy of individual residential units. For a t number of time-steps and l number of levels, the total number of scenarios for m number of uncertain parameters is l^{tm}. This has been conceptually shown for two uncertain parameters, X and Y, with two levels of uncertainty, H and L, for each, over a total of two timesteps—resulting in a combined total of 16 scenarios as indicated in Table 6-1. Each level H or L has its corresponding probability of occurrence which can be estimated using historical data. As the number of uncertain parameters or time-steps increases, the total number of scenarios will in-crease exponentially, resulting in an exponential rise in computational time [45]. This indicates that in order to solve the stochastic model with a large number of time-steps or uncertain parameters, scenario reduction techniques may be necessary [46,47].

The scenario-reduction method, however, reduces the accuracy in calculating the actual solution as it eliminates scenarios to decrease computational time. In this chapter, a sliding window approach is presented by considering a smaller number of time-steps that would significantly reduce the total number of scenarios to be computed at once. Hence, at each point in time, the proposed SP model is solved over a three-hour window to determine decision variables such as the battery SOC, the amount of loads shed/shift, and the volume of water in ST. This approach will provide a total of 4096 scenarios that are incorporated into the SP model. It should be noted that these scenarios are chosen for proof-of-concept purposes and do not affect the generality of the proposed methodology. Higher number of scenarios will improve the accuracy of the model, at the expense of the simulation time.

Table 6-1 Scenario table for uncertain parameters. L = Low, H = High

Scenario	Time 1		Time 2		Probability
	X	Y	X	Y	P
1				H	P1
2			H	L	P2
3		H		H	P3
4			L	L	P4
5	H			H	P5
6			H	L	P6
7		L		H	P7
8			L	L	P8
9				H	P9
10			H	L	P10
11		H		H	P11
12			L	L	P12
13	L			H	P13
14			H	L	P14
15		L		H	P15
16			L	L	P16

6.3 Scope and Contribution of Work

This chapter considers the quasi-steady-state operation of a microgrid and devises a strategy to maintain power balance under uncertainties. This is to ensure frequency stability in the

microgrid under various operating conditions. It has been assumed in this chapter that energy resources (PV, wind, and CES) are equipped with necessary local control systems to be able to operate in an islanded mode and generate the desired level of active power. As such, this aspect is considered outside scope for the current study.

The following are some of the contributions from the study presented in this chapter:

1) Although numerous papers in the literature have addressed the problem of optimal control and energy dispatch of electric microgrids, this thesis focuses on the co-optimization model, where both power, water, and wastewater networks are considered, along with the interconnection between the three. This aspect is less explored in the literature.
2) The proposed methodology ensures that the water distribution system, which is critical for post-disaster recovery, remains operational and available.
3) This research provides a case for investing in distributed community-scale water and energy technologies, for instance distributed wastewater treatment, rather than fully centralized approaches, which could provide a single point of failure during major disturbances.
4) Furthermore, this research demonstrates that the flexibility of a small-scale local water distribution network can be harnessed to balance load-generation in a microgrid with renewable energy resources.

6.4 Problem formulation

The main goal in this chapter is to propose a strategy to minimize the overall cost of meeting water and power demands over the dispatch period, while minimizing load shedding, given uncertainties in both water and power consumption. The problem is formulated in the form of a 2-stage stochastic optimization. The first-stage variables are assumed to be the amount of water to be purchased from an external resource and the amount of power to charge the battery before the dispatch period begins. The second stage variables consist of the dispatch (charge/discharge) schedule of the battery, operation schedule of the wastewater treatment plant, and the amounts of load shift or shed for individual users during each scenario.

6.4.1 Objective Function

The objective function is shown in (6.1). The first two terms indicate the costs of purchasing water to store in the storage tank and power to charge the battery. These are the first stage variables. The next term, weighed by the probabilities of individual scenarios, indicates the cost of discharging the battery as well as the penalties associated with load shedding. Batteries have a limited lifetime, which is typically modeled in terms of the number of deep discharge cycles. To prolong the life of a battery, it is desired to discharge it as little as possible. The discharging amount would change as the likely scenarios for power generation and demand change. This has been modeled as a cost function in (6.1). The fourth term in the objective function is used to ensure that, as much as possible, individual demands are met at the desired levels and at their desired times for each scenario. Here, when a shiftable load at time t and scenario s is served at the intended time, its corresponding binary variable will be 1 (i.e. $v_{i,t,t,s} = 1$), which indicates that the load will not be shed or shifted to a future time step and that there will be no penalty cost. Otherwise, any load

shed or shift (i.e., when $v_{i,t,t,s} = 0$) introduces a penalty into the objective function, which is weighed by the occupancy level of the house.

The cost-based approach in this formulation can be viewed in the form of penalties associated with each objective function. For instance, the cost function for the battery discourages battery usage when wind and PV system generate power. This is to prolong the life of the battery by minimizing the number of its charge/discharge cycles. Similarly, purchasing power from grid or water from an external source is discouraged using the cost (penalty) in the objective function. The big M represents a large number and is intended to, whenever technically possible, discourage load shedding in the microgrid. This is because supplying as many customers as possible if more important than the actual cost of dispatch, as is the case in any emergency dispatch strategy.

$$\min\left[c^{w}\cdot V^{\mathrm{ST,in}}+c^{u}\cdot P^{u}+\sum_{s\in S}p_{s}\cdot\left\{\sum_{t\in \mathrm{T}}c^{b}\,\frac{P_{t,s}^{b,d}}{P^{b,\max}}+M\cdot\sum_{i\in \mathrm{N}}\sum_{k\in \mathrm{T}}o_{i,t,s}\cdot(1-v_{i,t,k,s})\right\}\right] \tag{6.1}$$

6.4.2 Constraints

The multi-objective optimization problem in (6.1) is solved subject to the following constraints. It is assumed in this formulation that there will be no revenue from water distribution because water will be supplied to meet minimum demand without any cost to the users. Further, the pump operating cost is included in the battery discharging cost.

6.4.2.1 Power Balance:

At each time step and for each scenario, the total amount of power provided by the generation resources must equal the total demand, as given in (6.2). Power generation from wind and PV

resources depends on wind velocity and solar irradiance, respectively. This means that power generation level may change under different scenarios. Similarly, power demand and water demand may change according to scenarios considered, as modeled in (6.3).Since the power demand in the micro-grid is an uncertain parameter for a given time, it is divided among all customers connected to the grid using contribution factors as given in (6.4). These contribution factors can be estimated based on the historical demand profiles. This approach helps reduce the total number of scenarios to be considered for power demand. Equation (6.5)estimates contribution of shiftable and non-shiftable loads to the total power demand of a customer. It should be noted that since the system spans a small geographical area, power losses have not been considered. However, this is not necessary and actual power flow equations can be easily incorporated into the problem formulation.

$$\forall t \in \mathrm{T}, \forall s \in S : P_{t,s}^{w} + P_{t,s}^{b,d} - P_{t,s}^{b,c} = \sum_{i \in \mathrm{N}} (P_{i,t,s}^{d} - P_{i,t,s}^{\mathrm{PV}}) + P_{t,s}^{ww} \tag{6.2}$$

$$\forall i \in \mathrm{N}, \forall t \in \mathrm{T}, \forall s \in S : P_{i,t,s}^{d} = P_{i,t,s}^{\mathrm{d,NSH}} + \sum_{k=1}^{t} v_{i,k,t,s} \cdot P_{i,k,s}^{\mathrm{d,SH}} \tag{6.3}$$

$$\forall i \in \mathrm{N}, \forall t \in \mathrm{T}, \forall s \in S : P_{i,t,s}^{d,\mathrm{NSH}} = d_i \cdot P_{i,t,s}^{d} \tag{6.4}$$

$$\forall \boldsymbol{i} \in \mathrm{N}, \forall \boldsymbol{t} \in \mathrm{T}, \forall \boldsymbol{s} \in \boldsymbol{S} : \boldsymbol{P}_{i,t,s}^{d} = \boldsymbol{P}_{t,s}^{d} \cdot \boldsymbol{D}_i \tag{6.5}$$

6.4.2.2 Demand Response (load shifting and load shedding)

Demand shifting is a form of demand response, in which certain portion of demand is shifted to a future time. Since this may potentially introduce inconvenience for the customers, its application should be regulated. The constraints listed here limit the number of demand-shifting

instances. Equation (6.6)ensures that under each scenario, a shiftable load can only be shifted to one future time step, and not multiple time steps. Note that because of using an inequality, the load may be shed instead of being shifted to a future time step. This indicates a different category of demand response. In addition, (6.7)limits the number of times during the dispatch period that a customer may experience demand shifting. It should be noted that for a shiftable load at time *t* and scenario *s*, $v_{i,t,t,s} = 1$ indicates that the load will not be shifted to a future time step. Finally, it is assumed here that demand shifting is not performed partially and if scheduled, the entire load will be shifted to a future time step.

$$\forall i \in \mathrm{N}, \forall k \in \mathrm{T}, \forall s \in S : \sum_{t=k}^{\mathrm{T}} v_{i,k,t,s} \leq 1 \tag{6.6}$$

$$\forall i \in \mathrm{N}, \forall s \in S : \sum_{t=1}^{\mathrm{T}} v_{i,t,t,s} \geq T - \mathrm{TSH} \tag{6.7}$$

6.4.2.3 Battery Constraints:

In each scenario, the battery can be either charging or discharging at any point in time, but not both (see (6.8)). Also, the constraints for the state-of-charge (SOC) of the battery are represented by (6.9) and (6.10).Without loss of generality, it is assumed that prior to the dispatch period, the battery had been left depleted. It is possible to raise the charge on the battery prior to the start of the dispatch period by purchasing power from the utility. The amount of power to be purchased is a first stage variable, which is determined based on the severity and likelihoods of different scenarios. For future time steps, battery SOC will be determined based on the level at which it is charged or discharged, as well as a self-discharge rate. For any time step and any

scenario, the SOC must remain between the maximum and minimum acceptable limits, as indicated in (6.8).

$$\forall t \in \mathrm{T}, \forall s \in S : u_{t,s}^{b,c} + u_{t,s}^{b,d} \leq 1 \tag{6.8}$$

$$\begin{aligned} &\forall s \in S : SOC_{0,s} = SOC^{\min} + \frac{P^{u} \cdot \eta^{c}}{P^{\mathrm{B,max}}} \leq SOC^{\max} \\ &\forall t \in \mathrm{T}, \forall s \in S : SOC_{t,s} = (1-\gamma) \cdot SOC_{s,t-1} + \frac{P_{t,s}^{b,c} \eta^{c}}{P^{b,\max}} - \frac{P_{t,s}^{b,d}}{\eta^{d} P^{b,\max}} \end{aligned} \tag{6.9}$$

$$\forall t \in \mathrm{T}, \forall s \in S : SOC^{\min} \leq SOC_{t,s} \leq SOC^{\max} \tag{6.10}$$

6.4.2.4 Power Generation Constraints:

Power provided by the wind turbine and the PV panels depend on the wind speed and the solar irradiance, respectively (see (6.11)).The wind speed and solar irradiance vary randomly based on the scenarios in section 4, which will then be used to determine the power generated by each resource. It is assumed that all PV units receive the same amount of solar irradiance. The amount of power charged or discharged by the battery is bound by its maximum power for each time and scenario, as given in (6.12).

$$\begin{aligned} &\forall t \in \mathrm{T}, \forall s \in S : P_{t,s}^{\mathrm{Wind}} = \frac{0.5 \cdot \alpha \cdot \rho_{a} \cdot A \cdot (w_{t,s})^{3}}{1000} \\ &\forall i \in \mathrm{N}, \forall t \in \mathrm{T}, \forall s \in S : P_{i,t,s}^{\mathrm{PV}} = P_{i}^{\mathrm{PV,STC}} \frac{\Phi_{t,s}}{\Phi^{\mathrm{STC}}} \end{aligned} \tag{6.11}$$

$$\forall t \in \mathrm{T}, \forall s \in S : \begin{cases} 0 \leq P_{t,s}^{b,d} \leq P^{b,\max} u_{t,s}^{b,d} \\ 0 \leq P_{t,s}^{b,c} \leq P^{b,\max} u_{t,s}^{b,c} \end{cases} \tag{6.12}$$

6.4.2.5 Water Demand Constraints:

For each scenario, the total amount of water flow provided by the storage tank to the community should equal the total water demand, which is a sum of individual customer's water demands. At the beginning of the dispatch period, it has been assumed that the tank had been filled to the minimum level, and the neighborhood has the option of purchasing water from an external resource prior to the realization of various scenarios as given in (6.14). This amount of purchased water is a first stage variable. This water purchase from external sources may be necessary because the WWTP is assumed to take at least 2 hours to treat the water obtained from the residential neighborhood as given by zero outflow from WWTP in (6.15) during time steps 1 and 2. The volume of water in the ST is determined based on the amount of inflow to and outflow from it (see (6.16)).Total volume of water in the ST should be within the acceptable range as indicated in (6.17).

$$\forall t \in \mathrm{T}, \forall s \in S : \sum_{i \in \mathrm{N}} q_{i,t,s}^{d} = q_{t,s}^{\mathrm{ST,out}} = Q_{t,s}^{d} \tag{6.13}$$

$$\forall s \in S : V_{0,s}^{\mathrm{ST}} = V^{\mathrm{ST,in}} \tag{6.14}$$

$$\forall s \in S : q_{1,s}^{\mathrm{ww,out}} = q_{2,s}^{\mathrm{ww,out}} = 0 \tag{6.15}$$

$$\forall t \in \mathrm{T}, \forall s \in S : V_{t,s}^{\mathrm{ST}} = V_{t-1,s}^{\mathrm{ST}} + q_{t,s}^{\mathrm{ww,out}} \cdot \Delta - q_{t,s}^{\mathrm{ST,out}} \cdot \Delta \tag{6.16}$$

$$\forall \boldsymbol{t} \in \mathbf{T}, \forall \boldsymbol{s} \in \boldsymbol{S} : \boldsymbol{V}^{\mathrm{ST,min}} \leq \boldsymbol{V}_{\boldsymbol{t,s}}^{\mathrm{ST}} \leq \boldsymbol{V}^{\mathrm{ST,max}} \tag{6.17}$$

6.4.2.6 Wastewater Management Constraints:

A certain fraction of water discharged from the customers collects at the WWTP to be treated (see (6.18)).Considering the hourly timeline of this problem formulation, this has been considered to occur at the same time step *t*. Flow through pipes is limited by the maximum allowable rate, as indicated in (6.19). The volume of wastewater in the WWTP is determined based on the amount of inflow to and outflow from it (see (6.20)). This value should be within the acceptable range as shown in (6.21). Finally, the amount of power consumed for treating the wastewater and pumping it to the reservoir is assumed to be proportional to the volume of wastewater treated, as shown in (6.22). Constraint (6.23) ensures that there is no waste outflow during the first two hours of the study period because WWTP will take 2 hours of treatment.

$$\forall t \in \mathrm{T}, \forall s \in S : \sum_{i \in \mathrm{N}} q^{d}_{i,t,s} = k^{ww} \cdot q^{ww,\mathrm{in}}_{t,s} \tag{6.18}$$

$$\forall i \in \mathrm{N}, \forall t \in \mathrm{T}, \forall s \in S : q^{d}_{i,t,s} \leq q^{\max} \tag{6.19}$$

$$\forall t > 1, \forall s \in S : V^{ww}_{t,s} = V^{ww}_{t-1,s} + q^{ww,\mathrm{in}}_{t,s} \cdot \Delta - q^{ww,\mathrm{out}}_{t,s} \cdot \Delta - q^{ww,\mathrm{eff}}_{t,s} \cdot \Delta \tag{6.20}$$

$$\forall t \in \mathrm{T}, \forall s \in S : V^{ww,\min} \leq V^{ww}_{t,s} \leq V^{ww,\max} \tag{6.21}$$

$$\forall t \in \mathrm{T} : P^{ww}_{t,s} = (p^{ww} + p^{\mathrm{pump}}) \cdot q^{ww,\mathrm{out}}_{t,s} \tag{6.22}$$

$$\forall s \in S : q^{ww,\mathrm{eff}}_{1,s} = q^{ww,\mathrm{eff}}_{2,s} = 0 \tag{6.23}$$

6.5 Case study

6.5.1 Solution Methodology and Input Data

A hypothetical electrical microgrid is considered as the case study in this thesis that consists of 3 residential units. As discussed in section 4, four uncertain parameters are considered, i.e., wind power generation, PV power generation, total electrical demand in the network, and water demand in the water distribution system. Each of these parameters are assumed to have a high and a low level and change on an hourly basis. Data for wind and PV power generation and the energy demand of the customers are estimated using the data available from the US Department of Energy, National Renewable Energy Laboratory, National Solar Radiation, and Residential Energy Consumption Survey as explained in [171]. Similarly, household occupancy is estimated based on the data provided in the same paper. The water demand for customers is modeled considering the estimated data provided by U.S. Geological Survey (USGS) in [168] which indicates that on average each person uses about 100 gallons of water on the higher end per day. This study accounts for the occupancy levels of the households to estimate total water use per household per day. It should be noted that the values of all input parameters are chosen for demonstration purposes only and as such, they do not affect the generality of the problem. Further, it is assumed that each household consists of a combination of shiftable and non-shiftable loads as given in Table 6-2. It is assumed that approximately 60% of energy demand is for non-shiftable loads and 40% for shiftable loads. Table 6-2 provides energy per day for a typical single-family household adopted from EIA data [172].

Table 6-2 Energy consumption of a single-family household per day

Non-Shiftable Loads	kWh	Shiftable Loads	kWh
General lighting loads, cooking stove, oven, microwave, and refrigerator	18	Dishwasher, laundry machine and dryer, TV, and other non-essential electronics	12

Data in Table 6-2 is based on an average 30 kWh of energy usage per day for a single-family household (877 kWh per month) with two occupants. Loads such as general lighting, cooking and microwave, and refrigerator are considered basic non-shiftable loads since their interruption could lead to inconvenience. This accounts for 60% of total household energy consumption. However, other appliances such as the dishwasher, washer and dryer, and TVs are considered to be shiftable, since their operation times can be changed without significantly impacting the residents. This accounts for 40% of total household energy consumption. Since household occupancy affects the energy consumption of both shiftable and non-shiftable loads, different occupancy profiles (ranging from one occupant to five occupants) have been considered for the customers in the community in order to introduce diversity in energy consumption of the houses. Maximum allowable number of times during the study period that a customer may experience demand shifting (or TSH) is assumed to be 1. For the data on Φ^{STC}, α, SOC^{min}/ SOC^{max}, γ, c^B, and η^c/η^d readers are referred to [173]. A single wind turbine is considered for this study, with diameter of approximately 7 meters (200 m^2 swept area). The air density ρ_a is assumed to be 1.25 kg/m^3. $P_i^{PV,STC}$ values of 5 kW to 10 kW in each house have been assigned to reflect the PV generation of each customer [160]. The CES is considered to be sized at 140kW. It is assumed here that the water distribution system is already in place and the maximum flow per house is 0.0001262 m^3/s

(2.0 gallons per minute (GPM)) at 41 m head (approximately 60 pound per square inch (PSI)) as recommended in [161].

The proposed optimization formulation is solved using the GAMS software in an Intel® Core™ i7-8750H CPU @ 2.5 GHz – 2.21 GHz computer. As expected, the solution time increases with an increase in the number of scenarios. Two cases have been considered: The first case (case 1) considers two time-steps of analysis, hence a total of 256 different scenarios (4 variables, at 2 levels each, over 2 timesteps). The second case (case 2) considers three time-steps instead, raising the total number of scenarios to 4,096. The solution time for case 2 is approximately 19 minutes on average with median convergence time of 13 minutes and standard deviation of 23 minutes which is significantly higher than that of case 1 at less than 2 seconds on average. The model converged during all the test runs.

6.5.2 Results and Discussion

Table 6-3 lists the results of the analysis for both cases. For case 1, the community would need to purchase 12.92 kWh of electrical energy at the beginning of the study period in order to meet the energy needs for the next 2 hours (i.e., the duration of the study period). Similarly, 6.48 m^3 of water is necessary to properly meet the water needs of customers. The CES would need to supply 19.48 kWh of electricity at a cost of $13.88. On average, it would cost approximately $10.83 per hour for the community to meet their energy and water needs. Considering the dispatch over a 3-hour period, 3 kWh of electricity and 6.48 m^3 of water are needed from external sources in order to meet the energy and water needs. In this case, the CES would need to supply a total of 19.94 kWh to account for insufficient generation from wind and PV. This would cost approximately $7 per hour. It is important to note that having more information about the future

may support the decision process for the system operator since more possible scenarios are considered. However, in the general case, it does not indicate that more information will guarantee a more favorable (i.e., less expensive) solution.

Table 6-3 Solution of the proposed co-optimization problem

Case	**Case 1 (2 Time Steps)**		**Case 2 (3 Time Steps)**	
Objective Function	Value	Cost ($)	Value	Cost ($)
Power purchased from utility (kWh)	12.92	1.29	3.01	0.30
Water purchased (m3)	6.48	6.48	6.48	6.48
Average battery operation (kWh)	19.48	13.88	19.94	14.20
Total Cost ($)	21.65		20.98	
Probability of load shedding or shifting on average*	0.68%		0.043%	
Total cost per hour ($)	10.83		6.99	

*The average probability of demand response represents how likely it is for any customer to see either load shedding or shifting considering the probability of different scenarios for power generation and demand. A 0% value indicates that the microgrid has sufficient power generation to meet the demand for all possible scenarios considered in the study.

The following sections further discuss the results of the case studies for three strategically chosen scenarios. While the overall results are summarized in Table 6-3, these three individual scenarios are provided for demonstration purposes, and in general do not have any uniqueness over

other scenarios modeled. Instead, they represent the overall pattern in the output of the formulation as the uncertain parameters change their values.

The following scenarios are compared to demonstrate the results of case 2:

- Scenario 1: This scenario represents operating conditions during which power generation is less than power demand in the microgrid with high water demand.
- Scenario 2: This scenario represents operating conditions during which power generation is more than power demand in the microgrid with low water demand.
- Scenario 3: This scenario represents operating conditions during which power generation and demand in the microgrid are close in value with average water demand.

Figure 6-2 shows the power generation level from different sources (wind, PV, and battery discharging) and the power demand (household energy demand, WWTP power demand, and battery charging) for each time-step. During scenario 1, there is approximately 46 kW of demand during time step 3 in the microgrid which is being supplied from the primary generation sources of wind (26 kW) and PV (20 kW). Because generation is sufficient to supply the entire demand, the battery is neither charging nor discharging (also shown by the constant SOC level in Fig. 3 for scenario 1 time-step 3). On the other hand, for time-step 2 during scenario 1, the CES is discharging at the rate of approximately 45 kW because during that time, the total demand (approximately 103 kW) is more than the power generated by primary sources (approximately 58 kW from wind and PV). Similarly, during time-step 1 of scenario 1, the CES is discharging at the rate of 25 kW. For scenario 2, during which power generation is more than the demand, the battery is charging at the rates of approximately 4 kW and 13 kW at time-steps 1 and 3, respectively. This way, the stored energy can be utilized when needed. During scenario 3, the total generated power from wind and

PV is close to the power demand in time-steps 1 and 2 but not completely enough to meet the entire demand. Hence, CES discharges at a lower rate of 4 kW in both times compared to scenario 1. The primary sources meet the power demand during time-step 3, which means the CES system is offline, as shown in the graph.

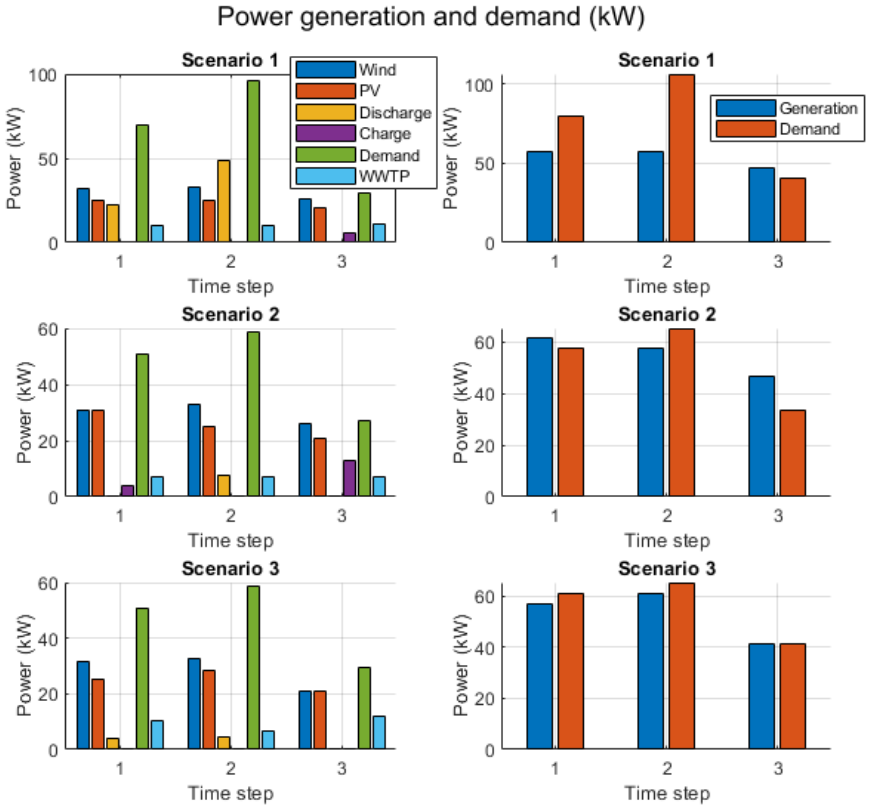

Figure 6-2 Graphs on the left show hourly power generation from individual sources at different time steps and power demand at corresponding times, during the three representative scenarios. The graphs on the right-side illustrate the total power generation (from wind and PV) and total power demand, for different scenarios and at different times.

The CES system stores power from the external source (grid) prior to time-step 1, as shown in Figure 6-3. The figure also shows the variations in the SOC of the battery as it undergoes charge

and discharge cycles. As expected, the battery can be either charging or discharging at a given time-step, but not both.

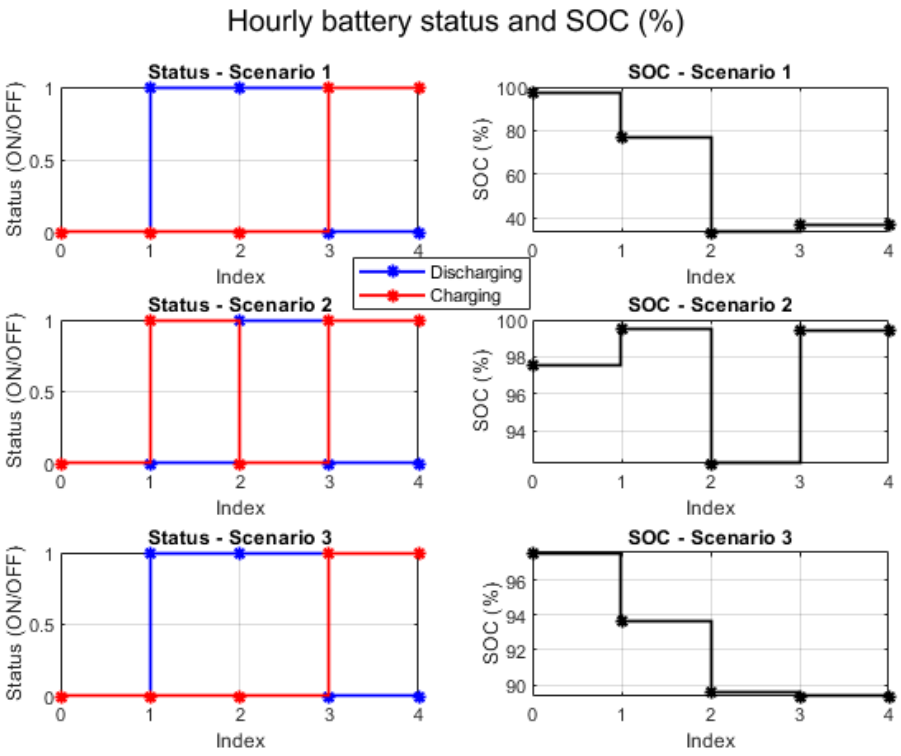

Figure 6-3 Hourly battery status (ON or OFF) and battery SOC for the three scenarios. For all scenarios, the battery is initially charged at 98%. As expected, scenario 1 indicates a significant drop in battery SOC, whereas in scenario 2, the battery undergoes some instances of charging. Scenario 3 also shows discharge; however, at a significantly lower rate than that of scenario 1.

Depending upon available generation and demand, there may be instances of demand response in order to ensure the power balance in the microgrid. Figure 6-4 shows the instances of load shedding in the microgrid. It can be seen that customer 3 experiences load shedding during time-step 1 of scenario 1 (when generation is not enough to meet the demand).

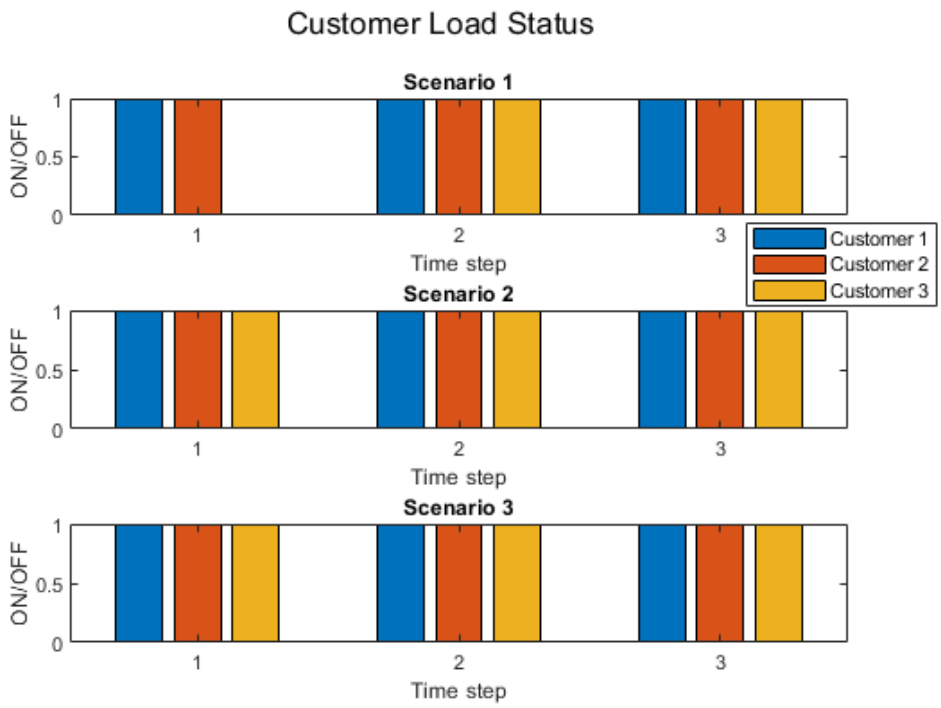

Figure 6-4 Load shedding or shifting instances during all three scenarios. During scenarios 2 and 3, there is sufficient generation to meet the demand; therefore, no load shedding or shifting is performed. However, during scenario 1, customer 3 experiences a load shed for time-step 3 (although not during times 1 or 2).

Finally, Figure 6-5 shows the operation state of the water network. It can be seen that the WWTP starts supplying water to the ST at the beginning of time-step 3, which is then used to meet the water demand for that time-step. During the first two hours of operation there is no outflow from the WWTP even though there is increase in its volume. This is because it takes time for the WWTP to treat the wastewater received from the residents. As expected, the water volume in the ST decreases to respond to the water demand in the system. Depending upon the water demand rate for a given scenario, the water level in the ST may change at a higher or lower rate than other scenarios for the same time step.

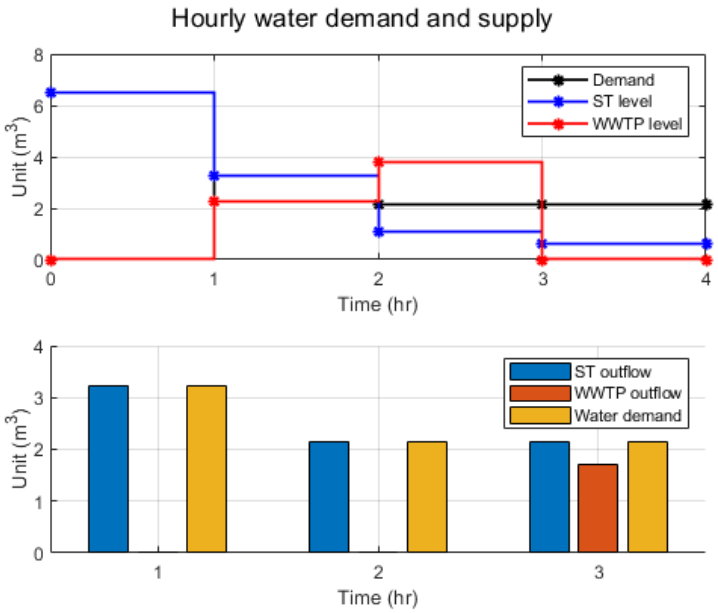

(a)

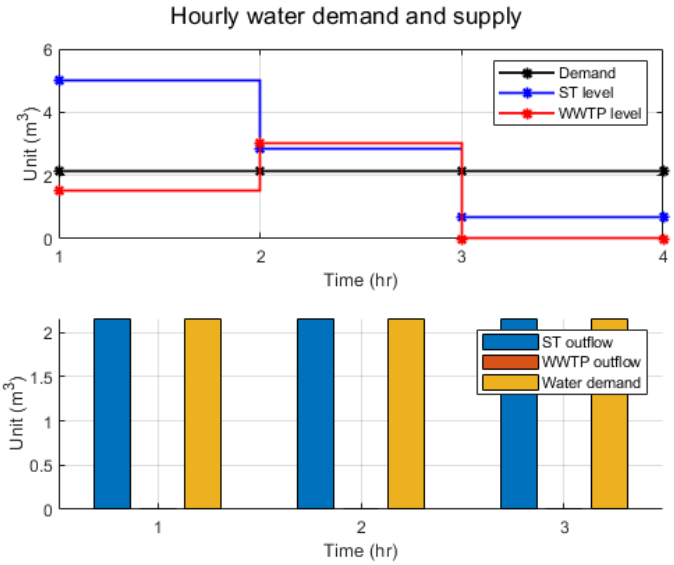

(b)

Figure 6-5 (a) Hourly water volume in ST and WWTP during scenarios 1 and 3. (b) Hourly water volume in ST and WWTP during scenario 2.

As given in Figure 6-5 (a), during time-steps 1 and 2, the total water demand is being supplied by the outflow of ST. There is no outflow from WWTP for first 2 hours of operation but

there is an increase in its volume as the customers use water during these time steps. During time-step 3, the WWTP starts supplying water to the ST, which in turn, supplies water to meet the demand, Since the ST tank has enough water to supply the low water demand for scenario 2 the WWTP does not need to be run for this scenario as shown by zero outflow in Figure 6-5 (b). The wastewater that was stored in time steps 1 and 2 will flow out of WWTP as effluent as indicated by the reduced water volume in WWTP for time step 3.

6.6 Conclusions

This chapter presented a strategy for combined water and energy operation in an isolated community that is operating as a microgrid/micro-net. It is assumed that the community has been disconnected from the main power grid and the water distribution network due to a large disturbance such as a natural disaster and is expected to operate in a standalone mode. To do this, the community is assumed to be equipped with a battery system, renewable energy resources such as a wind turbine and multiple rooftop PV panels, a water storage tank, and a wastewater treatment plant that is capable of providing potable water. The problem was formulated as a two-stage stochastic optimization one, where the main objective is to supply the demand (water and power) as much as possible, at minimum cost, subject to the uncertainties in both demand and renewable generation. In the first stage, the problem determines the amount of water to be purchased from the outside world (if any) and the amount of power to be purchased from the main grid to initially charge the battery (if any). These are then optimally allocated using the second-stage recourse variables during the dispatch period. Recourse variables consist of the amount of charge/discharge of the battery at any point in time, the level of load shift/shed for each customer at any point in time, the operation status of the wastewater treatment facility, and the amount of water to be

provided to the community by the storage tank. It was shown through a proof-of-concept case study that limited resources can be optimally allocated to allow for the continued operation of the community until services become available from the outside world. To improve tractability of the optimization problem, a sliding window approach was used where the problem was solved for a time horizon of 2-3 hours at a time. Extending the simulation time can significantly increase the number of variables to be considered, which for off-the-shelf optimization software packages, may negatively impact the convergence rate or simulation time. However, such limitation will not exist in commercial optimization packages.

CHAPTER 7

DECOMPOSING A POWER AND WATER NETWORK TO INTERCONNECTED ELECTRICAL MICROGRIDS AND WATER MICRONETS

In case of the loss of electrical grid due to natural or manmade disturbances millions of energy users can experience extended power outages across the region due to potential damages to generators, power transmission lines, power substations, communication network, or the fuel supply system. The changing climate is one of the major reasons for the recent increase in the frequency of natural disasters, and scientists predict that the number, duration, and severity of events are likely to increase year by year. Power restoration and recovery of other critical infrastructure can take weeks and months depending on the geographical region affected and the level of damages. One way to expediate power restoration efforts and reduce duration and number of power outages in a disaster affected area is to utilize locally available resources (e.g., water and energy) to allow the community to operate in a self-reliant manner until the time that service to the main power grid is restored. This has in part become possible due to the high penetration of renewable energy resources in the power grid at both transmission and distribution levels. For the latter, small-scale wind, rooftop PV, and community energy storage systems are being installed to help residential customers offset their electrical power demand and potentially sell electricity back to the grid when there is less energy need at the homes than power generation from the energy resource. Under emergency conditions, these resources can be coordinated and utilized to meet the local energy needs in case of power outages from the main grid. In 0 a solution was proposed to design a microgrid/micronet system using local energy and water resources. Then, in 0 an optimization dispatch strategy was proposed to operate the system. In this chapter, the problem is

viewed from the perspective of the power grid, i.e., how, in the wake of a natural disaster, a power distribution grid and water distribution network can be broken into multiple microgrids and micronets in order to allow for localized supply of energy and water. A graph theoretic approach is proposed, which is able to weigh nodes and edges based on their individual criticality levels as well as their overall impact on the integrity of the system.

7.1 Introduction

Electrical power network spans a large geographical area that extends from generation stations to load centers. Depending on the location of generators and loads, long transmission and distribution overhead lines are installed to connect the two. At the distribution level, the electrical power grid serves a wide range of energy users in terms of their load types, namely residential, commercial, and industrial. While the last two groups of loads may be equipped with some level of local generation for emergency conditions, residential loads are usually left without power during large-scale outages. Although the damages of long-term outages to residential loads is not financial (compared to commercial and industrial), the social and psychological impacts of long-term outages on users can be far more damaging. Losing power for several hours in cold winter, as was the case in Texas recently, can result in unsuitable living conditions specially for children or people with compromised health conditions. The same can be said about power outages during hot summer months and lack of A/C. In addition, losing power can have irreversible impacts on people who depend on electricity for health reasons, for instance to power their breathing devices. However, the impact of power outages are not limited to supply of electricity. Power grid provides supplies water treatment facilities, wastewater management plants, hospitals, communication

systems, traffic systems, and police stations, which are all critical facilities that must receive reliable power to ensure safety and security of the community.

Of all the critical infrastructure, power and water networks are most directly related to the health, safety, and security of a community. While reinforcing the entire power grid and water network against all possible disaster is neither cost-effective nor feasible, it is possible to adopt a self-healing approach to break the system into multiple small-scale systems (electric microgrids and water micronets) so that they can continue operating in a localized fashion. This can help reduce the social impacts of disaster-induced outages on a community that has been affected by a natural disaster.

This chapter is organized as follows. In section 7.2 a proposed methodology of breaking the original network into multiple clusters is presented with necessary assumptions. Section 7.3 presents case study and discussion. Finally, section 7.4 presents the concluding remarks of the chapter.

7.2 Proposed Methodology

7.2.1 Preliminaries and Assumptions

In this study, we model an electrical power grid or a water distribution system as a graph G(V, E) where V represents the vertices of the graph (or nodes), and E represents the edges connecting those nodes. The nodes represent load points or users of electricity or water, i.e., demand centers. It is assumed that some nodes in the network are equipped with DER for power supply or ST for water supply. The edges represent a connection between nodes and could be thought of as the power distribution lines in the energy network or water pipes in the water

network. It is assumed here that each node in the energy network has a certain weight depending upon the type (residential, commercial, or industrial) and criticality level of the loads connected to it. Nodes are particularly considered critical if they serve socially vulnerable neighborhoods in which residents may not be able to evacuate upon need or may be at higher risk against the natural disaster due to physical or financial limitations. The lines connecting the nodes also have weights which are determined based on their length and their resilience against natural disasters. Similarly, the graph for water distribution system has nodes and edges with their corresponding weights whose values are determined using the same logic as that of the power grid.

In addition, the proposed methodology considers that the power grid consists of several DERs that are capable of generating power on their own (i.e., without external help) after a power failure in the network. Such generators are referred to as black start capable units and do not relay on external power (for instance batteries or auxiliary generators) to run and supply power. Solar, wind, hydro, and battery storage units, if equipped with appropriate controllers, can be used as black start generators. The following step 1 describes in detail the methodology of graph formation and the weights computation for nodes and edges of the graph.

7.2.2 Decomposition Approach

7.2.2.1 Step 1: Graph Formation

The energy or water network is modeled as a single weighted graph. The following parameters are defined for each graph:

c_{ij} measure of closeness between node *i* and node *j*, based on the number of neighbors they share. If N(*i*) represents the set of neighbors of node *i* and |N(*i*)| is the dimension of this set (i.e., the number of its elements), closeness is defined as:

$$c_{ij} = \frac{|N(i \cap j)|}{|N(i \cup j)|}$$

The value of closeness ranges from 0 to 1, with larger numbers indicating nodes with a larger number of shared neighbors.

d_{ij} physical distance between node *i* and node *j*, normalized for the graph so that all distances are between 0 and 1. Larger values indicate longer distances between nodes.

r_{ij} resilience of the edge connecting nodes *i* and *j* against the natural disaster of interest. A number between 0 and 1, where 0 indicates least resilient and 1 indicates most resilient edge in the network.

v_i weight of node *i*, i.e., could indicate the criticality level of the node. The weights need to be normalized so that they all lie between 0 and 1, where smaller values indicate higher criticality

The edge weights are then updated using the above criteria as shown below. In this proposed heuristic model, larger weights indicate nodes that are likely not going to belong to the same microgrid or micronet. In other words, it represents a high cost for maintaining the (electrical or water) connection between the two.

$$w_{ij} = \frac{v_i + v_j}{2} \cdot \frac{d_{ij}}{c_{ij} \cdot r_{ij}} \tag{7.1}$$

Once the graph is formed and appropriate weights are assigned for the nodes and edges, the next step would be to identify initial clusters of the microgrid.

7.2.2.2 Step 2: Initial Clusters of Microgrids

The focus in this step is on the quasi-steady-state operation of the microgrids. In other words, it is assumed that microgrids are equipped with the well-known control algorithms based on master-client or droop-control for dispatching their generation units as well as means for resynchronization if two or more microgrids are to be connected to form a bigger network.

Here, we form microgrids around individual DER units with black start capability by assigning different load nodes and other non-black-start-capable DER resources to those units. These will be the medoids of the clusters and other nodes will be assigned to the closest medoid based on the weights derived above. Hence, the number of clusters will be equal to the number of black start capable units.

The outcome of this step is a series of microgrids that serve as the initial configuration of the post-disaster power system. Each node is now assigned to one cluster. The solution is acceptable if each cluster (microgrid) has sufficient generation capacity to supply its peak load. If this condition is met, it is considered that the cluster has load generation balance, and the cluster is self-sufficient in terms of power supply. Otherwise, there needs to be power exchange from neighboring clusters, as described in the next step.

7.2.2.3 Step 3: Microgrid Expansion

If the generation capacity condition is not met for one or more microgrids, they need to connect to (i.e., merge with) other microgrids with excess generation. Note that another option would have been to install backup local generation at the microgrids with power deficiency to be able to meet the load. However, our focus in this work is on edge reinforcement. This is because edges are used during both normal and post-disaster operation, whereas the usage of backup power will mostly be beneficial for emergency situations, so may not be the most effective investment.

Merging two microgrids is achieved by reinforcing the line connecting them. The cost of reinforcing a line connecting nodes *i* and *j* against the natural disaster is assumed to be inversely proportional to its resilience factor r_{ij}.

We first perform the following analysis:

- For each cluster, we find all edges that connect it to all other clusters
- Consider clusters c and k:
    - Consider all edges connecting the two clusters
    - Rank all edges based on their resilience and distance, i.e., r_{ij} / d_{ij}
    - The edge with the highest rank is selected as a candidate for reinforcement. The combination of the length of this edge and its resilience against the natural disaster makes it ideal for connecting the two clusters
    - For ease of representation, this edge is now referred to by index *ck*, since it is the candidate edge to connect clusters *c* and *k*. Every other edge is discarded.

For each cluster *c*, we then define the following:

D_c peak electric demand for cluster *c* (kW)

P_c maximum generation capacity for cluster c (kW)

S_c shortage of generation capacity in cluster c (kW), which is equivalent to loss of load

u_{ck} Binary value indicating if clusters c and k are connected (1 = connected, 0 = not connected). This connection is made through the candidate edges as found above

The goal is to simultaneously minimize the lost load and the cost of network reinforcement.

$$\min \left\{\sum_c S_c\right\}, \left\{\sum_c \sum_{k,k\neq c} u_{c,k} \frac{d_{c,k}}{r_{c,k}}\right\} \tag{7.2}$$

Subject to:

$$\forall c : S_c = P_c + \sum_{k,k\neq c} u_{k,c} P_k - D_c - \sum_{k,k\neq c} u_{k,c} D_k \tag{7.3}$$

7.2.2.4 Step 4: Water Network

The algorithm presented for the power system can also be applied to the water network. Steps 1 through 3 are the same, except that instead of generation capacity and peak demand, we consider water storage capacity and water demand. The critical nodes should be served with higher priority, and they will have lower weights (same as in the electrical network). For water network the following parameters are defined:

ST_c water storage capacity for cluster c (m^3)

WD_c average daily water demand for cluster c (m^3)

WS_c water shortage in cluster c (m^3)

u_{ck} Binary value indicating if clusters c and k are connected (1 = connected, 0 = not connected). This connection is made through the candidate edges as explained in step 3 above.

The goal is to simultaneously minimize the water shortage and the cost of network reinforcement.

$$\min \left\{ \sum_c WS_c \right\}, \left\{ \sum_c \sum_{k,k \neq c} u_{c,k} \frac{d_{c,k}}{r_{c,k}} \right\} \tag{7.4}$$

Subject to:

$$\forall c : WS_c = ST_c + \sum_{k,k \neq c} u_{k,c} ST_k - WD_c - \sum_{k,k \neq c} u_{k,c} WD_k \tag{7.5}$$

The initial clustering will be based on the storage tanks, i.e., nodes with a tank will be the medoids of the clusters. We assume that all storage tanks are equipped with the necessary pumping stations. Of course, this is not necessary if all demand points are located at a lower elevation compared to the storage tank, but we consider the more general case. Once the initial clusters are identified, all other nodes will be grouped based on their closeness to the medoids, similar to the microgrid expansion problem explained in step 3 above. In case of the water network, the goal would be to minimize the difference between water supply and water demand for each cluster and the cost of network reinforcement. Once the clusters for both water and power networks are identified, the last step is to interconnect the water micronets to the best power microgrids.

7.2.2.5 Step 5: Water-Energy Interconnection

The pumping stations and water treatment facilities in the water clusters need to be supplied with electricity in order to be able to treat and supply water to the community. For all water clusters, each node with ST will be connected to the "closest" electrical node. The closeness is defined here as having the smallest d_{ij} / r_{ij} which indicates that a short power line that is more resilient against potential disturbance will be chosen to interconnect the water cluster with a power cluster.

7.3 Case Study and Discussion

7.3.1 IEEE123 Electrical Power Grid

We consider an electrical power grid with 129 nodes as provided in the IEEE 123 bus test distribution system (Figure 7-1). This represents the original power network with no partitions. The nodes are presented by black circles and edges are represented by red lines. The information about nodes is provided in Appendix C, where the nodes, edges, edge weights, node weights, and the power generation and power demand at each node are listed.

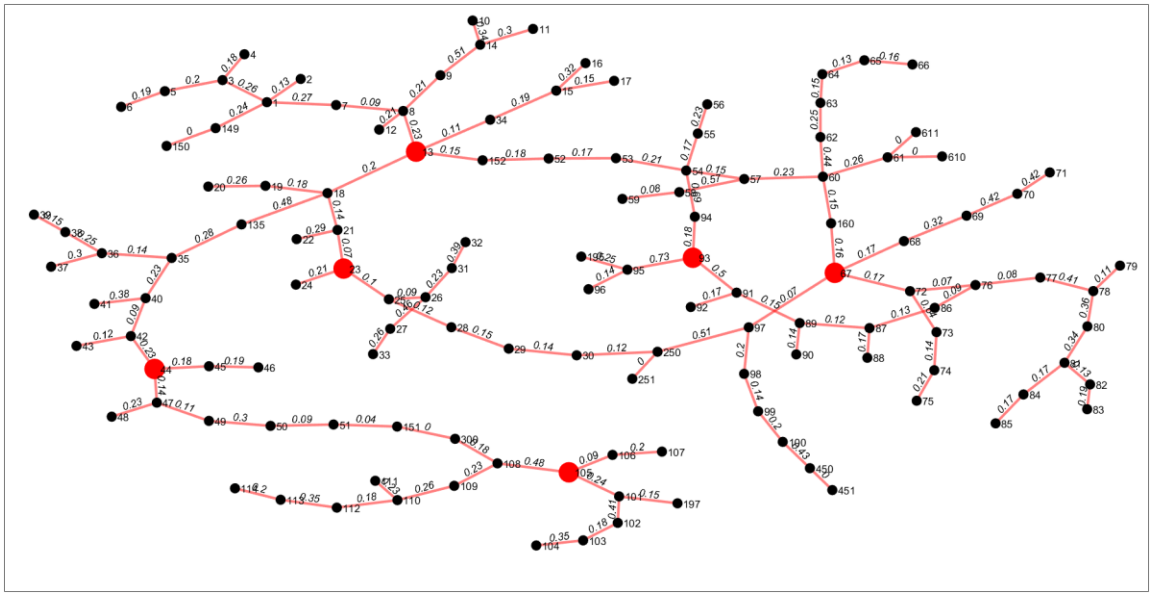

Figure 7-1 Graphical representation of IEEE 123 test distribution system. Red color nodes represent those with black start capable generators.

Six nodes (13, 23, 44, 67,93, 105 – all denoted in red) are assumed to be equipped with black start capable generators (i.e., the medoids of partitions). All other nodes are grouped around the medoids depending upon the edge weights as described above. Table 7-1 shows the weight assignment for different critical or non-critical nodes of the graph. It should be noted that this classification and the corresponding node assignment is made for demonstration purposes only and does not affect the generality of the problem.

Table 7-1 Node types and weights of nodes depending upon the nature of the node

Node Classification	**Node number**	**Node weight (v_i) depending upon the nature of the node**
Critical	21, 25, 51, 76, 86	Hospitals, pumping stations, water treatment systems, residential customers with vulnerable population Weight = 1
Essential but no critical	65, 113, 97	Essential commercial loads such as grocery stores and schools Weight = 0.6
Non-critical	Remaining nodes in the graph	All other loads in the network Weight = 0.4

The power distribution lines are usually overhead conductors and the distribution transformers serving customers are separated by a few spans of overhead lines. Longer spans are more vulnerable to disturbances compared to shorter ones. This indicates that generally longer lines are less resilient than shorter lines (although exceptions exist). Table 7-2 illustrates the resilience weights assigned to different edges (lines). Again, this is for demonstration purposes only.

Table 7-2 Edge length and resiliency weight in power network

Power line length	Edge resiliency weight (r_{ij})
Short edge (0 to 50 meters)	1
Medium edge (50 to 250 meters)	0.5
Long edge (> 250 meters)	0.2

Using the algorithm presented above, the graph in Figure 7-1 is partitioned into six clusters as shown in Figure 7-2 below.

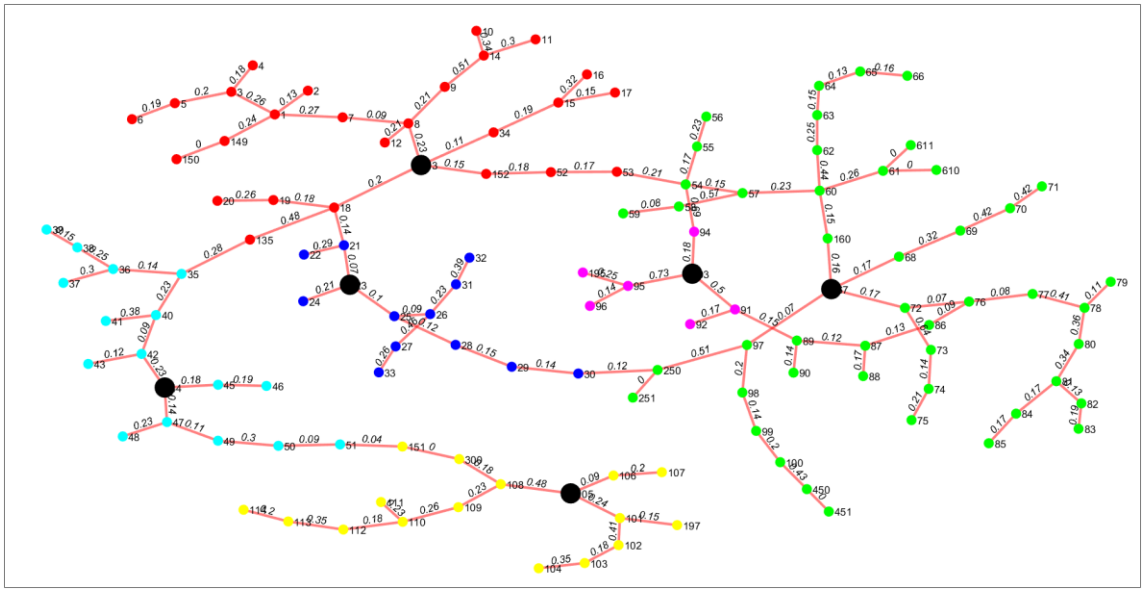

Figure 7-2 Electrical microgrid partitions based on node and edge weights. Six clusters are created (red, blue, cyan, green, magenta, and yellow) with center nodes (black) representing black start capable generators.

Once the partitions formed, the load and generation balance in each cluster is maintained by utilizing the available generation within the cluster as much as possible. However, when total load in a cluster is more than available generation in that cluster there needs to be power supply from

external sources (clusters). In order to import power from neighboring clusters, the edges are reinforced such that in case of disturbances power can still be exchanged between the clusters. Figure 7-3 shows the proposed edge reinforcements.

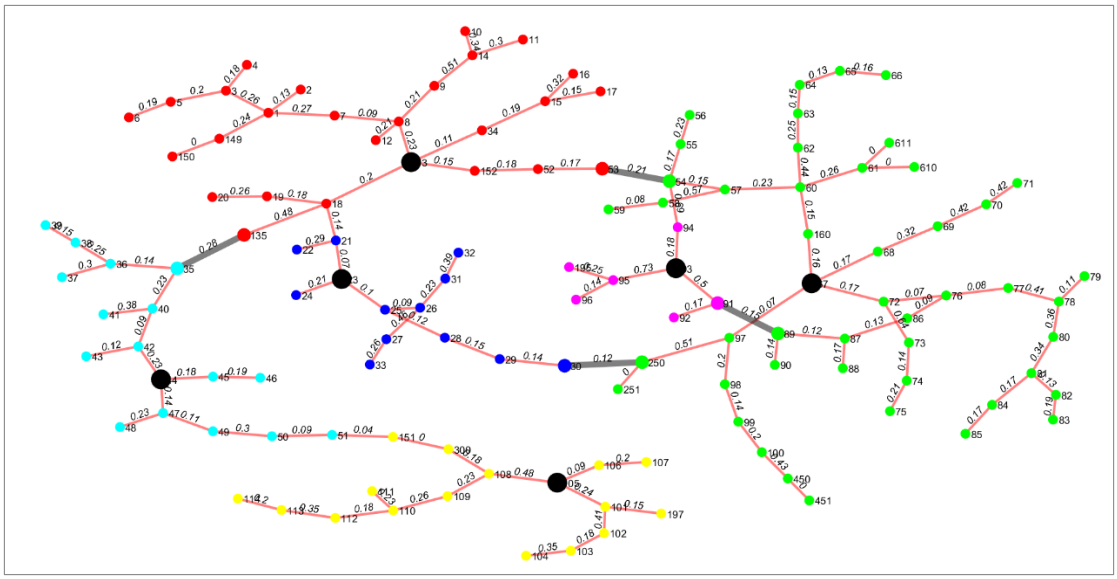

Figure 7-3 Edge reinforcement of microgrid. The brown highlighted edges represent reinforcement. There is power exchange between Cyan – Red clusters, Green – Magenta clusters, Red – Green cluster and Green – Blue clusters.

Table 7-3 shows power demand and generation in each cluster and connection made after solving the optimization model. In the table, 1 indicates that connection is made (reinforcement applied) whereas 0 represents no reinforcement applied. As shown in Figure 7-3 and Table 7-3, only edges connecting neighboring clusters are reinforced which indicates that the cost of reinforcement in the microgrid is small because there is no need to exchange power outside of the neighboring clusters. In other words, the neighboring clusters have sufficient generation in case a cluster has higher demand than its available generation.

Table 7-3 Power generation and load in each cluster and edge reinforcement

Cluster	Load	Generation	Red	Blue	Cyan	Green	Magenta	Yellow
Red	930	575	0	0	1	1	0	0
Blue	485	375	0	0	0	1	0	0
Cyan	790	880	0	0	0	0	0	0
Green	1265	1605	1	1	0	0	1	0
Magenta	0	230	0	0	0	0	0	0
Yellow	20	440	0	0	0	0	0	0

7.3.2 Water Distribution Network

The water distribution network given in [174] is taken as a case study and is modified for this study. This is a 130-node water network, whose data including the edge weights, node weights, water demands, and water storage capacities are provided in Table C.2 in the Appendix C.

Similar to the energy network described above, the water network nodes are represented by blue squares and pipes are represented by dashed grey lines. Since the pipes are generally underground, they are less vulnerable to natural disasters (compared to the overhead power lines). Table 7-4 is used to compute edge weights between any two nodes.

Table 7-4 Edge length and resiliency weight in water network

Water line length	**Edge resiliency weight (r_{ij})**
Short edge (0 to 250 meters)	1
Medium edge (250 to 500 meters)	0.6
Long edge (> 500 meters)	0.2

All nodes are considered being equally critical for water supply and they all have node weight of 0.5. The water nodes with storage tanks (12, 24, 27, 72, 77, 86) are highlighted by red starts in Fig. 4 below.

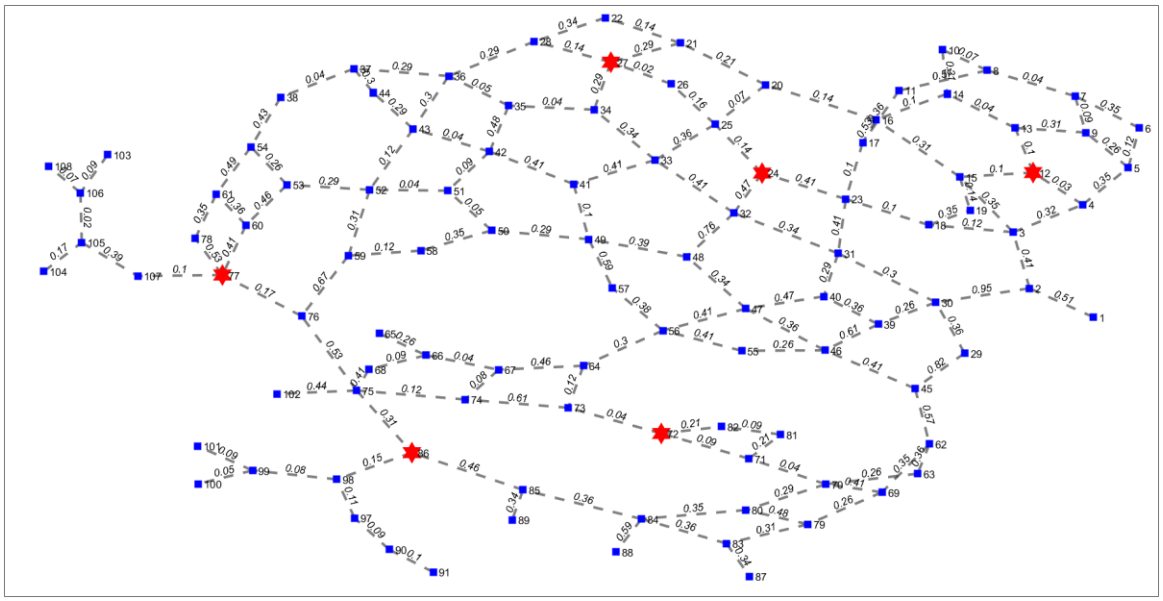

Figure 7-4 Graphical representation of the 130-node water distribution network. Red color star nodes represent the ST with pumping stations in the network. Blue squares are the nodes with water demand. Node number and edge weights connecting two nodes are provided in the diagram.

The edge weights and node weights are computed using the proposed methodology discussed above. Using the algorithm, the above graph is partitioned into six clusters as shown in Figure 7-5.

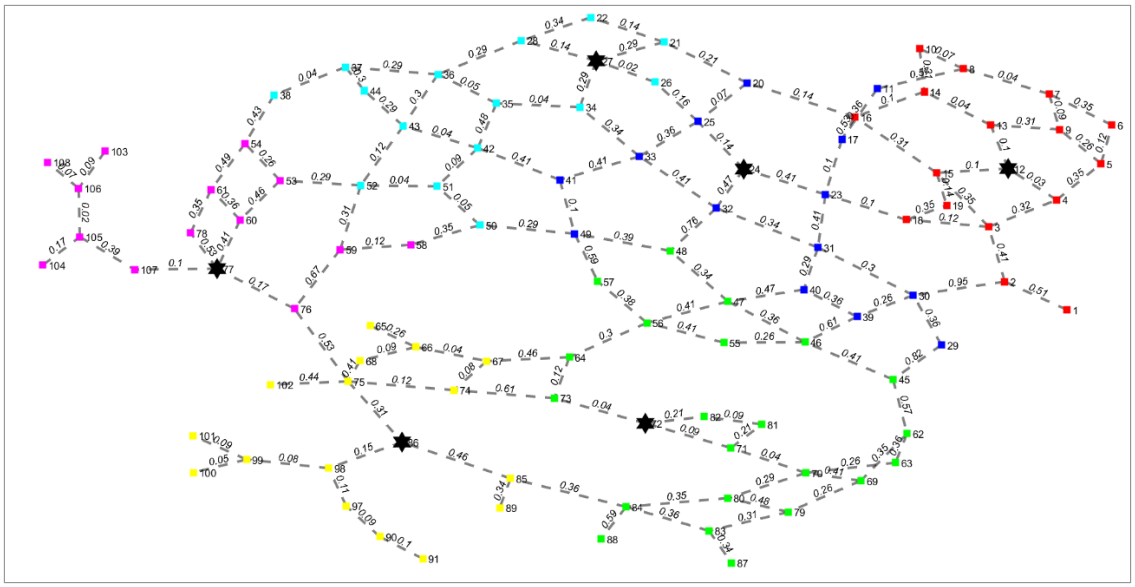

Figure 7-5 Water network partitions based on node and edge weights. Six clusters are created (red, blue, cyan, green, magenta, and yellow) with center nodes (black) representing STs.

Once the initial partitions are created, the water demand in each cluster is supplied from the ST available within the cluster as much as possible. However, when the demand in a cluster is more than ST capacity in that cluster, there needs to be water supply from neighboring clusters. In order to import water from neighboring clusters, the edges are reinforced such that in case of disturbances, those interconnecting edges can allow for supply of water between the clusters. Figure 7-6 shows the edge reinforcement performed.

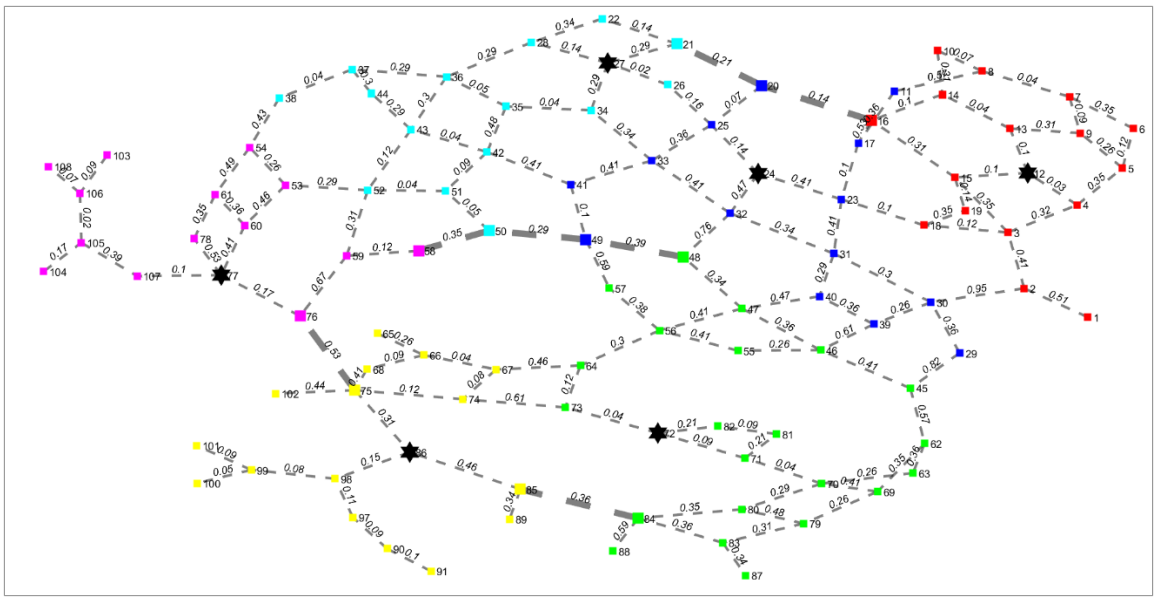

Figure 7-6 Edge reinforcement of the micronets. The brown highlighted edges represent reinforcement. There is water exchange between Cyan – Red clusters, Cyan – Magenta clusters, Blue – Green clusters, and Green – Yellow clusters.

Table 7-5 shows water demand and supply in each cluster and connection made after solving the optimization model. In the table, 1 indicates that a connection is made (reinforcement applied) whereas 0 represents no reinforcement applied. There is an additional cost of reinforcement in water networks compared to the power networks because there needs to be water exchange between clusters that are outside of neighboring clusters. As an example, water demand in the Green cluster is being supplied from the ST in Cyan and Magenta clusters via edges 58 – 50 – 49 – 48.

Table 7-5 Water supply and demand in each cluster and edge reinforcement

Cluster	Water Demand	ST Capacity	Red	Blue	Cyan	Green	Magenta	Yellow
Red	33	40	0	0	1	0	0	0
Blue	46	50	0	0	0	1	0	0
Cyan	48	100	1	0	0	1	0	0
Green	92	50	0	1	1	0	1	1
Magenta	42	150	0	0	0	1	0	1
Yellow	54	40	0	0	0	1	1	0

7.3.3 Water-Energy Interconnection

The next step is to connect the islanded water micronets (clusters) to a nearby power source such that the pumping stations at the ST or the water treatment facilities can be run to supply water to the communities as needed. This is done using the data in Table C.3 in the Appendix C for different pairs of microgrids and micronets. Figure 7-7 shows initial connection of ST nodes to nearby power nodes. In Figure 7-8, the closest energy node is connected to each ST. The highlighted edges represent the closest energy nodes supplying power to the pumping stations at the ST.

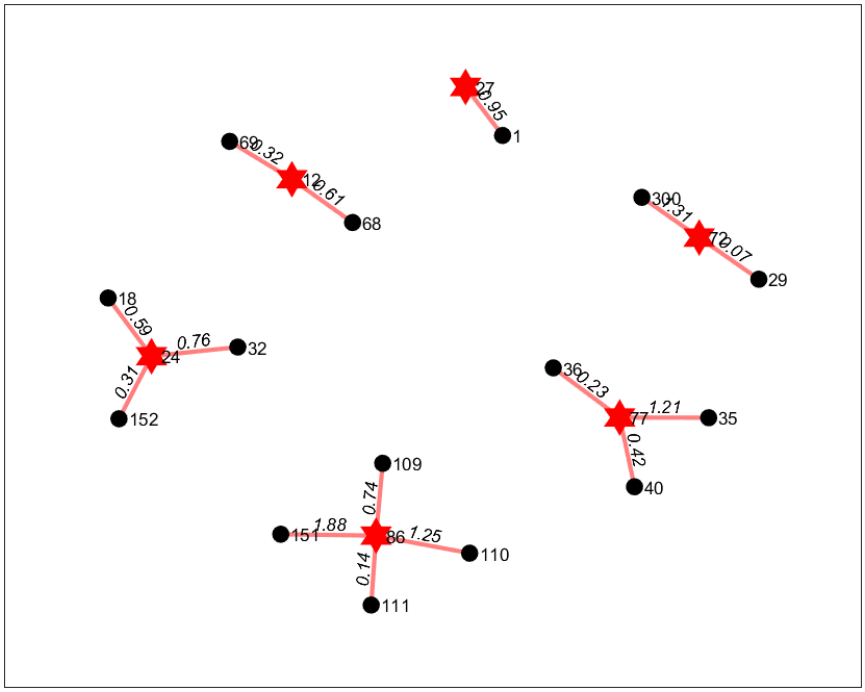

Figure 7-7 Water and energy interconnected clusters. Each cluster has one storage tank (red colored star nodes) which needs to be connected to the closest energy node (one of the black nodes).

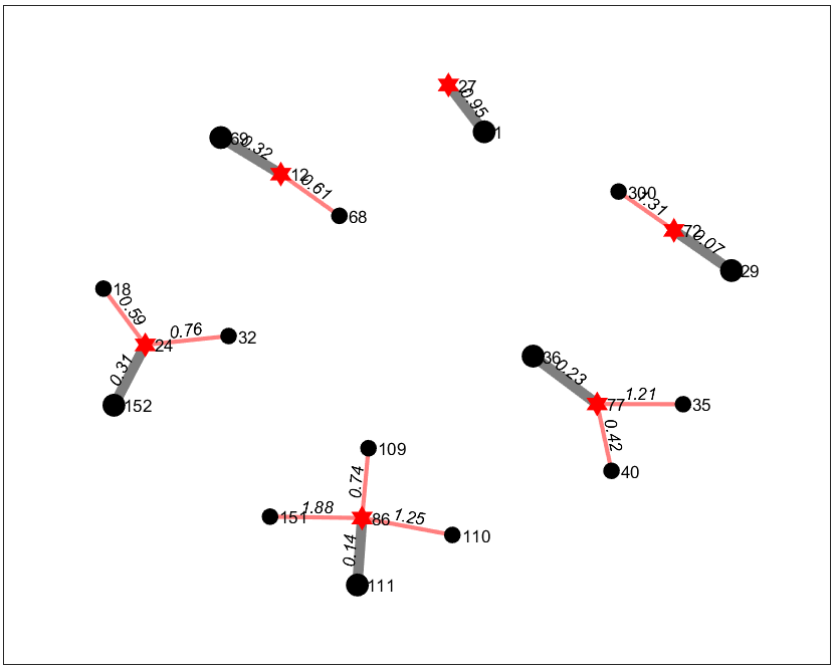

Figure 7-8 Water and energy interconnected clusters. The storage tanks are connected to the closest energy node as highlighted with solid grey colored edge.

7.4 Cost of Resilience

The critical edges need to be reinforced in advance in order to maintain a connection between the nodes connecting two clusters so that power or water exchange could occur between the clusters until the main power grid or water network is restored Such critical edges are identified considering the cost of reinforcement or cost of resilience. The edge length and resiliency of the edge is considered for cost computation because the financial burden to the community would increase as the length of edge connecting two or more clusters increases. Similarly, the cost would be higher for less resilient edge that connects two or more clusters. The graph partition algorithm presented in this chapter considers these two variables and selects the edge that has minimum cost for partition. In the optimization model, the cost parameter is used for candidate edges so that the optimal solution selects the edge which is shorter in length and more resilient that other candidate edges connecting two or more clusters.

Consider one example from the results presented in section 7.3.1: the weights for the edges in Figure 7-3 are computed using equation (7.1) which considers edge length and resiliency of the edge. The edge weight connecting the cluster green and cluster magenta is 0.15 and 0.69 for the edges 89 to 91 and 54 to 94, respectively. But only the edge 89 to 91 is selected for reinforcement because this cost is lower than cost of edge 54 to 94. Similarly, in Figure 7-6 edge reinforcement for the link connecting nodes 84 to 85 is considered over the links between 73 and 74 or 64 and 67. in the green and yellow clusters because the cost for the first is smaller (0.36) compared other two links (0.46 and 0.61).

7.5 Conclusions

In this chapter a centralize microgrid and micronet has been broken into decentralized sub networks. The smaller microgrid and micronets are interconnected such that they can exchange power and water as needed. In case of natural or manmade disturbance on power grid or water network, the main source or water or power could be damaged and wide area power outage or water shortage could occur. The concept of decentralized operation considers breaking the original power network into smaller sub networks such that locally available resources in each network could be utilized optimally to meet the critical needs of communities impacted by the disturbances. One example could be outage of major transmission lines due to a storm and communities experiencing extended power outages. Utilization of DER in the communities to meet the energy load via decentralized operation would increase the resiliency of the grid and expediate the power restoration efforts. Case studies for power network and water distribution systems have been presented as proof of concepts.

CHAPTER 8

SUMMARY AND FUTURE WORK

8.1 Summary

The focus of this work is on devising optimal strategies for design and operation of power and water networks. The work started by presenting an optimal control strategy for operation of a decentralized WWTP. Energy optimization of WWTPs is essential before they can be effectively deployed in the form of standalone systems in isolated communities or electric microgrids. The approach is then extended into the concept of combined power and energy networks (i.e., microgrid/micronet systems), first by proposing an optimal design strategy for allocating resources for such systems and then to devise a strategy for coordinated operation with minimal support from the outside world. The focus is then shifted to the formation of such networks by considering a combined power grid and water distribution network, which due to an external disturbance such as a natural disaster, needs to be decomposed into multiple smaller-scale microgrid/micronet combinations so that they can continue supplying their local loads while the main network is being repaired and restored.

The findings of this research work are applicable to communities that either need to operate independently from the main power and/or water networks (for instance, due to being remote) or have temporarily lost access to those networks due to large-scale disturbances such as natural disasters.

8.2 Novelty and Thesis Contribution

Literature study during the development of this thesis work revealed that many researchers have looked into microgrid design and operation in optimal way. As highlighted in CHAPTER 2 majority of existing research are focused on cost minimization of energy resources such as hybrid (both renewables and non-renewables generators) or non-hybrid (renewables and battery systems) generators. One of the common assumptions in the existing research is the presence of grid for battery charging in case of power shortage from renewable energy resources. However, this thesis is mainly focused on standalone mode of operation of microgrid where the main power grid is unavailable due to natural or manmade disturbances. In the research that do consider standalone operation of microgrid (for example in private island, military base, or other remote communities), the studies consider presence of non-renewable backup generators (diesel generator being common). However, this thesis only considers renewable energy generators which makes the problem challenging due to intermittent behavior of the renewables. Hence battery backup is essential in this thesis. In addition, this thesis identifies critical and non-critical loads in the microgrid and recommends demand response in such a way that the critical loads are supplied power as much as possible while shedding or shifting time of operation of non-critical loads. This part of the work highlights the design and operation of standalone microgrid from the humanitarian perspective during the aftermath of natural disasters or manmade disturbances in the power grid. This perspective of the power network operation lacks in the literature which mainly consider financial aspects of the energy system.

Furthermore, this thesis presents combined operation of water and energy networks in the communities. The literature study revealed that researchers have looked into the water-energy

nexus and the studies focus on optimal operational strategy for water and energy systems considering pump scheduling in water network, dynamic electricity pricing, and optimal size of power or energy system components to maintain system operation. Almost all literature consider availability of municipal water system in the studies. However, this thesis considers that municipal water system is unavailable due to some disturbances and the communities relay on external water purchase and WWTP to supply their water needs. The external water purchase is different from having continuously supply of water from municipal water system because the community would purchase water one time for the study horizon and store it in community ST as backup as opposed to community being supplied from a reservoir. In order to operate such standalone water system, a reliable optimal design and operation of water and energy systems is discussed in detail in this thesis.

The contributions of this work can be listed as follows:

- An optimal solution for energy management of a WWTP with the goal of minimizing its energy footprint,
- An optimal design solution for allocating energy and water resources to a standalone microgrid/micronet system that wishes to rely on local energy and water resources,
- An optimal operation solution for dispatching resources within such a system, subject to possible uncertainties, and
- A solution for dividing a power grid and/or a water distribution network into multiple such microgrid/micronet systems during emergency conditions.

The work has resulted in publications [171], [175].

8.3 Future Work

Some suggestions for extending the current work can be to expand the deterministic work conducted in the previous chapters into stochastic solutions that can handle a broader range of uncertainties. For instance, the work in CHAPTER 5 can be expanded by incorporating the variability of power generation and water or energy demand into the design problem. This could be done based on a stochastic programming model as performed in the work in [175], or by adopting a robust optimization model to ensure feasibility against the worst case conditions. Unlike stochastic programming proposed in CHAPTER 6, in robust optimization, the only information that will be used about the random variables is the range of values they may take (i.e., there will be no information available about the scenarios and their probabilities). Given the known range of uncertain variables, the optimization will be converted into a robust counterpart form, which will ensure optimality even under worst case conditions.

The proposed dispatch strategy in CHAPTER 6 provides a plan for resource allocation and demand response for smooth operation of a combined microgrid/micronet. In the analysis presented in this thesis, focus was on frequency stability and ensuring power balance within the microgrid. This is not unusual, as often we assume that one of the energy resources (CES in this case) can act as a grid-forming unit and dictate the voltage. However, for a more detailed analysis, AC power flow equations as well as operational constraints for the reactive power can be included to ensure voltage stability and sufficient node voltage support. From a mathematical perspective, this can negatively affect the tractability of the optimization problem as it introduces nonlinear terms. One way to avoid this, is to use Cartesian coordinates by breaking the node voltage equations into two, one for the real part and another for the imaginary part. Although this approach

may still leave certain bilinear terms, the highly nonlinear sine and cosine terms will be avoided. An example of how this can be done for an unbalanced distribution network is shown in [176].

Incorporating reactive power into the equations necessitates adding an inequality constraint for generation resources to ensure that the lower and upper limits are not exceeded, and another one to maintain the limit on the apparent power *S*. For instance, for a generic source *g*:

$$\forall g \in \mathrm{G}, \forall t \in \mathrm{T}, \forall s \in \mathrm{S}: Q_g^{\min} \le Q_{g,t,s} \le Q_g^{\max} \tag{8.1}$$

$$\forall g \in \mathrm{G}, \forall t \in \mathrm{T}, \forall s \in \mathrm{S}: S_{g,t,s}^2 = P_{g,t,s}^2 + Q_{g,t,s}^2 \le (S_g^{\max})^2 \tag{8.2}$$

If desired, an inequality equation can also be added to ensure acceptable power flow limits through different series elements such as lines or transformers (if any).

$$\forall l \in \mathrm{L}, \forall t \in \mathrm{T}, \forall s \in \mathrm{S}: S_{l,t,s} \le S_l^{\max} \tag{8.3}$$

It can be seen that these equations convert the optimization model into a nonlinear one, which requires special treatment for achieving acceptable tractability and convergence. Many researchers have proposed solution techniques based on quadratic programming, semidefinite programming, conic programming, or linearization and convexification of the model so that a solution can be obtained in polynomial time [177]–[180].

Currently, in CHAPTER 7 it has been considered that the total size of generation in the microgrid is designed in advanced in a similar way as presented in 0 and the total generation for the community grid is sufficient to meet the power demand of the network even though each cluster

might have power shortages. Because of this assumption there is no need for demand response or load curtailment since overall generation is sufficient to meet the demand of the network and the operator would need to coordinate among clusters to balance overall load and generation of the microgrid. The proposed optimization strategy identifies how much power or water needs to be exchanged between the clusters in order to maintain balance in supply and demand. However, in the case of microgrid where total size of generator for the microgrid has not been identified and installed in advance a demand response strategy can be implemented in the future work. This demand response strategy should be similar to the techniques presented in 0, 0, and 0 of this thesis so that the critical and non-critical loads in the network are prioritized accordingly.

REFERENCES

[1] Y. Wang, C. Chen, J. Wang, and R. Baldick, “Research on resilience of power systems under natural disasters—A review,” *IEEE Trans. Power Syst.*, vol. 31, no. 2, pp. 1604–1613, 2015.

[2] J. B. Halverson and T. Rabenhorst, “Hurricane Sandy: The science and impacts of a superstorm,” *Weatherwise*, vol. 66, no. 2, pp. 14–23, 2013.

[3] J. Vigdor, “The economic aftermath of Hurricane Katrina,” *J. Econ. Perspect.*, vol. 22, no. 4, pp. 135–154, 2008.

[4] K. Satake and B. F. Atwater, “Long-term perspectives on giant earthquakes and tsunamis at subduction zones,” *Annu. Rev. Earth Planet. Sci.*, vol. 35, pp. 349–374, 2007.

[5] T. Ohnishi, “The disaster at Japan’s Fukushima-Daiichi nuclear power plant after the March 11, 2011 earthquake and tsunami, and the resulting spread of radioisotope contamination,” *Radiat. Res.*, vol. 177, no. 1, pp. 1–14, 2012.

[6] D. S. K. Thomas, B. D. Phillips, A. Fothergill, and L. Blinn-Pike, *Social vulnerability to disasters*. CRC Press, 2009.

[7] T. G. Veenema, C. P. Thornton, R. P. Lavin, A. K. Bender, S. Seal, and A. Corley, “Climate change–related water disasters’ impact on population health,” *J. Nurs. Scholarsh.*, vol. 49, no. 6, pp. 625–634, 2017.

[8] M. A. Benevolenza and L. DeRigne, “The impact of climate change and natural disasters on vulnerable populations: A systematic review of literature,” *J. Hum. Behav. Soc. Environ.*, vol. 29, no. 2, pp. 266–281, 2019.

[9] M. Fordham, W. E. Lovekamp, D. S. K. Thomas, and B. D. Phillips, “Understanding social vulnerability,” *Soc. vulnerability to disasters*, vol. 2, pp. 1–29, 2013.

[10] H. Rodríguez and C. N. Russell, “Understanding disasters: Vulnerability, sustainable development, and resiliency,” *Public Sociol. Read.*, pp. 193–211, 2006.

[11] C. S. Holling, “Resilience and stability of ecological systems,” *Annu. Rev. Ecol. Syst.*, vol. 4, no. 1, pp. 1–23, 1973.

[12] C. Folke, S. R. Carpenter, B. Walker, M. Scheffer, T. Chapin, and J. Rockström, “Resilience thinking: integrating resilience, adaptability and transformability,” *Ecol. Soc.*, vol. 15, no. 4, 2010.

[13] M. J. Collier *et al.*, “Transitioning to resilience and sustainability in urban communities,” *Cities*, vol. 32, pp. S21–S28, 2013, doi: https://doi.org/10.1016/j.cities.2013.03.010.

[14] F. and A. O. of the U. N. (FAO), “The Water-Energy-Food Nexus: a New Approach in Support of Food Security and Sustainable Agriculture.” FAO Rome, 2014.

[15] A. Cheshmehzangi, “Preparedness Through Urban Resilience,” in *The City in Need*, Springer, 2020, pp. 41–103.

[16] R. C. Lewontin, “The meaning of stability.,” in *Brookhaven symposia in biology*, 1969, vol. 22, p. 13.

[17] J. Anderson and C. Bausch, “Climate Change and Natural Disasters: Scientific evidence of a possible relation between recent natural disasters and climate change,” *Policy Dep. Econ. Sci. Policy*, vol. 2, 2006.

[18] R. E. Munich, “Natural Catastrophe Year in Review. 2013.” 2012.

[19] S. Banholzer, J. Kossin, and S. Donner, “The impact of climate change on natural disasters,” in *Reducing disaster: Early warning systems for climate change*, Springer, 2014, pp. 21–49.

[20] C. Garcia and C. J. Fearnley, “Evaluating critical links in early warning systems for natural hazards,” *Environ. Hazards*, vol. 11, no. 2, pp. 123–137, 2012.

[21] R. Sauerborn and K. Ebi, “Climate change and natural disasters–integrating science and practice to protect health,” *Glob. Health Action*, vol. 5, no. 1, p. 19295, 2012.

[22] Y. Jin, P. Behrens, A. Tukker, and L. Scherer, “Water use of electricity technologies: A global meta-analysis,” *Renew. Sustain. Energy Rev.*, vol. 115, p. 109391, 2019, doi: https://doi.org/10.1016/j.rser.2019.109391.

[23] M. Howells *et al.*, “Integrated analysis of climate change, land-use, energy and water strategies,” *Nat. Clim. Chang.*, vol. 3, no. 7, pp. 621–626, 2013.

[24] P. Ganguli, D. Kumar, and A. R. Ganguly, “US power production at risk from water stress in a changing climate,” *Sci. Rep.*, vol. 7, no. 1, pp. 1–13, 2017.

[25] A. Bastaminia, M. R. Rezaei, and M. H. Saraei, “Evaluating the components of social and economic resilience: After two large earthquake disasters Rudbar 1990 and Bam 2003,” *Jàmbá J. Disaster Risk Stud.*, vol. 9, no. 1, pp. 1–12, 2017.

[26] I. Noy and R. Yonson, “Economic vulnerability and resilience to natural hazards: A survey of concepts and measurements,” *Sustainability*, vol. 10, no. 8, p. 2850, 2018.

[27] A. Fothergill and L. A. Peek, “Poverty and disasters in the United States: A review of recent sociological findings,” *Nat. hazards*, vol. 32, no. 1, pp. 89–110, 2004.

[28] E. Williams, “Environmental effects of information and communications technologies,”

Nature, vol. 479, no. 7373, pp. 354–358, 2011.

[29] M. Mutchek and E. Williams, "Moving towards sustainable and resilient smart water grids," *Challenges*, vol. 5, no. 1, pp. 123–137, 2014.

[30] T. Elmqvist *et al.*, "Response diversity, ecosystem change, and resilience," *Front. Ecol. Environ.*, vol. 1, no. 9, pp. 488–494, 2003.

[31] N. Lee and S. R. Stout, "Planning a Resilient Power Sector: Ensuring Reliable, Secure, Safe, and Affordable Electricity," National Renewable Energy Lab.(NREL), Golden, CO (United States), 2018.

[32] K. C. Desouza and T. H. Flanery, "Designing, planning, and managing resilient cities: A conceptual framework," *Cities*, vol. 35, pp. 89–99, 2013, doi: https://doi.org/10.1016/j.cities.2013.06.003.

[33] S. S. Patel, M. B. Rogers, R. Amlôt, and G. J. Rubin, "What do we mean by'community resilience'? A systematic literature review of how it is defined in the literature," *PLoS Curr.*, vol. 9, 2017.

[34] S. Romac, "The Importance of Community Resilience: Developing the American Red Cross International Services Department in the New Hampshire Region," 2014.

[35] S. Chen, S. Song, L. Li, and J. Shen, "Survey on smart grid technology," *Power Syst. Technol.*, vol. 33, no. 8, pp. 1–7, 2009.

[36] J. Doss-Gollin, D. J. Farnham, U. Lall, and V. Modi, "How unprecedented was the February 2021 Texas cold snap?," 2021.

[37] D. Wu *et al.*, "An Open-source Model for Simulation and Corrective Measure Assessment of the 2021 Texas Power Outage," *arXiv Prepr. arXiv2104.04146*, 2021.

[38] P. Hines, J. Apt, and S. Talukdar, "Trends in the history of large blackouts in the United States," in *2008 IEEE Power and Energy Society General Meeting-Conversion and Delivery of Electrical Energy in the 21st Century*, 2008, pp. 1–8.

[39] A. Hussain, V.-H. Bui, and H.-M. Kim, "Microgrids as a resilience resource and strategies used by microgrids for enhancing resilience," *Appl. Energy*, vol. 240, pp. 56–72, 2019.

[40] C. Abbey *et al.*, "Powering through the storm: Microgrids operation for more efficient disaster recovery," *IEEE power energy Mag.*, vol. 12, no. 3, pp. 67–76, 2014.

[41] T. S. Ustun, U. Cali, and M. C. Kisacikoglu, "Energizing microgrids with electric vehicles during emergencies—Natural disasters, sabotage and warfare," in *2015 IEEE International Telecommunications Energy Conference (INTELEC)*, 2015, pp. 1–6.

[42] J. W. Hurtt, “Residential Microgrids for Disaster Recovery Operations.” Virginia Tech, 2013.

[43] N. Hatziargyriou, H. Asano, R. Iravani, and C. Marnay, “Microgrids,” *IEEE Power Energy Mag.*, vol. 5, no. 4, pp. 78–94, 2007, doi: 10.1109/MPAE.2007.376583.

[44] S. Parhizi, H. Lotfi, A. Khodaei, and S. Bahramirad, “State of the art in research on microgrids: A review,” *Ieee Access*, vol. 3, pp. 890–925, 2015.

[45] D. Parra *et al.*, “An interdisciplinary review of energy storage for communities: Challenges and perspectives,” *Renew. Sustain. Energy Rev.*, vol. 79, pp. 730–749, 2017, doi: https://doi.org/10.1016/j.rser.2017.05.003.

[46] D. Parra, S. A. Norman, G. S. Walker, and M. Gillott, “Optimum community energy storage system for demand load shifting,” *Appl. Energy*, vol. 174, pp. 130–143, 2016, doi: https://doi.org/10.1016/j.apenergy.2016.04.082.

[47] C. Biggs, C. Ryan, J. Wiseman, and K. Larsen, “Distributed Water Systems: A networked and localised approach for sustainable water services,” 2009.

[48] G. Hallsmith, *The key to sustainable cities: Meeting human needs, transforming community systems*. New Society Publishers, 2003.

[49] C. K. Makropoulos and D. Butler, “Distributed water infrastructure for sustainable communities,” *Water Resour. Manag.*, vol. 24, no. 11, pp. 2795–2816, 2010.

[50] G. J. Falco and W. R. Webb, “Water Microgrids: The Future of Water Infrastructure Resilience,” *Procedia Eng.*, vol. 118, pp. 50–57, 2015, doi: https://doi.org/10.1016/j.proeng.2015.08.403.

[51] J. Eddy, N. E. Miner, and J. Stamp, “Sandia’s Microgrid Design Toolkit,” *Electr. J.*, vol. 30, no. 4, pp. 62–67, 2017, doi: https://doi.org/10.1016/j.tej.2017.04.002.

[52] M. S. Mahmoud, *Microgrid: advanced control methods and renewable energy system integration*. Elsevier, 2016.

[53] J. Lee and S.-K. Chae, “Hourly water demand forecasting for micro water grids,” *J. Water Supply Res. Technol.*, vol. 65, no. 1, pp. 12–17, 2016.

[54] K. Adeyeye, A. Bairi, S. Emmitt, and K. Hyde, “Socially-integrated resilience in building-level water networks using smart microgrid+net,” *Procedia Eng.*, vol. 212, pp. 39–46, 2018, doi: https://doi.org/10.1016/j.proeng.2018.01.006.

[55] D. Zhang, N. Shah, and L. G. Papageorgiou, “Efficient energy consumption and operation management in a smart building with microgrid,” *Energy Convers. Manag.*, vol. 74, pp. 209–222, 2013.

[56] R. Goldstein and W. Smith, *Water & sustainability (volume 4): US electricity consumption for water supply & treatment-the next half century*. Electric Power Research Institute, 2002.

[57] E. Efficiency, "Energy Efficiency in Water and Wastewater Facilities," 2009.

[58] J. Daw, K. Hallett, J. DeWolfe, and I. Venner, "Energy efficiency strategies for municipal wastewater treatment facilities," National Renewable Energy Lab.(NREL), Golden, CO (United States), 2012.

[59] E. Grubert and K. T. Sanders, "Water use in the United States energy system: A national assessment and unit process inventory of water consumption and withdrawals," *Environ. Sci. Technol.*, vol. 52, no. 11, pp. 6695–6703, 2018.

[60] M. A. Maupin, "Summary of estimated water use in the united states in 2015," US Geological Survey, 2018.

[61] N. Ando, S. Yoshikawa, S. Fujimori, and S. Kanae, "Long-term projections of global water use for electricity generation under the shared socioeconomic pathways and climate mitigation scenarios," *Hydrol. Earth Syst. Sci. Discuss.*, pp. 1–25, 2017.

[62] M. D. Bartos and M. V Chester, "Impacts of climate change on electric power supply in the Western United States," *Nat. Clim. Chang.*, vol. 5, no. 8, pp. 748–752, 2015.

[63] A. Zohrabian, S. L. Plata, D. M. Kim, A. E. Childress, and K. T. Sanders, "Leveraging the water-energy nexus to derive benefits for the electric grid through demand-side management in the water supply and wastewater sectors," *Wiley Interdiscip. Rev. Water*, vol. 8, no. 3, p. e1510, 2021.

[64] A. P. P. da Silveira and H. Mata-Lima, "Energy audit in water supply systems: a proposal of integrated approach towards energy efficiency," *Water Policy*, vol. 22, no. 6, pp. 1126–1141, 2020.

[65] Y. Zhang, J. Fang, S. Wang, and H. Yao, "Energy-water nexus in electricity trade network: A case study of interprovincial electricity trade in China," *Appl. Energy*, vol. 257, p. 113685, 2020.

[66] S. Wang, B. Fath, and B. Chen, "Energy–water nexus under energy mix scenarios using input–output and ecological network analyses," *Appl. Energy*, vol. 233, pp. 827–839, 2019.

[67] A. Stuhlmacher and J. L. Mathieu, "Water distribution networks as flexible loads: A chance-constrained programming approach," *Electr. Power Syst. Res.*, vol. 188, p. 106570, 2020.

[68] E. Dall'Anese, P. Mancarella, and A. Monti, "Unlocking flexibility: Integrated

optimization and control of multienergy systems," *IEEE Power Energy Mag.*, vol. 15, no. 1, pp. 43–52, 2017.

[69] H. Cherif, S. Tnani, J. Belhadj, and A. R. Silva, "Optimal sizing and technical evaluation of energy and water system based on micro-hydric solar and wind sources," in *2018 IEEE 16th International Conference on Industrial Informatics (INDIN)*, 2018, pp. 1018–1023.

[70] D. Fooladivanda, A. D. Domínguez-García, and P. W. Sauer, "Utilization of water supply networks for harvesting renewable energy," *IEEE Trans. Control Netw. Syst.*, vol. 6, no. 2, pp. 763–774, 2018.

[71] F. Wang, J. Xu, L. Liu, G. Yin, J. Wang, and J. Yan, "Optimal design and operation of hybrid renewable energy system for drinking water treatment," *Energy*, vol. 219, p. 119673, 2021.

[72] F. Moazeni and J. Khazaei, "Optimal operation of water-energy microgrids; a mixed integer linear programming formulation," *J. Clean. Prod.*, vol. 275, p. 122776, 2020.

[73] R. L. Siegrist, J. E. McCray, K. S. Lowe, T. Y. Cath, and J. Munakata-Marr, "Onsite and Decentralised Wastewater Systems." Water, 2013.

[74] D. Geisinger and G. Chartier, "Managed onsite/decentralized wastewater systems as long-term solutions," *Clearwaters*, vol. 35, pp. 6–11, 2005.

[75] R. Crites and G. Tchobanoglous, *Small and decentralized wastewater management systems*, no. 628.3 C934s. Mc Graw Hill, 1998.

[76] A. Shehabi, J. R. Stokes, and A. Horvath, "Energy and air emission implications of a decentralized wastewater system," *Environ. Res. Lett.*, vol. 7, no. 2, p. 24007, 2012.

[77] K. L. Nelson, "Small and decentralized systems for wastewater treatment and reuse," in *Water Conservation, Reuse, and Recycling: Proceedings of an Iranian-American Workshop*, 2005, vol. 10, no. 29, p. 54.

[78] *Methodology and Findings for the Exposure Analysis of the Chinese Wastewater Sector to Flooding and Earthquakes Hazards*. The World Bank, 2019.

[79] N. K. Singh, A. A. Kazmi, and M. Starkl, "A review on full-scale decentralized wastewater treatment systems: techno-economical approach," *Water Sci. Technol.*, vol. 71, no. 4, pp. 468–478, 2015.

[80] M. A. Massoud, A. Tarhini, and J. A. Nasr, "Decentralized approaches to wastewater treatment and management: Applicability in developing countries," *J. Environ. Manage.*, vol. 90, no. 1, pp. 652–659, 2009, doi: https://doi.org/10.1016/j.jenvman.2008.07.001.

[81] D. Vuono *et al.*, "Flexible hybrid membrane treatment systems for tailored nutrient

management: A new paradigm in urban wastewater treatment," *J. Memb. Sci.*, vol. 446, pp. 34–41, 2013.

[82] D. C. Vuono *et al.*, "Disturbance and temporal partitioning of the activated sludge metacommunity," *ISME J.*, vol. 9, no. 2, pp. 425–435, 2015.

[83] R. G. Hunter, J. W. Day, A. R. Wiegman, and R. R. Lane, "Municipal wastewater treatment costs with an emphasis on assimilation wetlands in the Louisiana coastal zone," *Ecol. Eng.*, vol. 137, pp. 21–25, 2019, doi: https://doi.org/10.1016/j.ecoleng.2018.09.020.

[84] G. Rodriguez-Garcia, M. Molinos-Senante, A. Hospido, F. Hernández-Sancho, M. T. Moreira, and G. Feijoo, "Environmental and economic profile of six typologies of wastewater treatment plants," *water Res.*, vol. 45, no. 18, pp. 5997–6010, 2011.

[85] A. Fenu *et al.*, "Energy audit of a full scale MBR system," *Desalination*, vol. 262, no. 1, pp. 121–128, 2010, doi: https://doi.org/10.1016/j.desal.2010.05.057.

[86] M. Gander, B. Jefferson, and S. Judd, *Aerobic MBRs for domestic wastewater treatment: A review with cost considerations*, vol. 18. 2000.

[87] B. Verrecht, S. Judd, G. Guglielmi, C. Brepols, and J. W. Mulder, "An aeration energy model for an immersed membrane bioreactor," *Water Res.*, vol. 42, no. 19, pp. 4761–4770, 2008, doi: https://doi.org/10.1016/j.watres.2008.09.013.

[88] I. Martin, M. Pidou, A. Soares, S. Judd, and B. Jefferson, "Modelling the energy demands of aerobic and anaerobic membrane bioreactors for wastewater treatment," *Environ. Technol.*, vol. 32, no. 9, pp. 921–932, Jul. 2011, doi: 10.1080/09593330.2011.565806.

[89] X. Wei, "Modeling and optimization of wastewater treatment process with a data-driven approach," 2013.

[90] K. V Gernaey, M. C. M. van Loosdrecht, M. Henze, M. Lind, and S. B. Jørgensen, "Activated sludge wastewater treatment plant modelling and simulation: state of the art," *Environ. Model. Softw.*, vol. 19, no. 9, pp. 763–783, 2004, doi: https://doi.org/10.1016/j.envsoft.2003.03.005.

[91] A. G. El-Din and D. W. Smith, "A combined transfer-function noise model to predict the dynamic behavior of a full-scale primary sedimentation tank," *Water Res.*, vol. 36, no. 15, pp. 3747–3764, 2002, doi: https://doi.org/10.1016/S0043-1354(02)00089-1.

[92] D. S. Lee, M. W. Lee, S. H. Woo, Y.-J. Kim, and J. M. Park, "Nonlinear dynamic partial least squares modeling of a full-scale biological wastewater treatment plant," *Process Biochem.*, vol. 41, no. 9, pp. 2050–2057, 2006, doi: https://doi.org/10.1016/j.procbio.2006.05.006.

[93] K. B. Newhart, R. W. Holloway, A. S. Hering, and T. Y. Cath, "Data-driven performance

analyses of wastewater treatment plants: A review," *Water Res.*, vol. 157, pp. 498–513, 2019.

[94] G. E. P. Box, G. M. Jenkins, G. C. Reinsel, and G. M. Ljung, *Time series analysis: forecasting and control*. John Wiley & Sons, 2015.

[95] IEA, "Status of Power System Transformation," *IEA*, Paris, 2019.

[96] S. M. Ismael, S. H. E. Abdel Aleem, A. Y. Abdelaziz, and A. F. Zobaa, "State-of-the-art of hosting capacity in modern power systems with distributed generation," *Renew. Energy*, vol. 130, pp. 1002–1020, 2019, doi: https://doi.org/10.1016/j.renene.2018.07.008.

[97] D. Chattopadhyay and T. Alpcan, "Capacity and Energy-Only Markets Under High Renewable Penetration," *IEEE Trans. Power Syst.*, vol. 31, no. 3, pp. 1692–1702, 2016, doi: 10.1109/TPWRS.2015.2461675.

[98] A. Tuohy, P. Meibom, E. Denny, and M. O'Malley, "Unit commitment for systems with significant wind penetration," *IEEE Trans. power Syst.*, vol. 24, no. 2, pp. 592–601, 2009.

[99] P. Palensky and D. Dietrich, "Demand side management: Demand response, intelligent energy systems, and smart loads," *IEEE Trans. Ind. informatics*, vol. 7, no. 3, pp. 381–388, 2011.

[100] H. Liang and W. Zhuang, "Stochastic modeling and optimization in a microgrid: A survey," *Energies*, vol. 7, no. 4, pp. 2027–2050, 2014.

[101] S. X. Chen, H. B. Gooi, and M. Wang, "Sizing of energy storage for microgrids," *IEEE Trans. Smart Grid*, vol. 3, no. 1, pp. 142–151, 2011.

[102] S. Kahrobaee, S. Asgarpoor, and W. Qiao, "Optimum sizing of distributed generation and storage capacity in smart households," *IEEE Trans. Smart Grid*, vol. 4, no. 4, pp. 1791–1801, 2013.

[103] R. Atia and N. Yamada, "Sizing and analysis of renewable energy and battery systems in residential microgrids," *IEEE Trans. Smart Grid*, vol. 7, no. 3, pp. 1204–1213, 2016.

[104] C. D. Rodríguez-Gallegos, D. Yang, O. Gandhi, M. Bieri, T. Reindl, and S. K. Panda, "A multi-objective and robust optimization approach for sizing and placement of PV and batteries in off-grid systems fully operated by diesel generators: An Indonesian case study," *Energy*, vol. 160, pp. 410–429, 2018.

[105] H. Alharbi and K. Bhattacharya, "Optimal sizing of battery energy storage systems for microgrids," in *2014 IEEE Electrical Power and Energy Conference*, 2014, pp. 275–280.

[106] H. Bludszuweit and J. A. Domínguez-Navarro, "A probabilistic method for energy storage sizing based on wind power forecast uncertainty," *IEEE Trans. power Syst.*, vol. 26, no. 3,

pp. 1651–1658, 2010.

[107] B. Hartmann and A. Dán, “Methodologies for storage size determination for the integration of wind power,” *IEEE Trans. Sustain. Energy*, vol. 5, no. 1, pp. 182–189, 2013.

[108] S. Bahramirad, W. Reder, and A. Khodaei, “Reliability-constrained optimal sizing of energy storage system in a microgrid,” *IEEE Trans. Smart Grid*, vol. 3, no. 4, pp. 2056–2062, 2012.

[109] B. Cao, W. Dong, Z. Lv, Y. Gu, S. Singh, and P. Kumar, “Hybrid microgrid many-objective sizing optimization with fuzzy decision,” *IEEE Trans. Fuzzy Syst.*, vol. 28, no. 11, pp. 2702–2710, 2020.

[110] A. R. Jordehi, “Optimisation of demand response in electric power systems, a review,” *Renew. Sustain. energy Rev.*, vol. 103, pp. 308–319, 2019.

[111] P. Denholm and T. Mai, “Timescales of energy storage needed for reducing renewable energy curtailment,” *Renew. energy*, vol. 130, pp. 388–399, 2019.

[112] D. Fooladivanda and J. A. Taylor, “Energy-optimal pump scheduling and water flow,” *IEEE Trans. Control Netw. Syst.*, vol. 5, no. 3, pp. 1016–1026, 2017.

[113] P. W. Jowitt and G. Germanopoulos, “Optimal pump scheduling in water-supply networks,” *J. Water Resour. Plan. Manag.*, vol. 118, no. 4, pp. 406–422, 1992.

[114] S. A. Moosavian, “Optimal design of water distribution networks under uncertainty.” University of British Columbia, 2018.

[115] E. Batchabani and M. Fuamba, “Optimal tank design in water distribution networks: review of literature and perspectives,” *J. water Resour. Plan. Manag.*, vol. 140, no. 2, pp. 136–145, 2014.

[116] M. Cunha and J. Marques, “A new multiobjective simulated annealing algorithm—MOSA-GR: Application to the optimal design of water distribution networks,” *Water Resour. Res.*, vol. 56, no. 3, p. e2019WR025852, 2020.

[117] E. Yuksel, V. Eroglu, H. Z. Sarikaya, and I. Koyuncu, “Current and future strategies for water and wastewater management of Istanbul City,” *Environ. Manage.*, vol. 33, no. 2, pp. 186–195, 2004.

[118] S. Yerri and K. R. Piratla, “Decentralized water reuse planning: Evaluation of life cycle costs and benefits,” *Resour. Conserv. Recycl.*, vol. 141, pp. 339–346, 2019.

[119] D. A. Kendrick, H. S. Rao, and C. H. Wells, “Optimal operation of a system of waste water treatment facilities,” in *1970 IEEE Symposium on Adaptive Processes (9th)*

Decision and Control, 1970, p. 123.

[120] J. Hakanen, K. Sahlstedt, and K. Miettinen, "Wastewater treatment plant design and operation under multiple conflicting objective functions," *Environ. Model. Softw.*, vol. 46, pp. 240–249, 2013.

[121] D. Parra *et al.*, "An interdisciplinary review of energy storage for communities: Challenges and perspectives," *Renew. Sustain. Energy Rev.*, vol. 79, pp. 730–749, 2017, doi: https://doi.org/10.1016/j.rser.2017.05.003.

[122] T. Mai, D. Sandor, R. Wiser, and T. Schneider, "Renewable electricity futures study. executive summary," National Renewable Energy Lab.(NREL), Golden, CO (United States), 2012.

[123] S. Eckroad and I. Gyuk, "EPRI-DOE handbook of energy storage for transmission & distribution applications," *Electr. Power Res. Institute, Inc*, pp. 3–35, 2003.

[124] S. H. Madaeni and R. Sioshansi, "The impacts of stochastic programming and demand response on wind integration," *Energy Syst.*, vol. 4, no. 2, pp. 109–124, 2013.

[125] A. Papavasiliou and S. S. Oren, "Coupling wind generators with deferrable loads," in *2008 IEEE Energy 2030 Conference*, 2008, pp. 1–7.

[126] A. Santhosh, A. M. Farid, and K. Youcef-Toumi, "Real-time economic dispatch for the supply side of the energy-water nexus," *Appl. Energy*, vol. 122, pp. 42–52, 2014.

[127] R. Menke, E. Abraham, P. Parpas, and I. Stoianov, "Demonstrating demand response from water distribution system through pump scheduling," *Appl. Energy*, vol. 170, pp. 377–387, 2016, doi: https://doi.org/10.1016/j.apenergy.2016.02.136.

[128] A. Ioannou, G. Fuzuli, F. Brennan, S. W. Yudha, and A. Angus, "Multi-stage stochastic optimization framework for power generation system planning integrating hybrid uncertainty modelling," *Energy Econ.*, vol. 80, pp. 760–776, 2019.

[129] K. Huang and S. Ahmed, "The value of multistage stochastic programming in capacity planning under uncertainty," *Oper. Res.*, vol. 57, no. 4, pp. 893–904, 2009.

[130] X. Peng and P. Jirutitijaroen, "A probabilistic unit commitment problem with photovoltaic generation system," in *TENCON 2009-2009 IEEE Region 10 Conference*, 2009, pp. 1–6.

[131] M. Lubin, C. G. Petra, M. Anitescu, and V. Zavala, "Scalable stochastic optimization of complex energy systems," in *SC'11: Proceedings of 2011 International Conference for High Performance Computing, Networking, Storage and Analysis*, 2011, pp. 1–10.

[132] L. Kuznia, B. Zeng, G. Centeno, and Z. Miao, "Stochastic optimization for power system configuration with renewable energy in remote areas," *Ann. Oper. Res.*, vol. 210, no. 1,

pp. 411–432, 2013.

[133] G. Strbac, “Demand side management: Benefits and challenges,” *Energy Policy*, vol. 36, no. 12, pp. 4419–4426, 2008, doi: https://doi.org/10.1016/j.enpol.2008.09.030.

[134] E. D. Thomasson *et al.*, “Acute Health Effects After the Elk River Chemical Spill, West Virginia, January 2014,” *Public Health Rep.*, vol. 132, no. 2, pp. 196–202, Feb. 2017, doi: 10.1177/0033354917691257.

[135] S. Cisneros, “Portland To Empty Water In Mt. Tabor Reservoir After Contamination,” Apr. 16, 2014.

[136] A. M. Hamiche, A. B. Stambouli, and S. Flazi, “A review of the water-energy nexus,” *Renew. Sustain. Energy Rev.*, vol. 65, pp. 319–331, 2016, doi: https://doi.org/10.1016/j.rser.2016.07.020.

[137] X. Zhang and V. V Vesselinov, “Energy-water nexus: Balancing the tradeoffs between two-level decision makers,” *Appl. Energy*, vol. 183, pp. 77–87, 2016, doi: https://doi.org/10.1016/j.apenergy.2016.08.156.

[138] M. Wakeel, B. Chen, T. Hayat, A. Alsaedi, and B. Ahmad, “Energy consumption for water use cycles in different countries: A review,” *Appl. Energy*, vol. 178, pp. 868–885, 2016, doi: https://doi.org/10.1016/j.apenergy.2016.06.114.

[139] K. E. Lansey and L. W. Mays, “Optimization model for water distribution system design,” *J. Hydraul. Eng.*, vol. 115, no. 10, pp. 1401–1418, 1989.

[140] H. M. V Samani and A. Mottaghi, “Optimization of water distribution networks using integer linear programming,” *J. Hydraul. Eng.*, vol. 132, no. 5, pp. 501–509, 2006.

[141] T. D. Prasad and N.-S. Park, “Multiobjective genetic algorithms for design of water distribution networks,” *J. Water Resour. Plan. Manag.*, vol. 130, no. 1, pp. 73–82, 2004.

[142] J. Burgschweiger, B. Gnädig, and M. C. Steinbach, “Optimization models for operative planning in drinking water networks,” *Optim. Eng.*, vol. 10, no. 1, pp. 43–73, 2009.

[143] K. Oikonomou and M. Parvania, “Optimal coordination of water distribution energy flexibility with power systems operation,” *IEEE Trans. Smart Grid*, vol. 10, no. 1, pp. 1101–1110, 2018.

[144] M. H. Albadi and E. F. El-Saadany, “A summary of demand response in electricity markets,” *Electr. Power Syst. Res.*, vol. 78, no. 11, pp. 1989–1996, 2008, doi: https://doi.org/10.1016/j.epsr.2008.04.002.

[145] Matlab, “ARIMAX Model Specifications,” *Mathworks*. https://www.mathworks.com/help/econ/arimax-model-specifications.html#.

[146] The Mathworks Inc., “Matlab. 9.6.0 (R2019a).” 2019, [Online]. Available: https://www.mathworks.com/.

[147] GAMS Development Corp., “https://www.gams.com/.” The General Algebraic Modeling System Inc., version 24.4.6, 2014, [Online]. Available: https://www.gams.com/.

[148] W. E. Forsthoffer and W. E. Forsthoffer, “Pump Best Practices,” *Forsthoffer’s Best Pract. Handb. Rotating Mach.*, pp. 25–91, Jan. 2011, doi: 10.1016/B978-0-08-096676-2.10002-5.

[149] D. Jones and M. Tamiz, “Goal Programming Variants BT - Practical Goal Programming,” D. Jones and M. Tamiz, Eds. Boston, MA: Springer US, 2010, pp. 11–22.

[150] R. L. Rardin and R. L. Rardin, *Optimization in operations research*, vol. 166. Prentice Hall Upper Saddle River, NJ, 1998.

[151] M. Choobineh, A. Speake, M. Harris, P. C. Tabares-Velasco, and S. Mohagheghi, “End-User-Aware Community Energy Management in a Distribution System Exposed to Extreme Temperatures,” *IEEE Trans. Smart Grid*, vol. 10, no. 4, pp. 3753–3764, 2019, doi: 10.1109/TSG.2018.2834572.

[152] E. Wilson, “Commercial and residential hourly load profiles for all tmy3 locations in the united states,” *O. o. EE a. R. Energy, Ed., ed. US Dep. Energy Open Data Cat. US Dep. Energy*, 2014.

[153] US Energy Information Administration, “Residential Energy Consumption Survey (RECS),” 2015. https://www.eia.gov/consumption/residential/ (accessed Feb. 27, 2020).

[154] G. Venkatesh and H. Brattebø, “Energy consumption, costs and environmental impacts for urban water cycle services: Case study of Oslo (Norway),” *Energy*, vol. 36, no. 2, pp. 792–800, 2011, doi: https://doi.org/10.1016/j.energy.2010.12.040.

[155] A. Guerrini, G. Romano, and A. Indipendenza, “Energy efficiency drivers in wastewater treatment plants: A double bootstrap DEA analysis,” *Sustainability*, vol. 9, no. 7, p. 1126, 2017.

[156] L. A. Benefield, “Rule Development Committee Issue Research Report Draft-Residential Flow Rates,” Washington, 2002. [Online]. Available: https://www.doh.wa.gov/Portals/1/Documents/Pubs/337-103.pdf.

[157] C. A. Dieter and M. A. Maupin, “Public supply and domestic water use in the United States, 2015,” US Geological Survey, 2017.

[158] M. Sengupta, Y. Xie, A. Lopez, A. Habte, G. Maclaurin, and J. Shelby, “The national solar radiation data base (NSRDB),” *Renew. Sustain. Energy Rev.*, vol. 89, pp. 51–60, 2018.

[159] NSRDB, “National Solar Radiation Data Base,” 2005. https://rredc.nrel.gov/solar/old_data/nsrdb/1991-2005/tmy3/ (accessed Feb. 27, 2020).

[160] A. Goodrich, T. James, and M. Woodhouse, “Residential, commercial, and utility-scale photovoltaic (PV) system prices in the United States: current drivers and cost-reduction opportunities,” National Renewable Energy Lab.(NREL), Golden, CO (United States), 2012.

[161] (CEC) Commission California Energy, “California Code of Regulations Title 20,” 2016. https://www.epa.gov/sites/production/files/2017-10/documents/ws-commercialbuildings-waterscore-residential-kitchen-laundry-guide.pdf (accessed Feb. 27, 2020).

[162] G. R. Joshi and E. D. Wollega, “Planning Hydroelectric Power Distribution Under Uncertain Supply.”

[163] Office of Energy Efficiency & Renewable Energy (EERE)., “Commercial and Residential Hourly Load Profiles for all TMY3 Locations in the United States,” 2014. https://data.openei.org/submissions/153.

[164] National Renewable Energy Lab, “Wind Integration National Dataset Toolkit,” 2021. https://www.nrel.gov/grid/wind-toolkit.html.

[165] U. S. C. Bureau, “Characteristics of New Housing,” 2021. https://www.census.gov/construction/chars/highlights.html.

[166] Wind Power, “Wind Power,” 2021. https://www.thewindpower.net/turbine_en_348_nordtank_ntk300-31.php.

[167] Ryse Energy, “Ryse Energy 5 kW Wind Turbines,” 2021. https://www.ryse.energy/5kw-wind-turbines/.

[168] USGS, “Water Science School,” *Water Science,* 2020. https://www.usgs.gov/special-topic/water-science-school/science.

[169] M. Milnes, “The mathematics of pumping water,” *R. Acad. Eng.,* 2010.

[170] B. Peacock, “Energy and Cost Required to Lift or Pressurize Water,” *Univ. California, Pub. IG6-96,* 1996.

[171] G. Joshi and S. Mohagheghi, “Energy and Water Co-Optimization for the Resilient Neighborhood of Future,” in *2020 IEEE Industry Applications Society Annual Meeting,* 2020, pp. 1–8.

[172] US Energy Information Administration, “Electricity explained Use of electricity,” 2020. https://www.eia.gov/energyexplained/electricity/use-of-electricity.php.

[173] M. Choobineh, A. Speake, M. Harris, P. C. Tabares-Velasco, and S. Mohagheghi, “End-user-aware community energy management in a distribution system exposed to extreme temperatures,” *IEEE Trans. Smart Grid*, vol. 10, no. 4, pp. 3753–3764, 2018.

[174] K. B. Adedeji, “Development of a leakage detection and localization technique for real-time applications in water distribution networks.,” 2018.

[175] G. Joshi and S. Mohagheghi, “Optimal Operation of Combined Energy and Water Systems for Community Resilience against Natural Disasters,” *Energies* , vol. 14, no. 19. 2021, doi: 10.3390/en14196132.

[176] K. Alboaouh and S. Mohagheghi, “Voltage, var and watt optimization for a distribution system with high PV penetration: A probabilistic study,” *Electr. Power Syst. Res.*, vol. 180, p. 106159, 2020.

[177] H.-G. Yeh, D. F. Gayme, and S. H. Low, “Adaptive VAR control for distribution circuits with photovoltaic generators,” *IEEE Trans. Power Syst.*, vol. 27, no. 3, pp. 1656–1663, 2012.

[178] R. A. Jabr, “A conic quadratic format for the load flow equations of meshed networks,” *IEEE Trans. Power Syst.*, vol. 22, no. 4, pp. 2285–2286, 2007.

[179] X. Bai, H. Wei, K. Fujisawa, and Y. Wang, “Semidefinite programming for optimal power flow problems,” *Int. J. Electr. Power Energy Syst.*, vol. 30, no. 6–7, pp. 383–392, 2008.

[180] G. C. Contaxis, C. Delkis, and G. Korres, “Decoupled optimal load flow using linear or quadratic programming,” *IEEE Trans. Power Syst.*, vol. 1, no. 2, pp. 1–7, 1986.

APPENDIX A

SBMBR EQUIPMENT DATA

Summary of equipment nameplate data that have been used for SBMBR study are summarized below.

Table A-1 Electromechanical equipment ratings

Summary of equipment nameplate data		
Rated speed (RPM)	Grinder pump	3450.00
	G-BH1 Blower	3450.00
	Mixer	1160.00
	RAS pump	1755.00
	Air scour blower	1755.00
	Permeate pumps	1755.00
Rated power (kW)	Grinder pump	2.00
	G-BH1 Blower	2.55
	Mixer	0.75
	RAS pump	1.10
	Air scour blower	1.27
	Permeate pumps	0.75
Flow rate at rated power and pressure (m^3/s)	Grinder pump	0.0027 (43 GPM)
	RAS pump	0.0044 (70 GPM)
	Permeate pumps	0.0000088 (22 GPM)

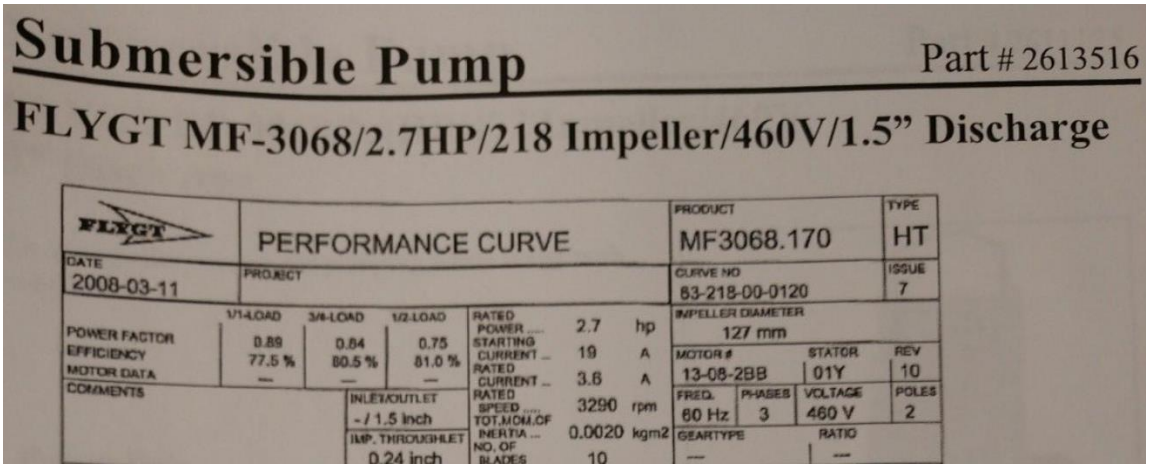

Figure A-1 Nameplate Data for Grinder Pump (Submersible Pump FLYGT MF-3068)

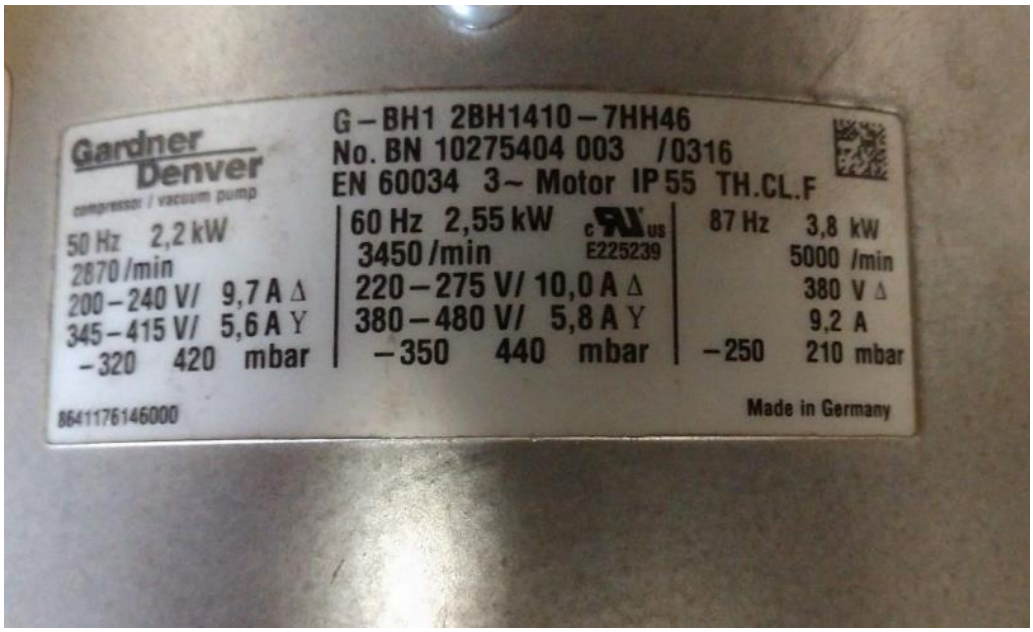

Figure A-2 Nameplate Data for Blower (G-BH1 Side channel blower, Gardner, Denver, CO)

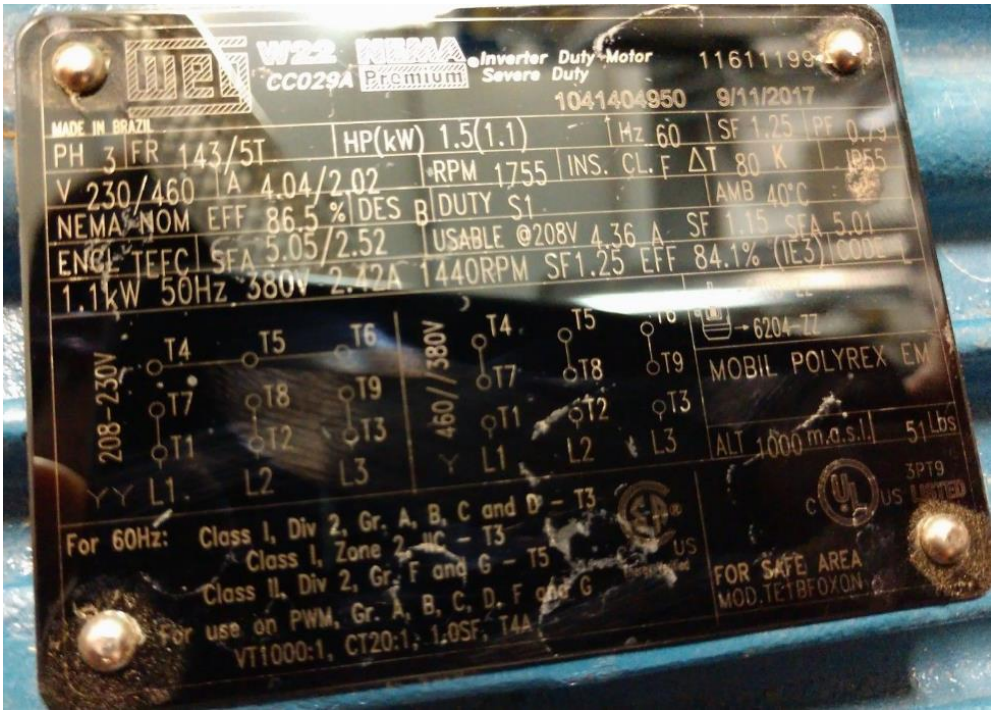

Figure A-3 Nameplate Data for RAS Pump (81 1/2A52-B centrifugal pump, Gorman-Rupp, Mansfield, OH)

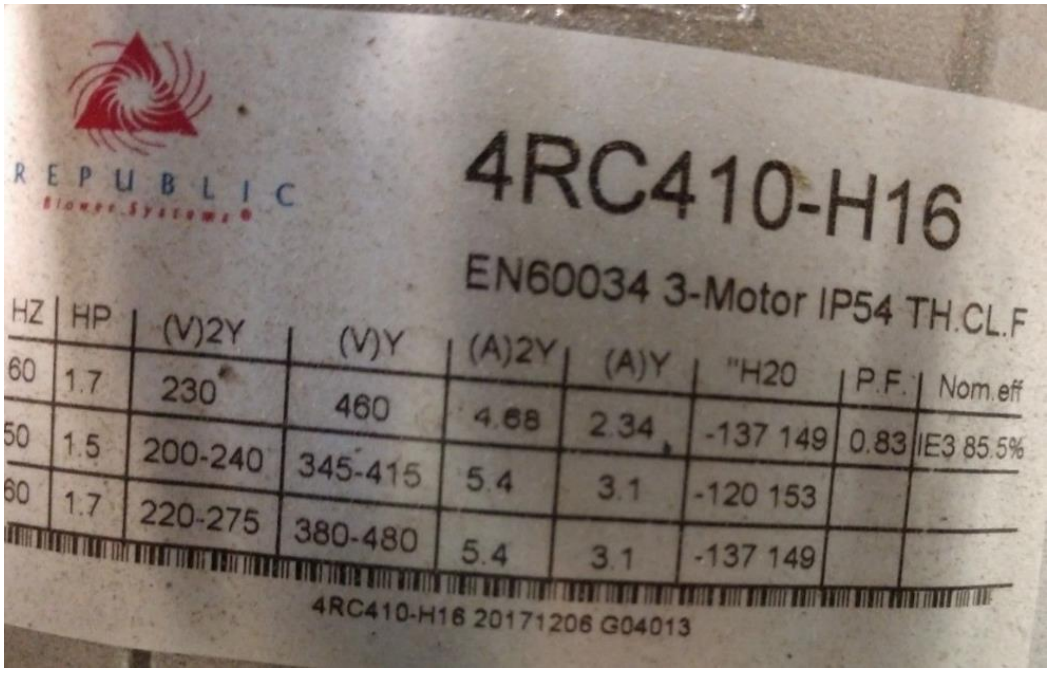

Figure A-4 Nameplate Data for Air Scour Blower (Republic Blower Systems 4RC410-H16

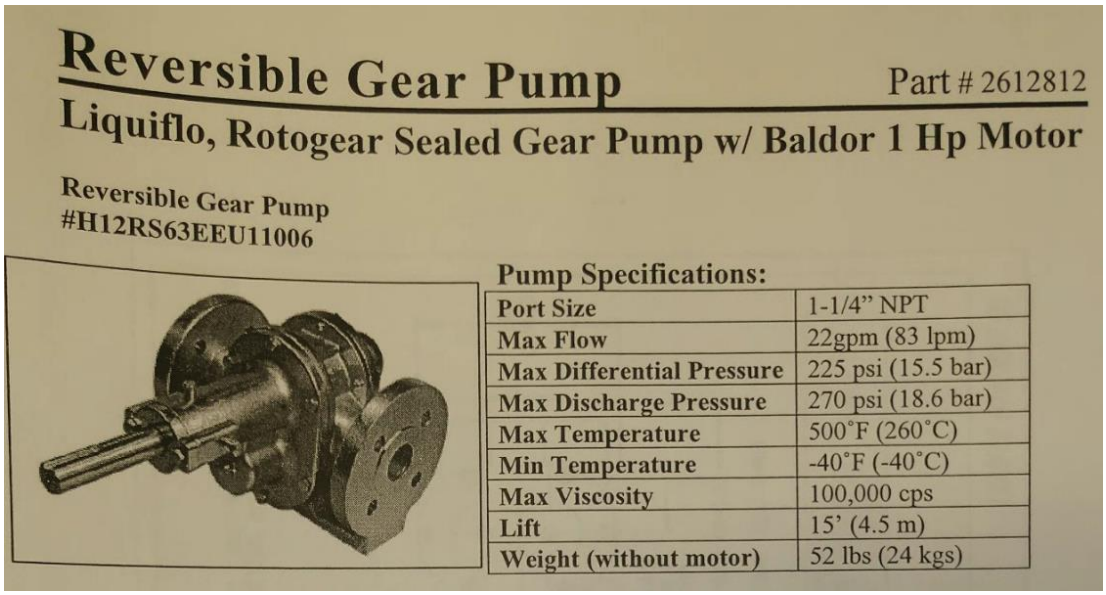

Figure A-5 Nameplate Data for Permeate Pumps (H12 Reversible Gear Pump, Liquiflo, Garwood, NJ)

APPENDIX B

RESIDENTIAL LOAD AND PUMP LOAD DATA

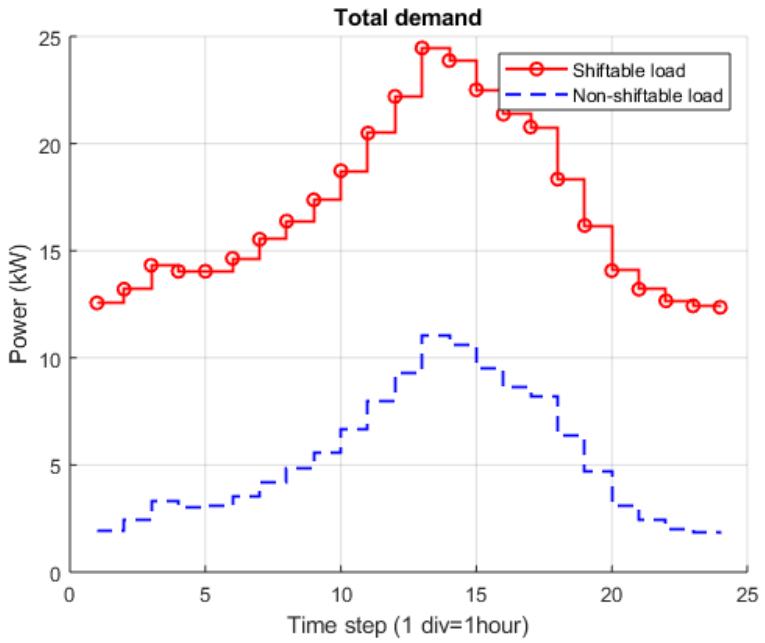

Figure B-6 Total kW for shiftable and non-shiftable loads in the community.

1. Water Pump Sizing

The size of water pump required is estimated using the following equation [169]:

$$P_t = \frac{\rho \cdot g \cdot q_t^{ww,out} \cdot H}{\eta} \tag{B.1}$$

where ρ and g are the density of water (1000 kg/m3) and acceleration due to gravity (9.81 m/s^2), respectively. Parameter η represents the efficiency of the pump (assumed to be 0.7 [112]). Parameters $q_t^{ww,out}$ and H represent water flow rate from the WWTP (at least 0.0007 m^3/s per house

or 0.007 m^3/s for 10 houses) and water head difference between of top of ST and WWTP, respectively. Total head from WWTP and ST needs to be at least 41 m (or 60 PSI pressure difference). With these parameter values, a power of 4.022 kW (5.39 Hp) is needed to pump 25.2 m^3 of water in 1 hour. A 7 Hp pump is therefore chosen for this case study.

This implies that the pump would consume 5.22 kWh of energy to lift 25.2 m^3 water at 60 PSI or 0.21 kWh energy per unit volume of water lift at that pressure. This number is close to 0.19 kWh/m^3 requirement of water pumping given in [170].

APPENDIX C

MICROGRID AND MICRONET CASE STUDY DATA

Table C-1 IEEE 123 Nodes Microgrid Data

Energy Graph - Edges			Energy Graph - Node Data		
From Node	**To Node**	**Weight**	**Node**	**Load (kW)**	**Generator kW**
1	2	0.132	1	40	10
1	3	0.260	2	20	20
1	7	0.274	4	40	20
3	4	0.183	5	20	20
3	5	0.196	6	40	30
5	6	0.188	7	20	0
7	8	0.090	9	40	0
8	12	0.206	10	20	0
8	9	0.206	11	40	50
8	13	0.226	12	20	60
9	14	0.513	16	40	30
13	34	0.113	17	20	25
13	18	0.199	19	40	35
13	152	0.151	20	40	50
11	14	0.302	22	40	60
10	14	0.343	24	40	100
15	16	0.320	28	40	20
15	17	0.151	29	40	10
18	19	0.181	30	40	0
18	21	0.140	31	20	0
18	135	0.480	32	20	50
19	20	0.260	33	40	0
21	22	0.287	34	40	70
21	23	0.071	35	40	100
23	24	0.211	37	40	0
23	25	0.104	38	20	0
25	26	0.095	39	20	80
25	28	0.117	41	20	0
26	27	0.457	42	20	30
26	31	0.226	43	40	0
27	33	0.264	45	20	10

Table C-1 Continued

28	29	0.151	46	20	10
29	30	0.135	47	105	0
30	250	0.121	48	210	0
31	32	0.392	49	140	0
15	34	0.188	50	40	20
35	36	0.135	51	20	10
35	40	0.228	52	40	5
36	37	0.297	53	40	60
36	38	0.245	55	20	70
38	39	0.151	56	20	90
40	41	0.377	58	20	0
40	42	0.090	59	20	0
42	43	0.121	60	20	80
42	44	0.228	62	40	90
44	45	0.181	63	40	100
44	47	0.137	64	75	120
45	46	0.188	65	140	125
47	48	0.228	66	75	60
47	49	0.113	68	20	70
49	50	0.302	69	40	60
50	51	0.086	70	20	0
51	151	0.043	71	40	0
52	53	0.166	73	40	50
53	54	0.211	74	40	20
54	55	0.166	75	40	60
54	57	0.151	76	245	90
54	94	0.685	77	40	75
55	56	0.228	79	40	40
57	58	0.572	80	40	30
57	60	0.228	82	40	50
58	59	0.079	83	20	10
60	61	0.264	84	20	0
60	62	0.442	85	40	0
60	160	0.146	86	20	0
61	611	0.000	87	40	15
61	610	0.000	88	40	60
62	63	0.251	90	40	80
63	64	0.151	92	40	20

Table C-1 Continued

64	65	0.133	94	40	30
65	66	0.157	95	20	10
67	68	0.166	96	20	0
67	72	0.166	98	40	0
67	97	0.072	99	40	0
68	69	0.320	100	40	0
69	70	0.416	102	20	0
70	71	0.416	103	40	0
72	73	0.640	104	40	60
72	76	0.069	106	40	90
73	74	0.136	107	40	10
74	75	0.214	109	40	50
76	77	0.075	111	20	60
76	86	0.091	112	20	30
77	78	0.407	113	40	20
78	79	0.113	114	20	90
78	80	0.358	3	0	0
80	81	0.339	8	0	0
81	82	0.132	13	0	100
81	84	0.166	14	0	0
82	83	0.188	15	0	0
84	85	0.170	18	0	0
86	87	0.129	21	0	0
87	88	0.170	23	0	150
87	89	0.124	25	0	60
89	90	0.135	26	0	90
89	91	0.151	27	0	80
91	92	0.166	36	0	70
91	93	0.503	40	0	60
93	94	0.181	44	0	75
93	95	0.731	54	0	90
95	96	0.136	57	0	20
95	195	0.251	61	0	10
97	98	0.196	67	0	50
97	250	0.512	72	0	0
98	99	0.136	78	0	0
99	100	0.196	81	0	0
100	450	0.433	89	0	0

Table C-1 Continued

101	102	0.411	91	0	0
101	105	0.241	93	0	100
102	103	0.181	97	0	0
103	104	0.347	101	0	0
105	106	0.094	105	0	150
105	108	0.480	108	0	20
106	107	0.196	110	0	10
108	109	0.226	135	0	0
108	300	0.180	149	0	0
109	110	0.264	150	0	0
110	111	0.228	151	0	0
110	112	0.180	152	0	0
112	113	0.347	160	0	0
113	114	0.196	195	0	0
35	135	0.283	197	0	0
1	149	0.241	250	0	40
149	150	0.000	251	0	30
151	300	0.000	300	0	0
52	152	0.180	450	0	0
67	160	0.158	451	0	0
101	197	0.151	610	0	0
250	251	0.000	611	0	0
450	451	0.000			

Table C -2 130 Nodes Water Distribution Network Data

Water Graph - Edges			Water Graph - Node Data		
From Node	**To Node**	**Weight**	**Node**	**Demand (m3)**	**Water storage (m3)**
1	2	0.510	1	0	0
2	3	0.410	2	0	0
3	4	0.322	3	0	0
4	5	0.352	4	3	0
5	6	0.119	5	3	0
6	7	0.352	6	3	0
9	7	0.090	7	3	0
7	8	0.036	8	3	0
10	8	0.074	9	3	0
8	11	0.567	10	3	0
5	9	0.255	11	0	0
13	9	0.309	12	3	40
14	10	0.309	13	3	0
4	12	0.030	14	3	0
12	13	0.099	15	0	0
13	14	0.036	16	0	0
15	12	0.099	17	0	0
16	14	0.099	18	3	0
17	11	0.361	19	3	0
3	15	0.352	20	0	0
15	16	0.309	21	3	0
16	17	0.528	22	3	0
2	30	0.952	23	3	0
3	18	0.120	24	3	0
18	19	0.352	25	3	0
15	19	0.137	26	3	0
16	20	0.137	27	3	50
17	23	0.099	28	3	0
18	23	0.103	29	1	0
23	24	0.412	30	3	0
25	24	0.137	31	3	0
25	20	0.074	32	3	100
27	21	0.293	33	3	0
20	21	0.213	34	3	0
21	22	0.137	35	3	0
28	22	0.340	36	3	0
23	31	0.410	37	3	0

Table C-2 Continued

24	32	0.469	38	3	0
33	25	0.361	39	8	0
25	26	0.159	40	7	0
26	27	0.018	41	3	0
34	27	0.293	42	3	0
27	28	0.137	43	3	0
36	28	0.293	44	3	0
30	29	0.361	45	5.5	0
30	31	0.298	46	3	0
32	31	0.340	47	6.5	0
33	32	0.410	48	7	0
33	34	0.340	49	3	0
34	35	0.041	50	3	0
35	36	0.048	51	3	0
36	37	0.293	52	3	0
38	37	0.041	53	3	0
29	45	0.821	54	3	0
30	39	0.258	55	3	0
31	40	0.293	56	3	0
48	32	0.762	57	3	0
41	33	0.410	58	3	0
35	42	0.476	59	3	0
43	36	0.298	60	3	0
44	37	0.298	61	3	0
54	38	0.425	62	6	0
39	40	0.361	63	5	0
40	47	0.469	64	3	0
41	42	0.410	65	3	0
42	43	0.041	66	3	0
43	44	0.293	67	3	50
39	46	0.612	68	3	0
49	41	0.103	69	3	0
51	42	0.090	70	3	0
52	43	0.119	71	3	0
46	45	0.410	72	3	0
46	47	0.361	73	3	0
48	47	0.340	74	3	0
49	48	0.386	75	3	0
49	50	0.293	76	3	0

Table C-2 Continued

50	51	0.048	77	3	150
51	52	0.041	78	3	0
52	53	0.293	79	3	0
53	54	0.258	80	8	0
45	62	0.567	81	3	40
46	55	0.255	82	3	0
47	56	0.410	83	3	0
57	49	0.586	84	9	0
50	58	0.352	85	3	0
58	59	0.120	86	3	0
52	59	0.309	87	3	0
53	60	0.464	88	3	0
61	54	0.489	89	3	0
63	62	0.361	90	3	0
55	56	0.410	91	3	0
57	56	0.383	92	3	0
76	59	0.670	93	3	0
61	60	0.361	94	3	0
69	62	0.352	95	3	0
63	70	0.255	96	3	0
64	56	0.298	97	3	0
66	65	0.258	98	3	0
66	67	0.036	99	3	0
64	67	0.464	100	3	0
73	64	0.120	101	3	0
74	67	0.079	102	0	0
75	68	0.412	103	3	0
68	66	0.087	104	3	0
77	60	0.412	105	3	0
78	61	0.352	106	3	0
70	69	0.410	107	3	0
69	79	0.258	108	3	0
70	80	0.293	109	3	0
71	70	0.041	110	0	0
72	71	0.090	111	3	0
71	81	0.213	112	3	0
81	82	0.090	113	3	0
72	82	0.213	114	0	0
73	72	0.036	115	0	0

Table C-2 Continued

74	73	0.612	116	0	0
75	74	0.119	117	3	0
80	79	0.476	118	3	0
79	83	0.309	119	3	0
84	80	0.352	120	3	0
84	83	0.361	121	3	0
85	84	0.361	122	3	0
86	85	0.464	123	3	0
75	86	0.309	124	3	0
75	76	0.528	125	3	0
76	77	0.170	126	3	0
77	78	0.528	127	3	0
83	87	0.340	128	3	0
84	88	0.586	129	3	0
85	89	0.340	130	3	0
90	91	0.096	131	3	0
97	90	0.089	132	3	0
97	98	0.105	133	3	0
86	98	0.152	134	3	0
99	100	0.050	135	3	0
98	99	0.084	136	3	0
99	101	0.093	137	3	0
102	75	0.442	138	3	0
105	104	0.170	139	3	0
106	103	0.085	140	3	0
106	105	0.020	141	3	0
105	107	0.386	142	3	0
77	107	0.102	143	3	0
108	106	0.069	144	3	0

Table C -3 Energy and Water Interconnection Data

ST Nodes	Energy Nodes	Distance (d_{ij})	Resilience (r_{ij})	Weight (d_{ij}/r_{ij})
12	68	0.30	0.5	0.61
12	69	0.24	0.75	0.32
24	152	0.24	0.8	0.31
24	32	0.30	0.4	0.76
24	18	0.53	0.9	0.59
27	1	0.47	0.5	0.95
72	29	0.03	0.35	0.07
72	300	0.59	0.45	1.31
77	35	0.42	0.35	1.21
77	40	0.38	0.9	0.42
77	36	0.23	1	0.23
86	110	0.75	0.6	1.25
86	111	0.07	0.5	0.14
86	109	0.63	0.85	0.74
86	151	0.84	0.45	1.88